Transportation Research Part E 208 (2026) 104707

Contents lists available at ScienceDirect

Transportation Research Part E

journal homepage: www.elsevier.com/locate/tre

Digital twin-based dynamic co-scheduling with AGV energy management in sea-rail intermodal automated container terminals

Jiaqi Li [a,b], Daofang Chang [c], Furong Wen [d], Ilkyeong Moon [b,*]

[a] Institute of Logistics Science and Engineering, Shanghai Maritime University, 1550 Haigang Avenue, Shanghai, 201306, China
[b] Department of Industrial Engineering, Seoul National University, 1 Gwanak-ro Gwanak-gu, Seoul, 08826, Republic of Korea
[c] Logistics Engineering College, Shanghai Maritime University, 1550 Haigang Avenue, Shanghai, 201306, China
[d] Guangxi Bagui Engineering Supervision, Guangxi, China

ARTICLE INFO

Keywords:
Sea-rail intermodal automated container terminal
Multi-equipment co-scheduling
Battery scheduling
Decomposition-iteration optimization
Digital twin

ABSTRACT

To fully leverage the advantages of sea-rail intermodal transport, the automation upgrade of the railway center station (RCS) is essential for enabling seamless connectivity between the RCS and the terminal via automated guided vehicles (AGVs). This transformation introduces complex scheduling challenges for sea-rail intermodal automated container terminals (SRIACTs), including multi-directional container flows, coordination among diverse equipment, and AGV charging requirements with battery management. To address these challenges, this paper investigates the multi-equipment collaborative scheduling problem in SRIACTs with consideration of AGV charging. A mixed-integer programming model is formulated with sequencing, timing, and energy constraints, aiming to jointly minimize makespan and total charging time. To improve computational efficiency in large-scale cases, an improved genetic algorithm based on a decomposition-iteration framework is developed according to problem-specific features. Furthermore, to address operational uncertainties, a digital twin-based hybrid rescheduling framework is extended to enable real-time monitoring, disturbance detection, and rapid response to AGV status and battery levels, thereby enhancing system resilience and scheduling flexibility. Extensive numerical experiments are conducted to validate the effectiveness of the proposed algorithm and rescheduling framework. On this basis, comparative analyses are performed on bi-objective formulations and the flexible charging strategy. Additionally, sensitivity analyses examine the impacts of key factors, including objective weights, charging thresholds, rescheduling thresholds, and the number and layout of charging facilities. The findings provide valuable insights for terminal operators in formulating integrated scheduling strategies, optimizing AGV charging plans, and scientifically deploying charging infrastructure during the RCS automation process, thereby promoting sustainable and intelligent terminal operations.

1. Introduction

With the continuous growth of global logistics demand, maritime transport, leveraging its advantages of high capacity and low cost, accounts for over 80% of global trade volume (Trade and Development, 2024). As core nodes of global logistics networks, the operational efficiency of container terminals has increasingly become a focal point of attention. Driven by low-carbon and sustainable

* Corresponding author.
E-mail addresses: jiaqili@stu.shmtu.edu.cn (J. Li), dfchang@shmtu.edu.cn (D. Chang), wenfr@bbwport.com (F. Wen), ikmoon@snu.ac.kr (I. Moon).

https://doi.org/10.1016/j.tre.2026.104707
Received 25 August 2025; Received in revised form 19 January 2026; Accepted 19 January 2026
Available online 28 January 2026

Fig. 1. Layout of Qinzhou Port and its container flows.

development goals, sea-rail intermodal transport, as a multimodal transport mode with advantages such as low carbon emissions, high accessibility, and resource intensification, is gradually becoming an important pathway for port transformation and upgrading, attracting widespread attention.

In recent years, representative hub ports in China, such as Qinzhou Port, have made notable progress in the development of sea-rail intermodal services, with continuous growth in both container throughput and rail-handled volumes. On June 30, 2023, Qinzhou Port removed the physical barriers between the terminal and the railway center station (RCS), achieving preliminary connectivity of operational spaces (see Fig. 1). However, the RCS has not yet completed its automation upgrade, and containers still rely on internal container trucks (ICTs) for transportation between the RCS and the terminal yard. Additionally, efficient direct transport between ships and trains cannot be achieved, which constrains the overall operational efficiency and intelligent level. To further unlock the synergistic potential of sea-rail intermodal transport, Qinzhou Port has initiated the planning for the automation upgrade of the RCS, aiming to introduce an automated guided vehicle (AGV) system to establish an automated transportation and coordinated scheduling system covering the RCS, terminal yard, and seaside area (see Fig. 1).

Notably, the yard area of Qinzhou Port features a distinctive U-shaped road layout for container trucks, consisting of a one-way U-shaped road used exclusively by container trucks. Following the automation upgrade of the RCS and the deployment of AGVs, ICTs previously responsible for horizontal transport between the RCS and the yard were phased out. AGVs have since taken over the container transfer tasks among the RCS, the yard, and the seaside, including the direct train-ship transfers that were not feasible under the traditional ICT-based operation. The U-shaped road remains dedicated to external container trucks (ECTs) for entering the yard and performing pickup and delivery activities.

Under this layout, the operational scope of AGVs expands considerably compared with that in conventional automated container terminals, where AGVs typically operate only in the seaside area. AGVs must now enter handling lanes within the yard blocks as well as those at the RCS, and position themselves near the designated bays to complete handover operations with rail cranes (RCs) and yard cranes (YCs). As the temporal arrival of AGVs more directly affects the initiation and completion of equipment operations, their spatio-temporal alignment with handling equipment becomes more critical. Consequently, task-timing coordination requirements in multi-equipment collaborative scheduling are substantially intensified, leading to higher overall system coordination complexity.

Academic research on scheduling optimization for automated container terminals has been extensively conducted, focusing primarily on multi-equipment collaborative scheduling modeling, AGV path and energy consumption optimization, robust scheduling under disturbance conditions, and the application of digital twin (DT) technology in scheduling optimization. In terms of multi-equipment collaboration, existing studies have generally adopted mixed-integer programming (MIP) models combined with heuristic algorithms to achieve task allocation and job sequencing optimization for RCs, YCs, quay cranes (QCs), and AGVs (Qin et al., 2020; Yu et al., 2023). In terms of AGV scheduling and energy control, existing literature has introduced battery constraints, charging strategies, and fast-charging behaviors into optimization models (Gong et al., 2024; Song et al., 2024). Additionally, to address dynamic disturbances in terminal operations, researchers have proposed methods based on stochastic optimization models (Zhen et al., 2022; Zhang et al., 2025), rolling horizon strategies (Li et al., 2025c), and predictive optimization (Tang et al., 2024b; Kim et al., 2026). In recent years, DT technology has been increasingly applied in terminal scheduling research, enabling real-time perception of operational status and dynamic feedback through virtual-physical mapping, and showing promising potential in enhancing system responsiveness and scheduling efficiency (Gao et al., 2024; Li et al., 2025a).

Although the aforementioned studies have made significant progress in scheduling methods, scheduling optimization for SRIACTs still faces three major challenges:

(1) Complex decision variables and enhanced coupling with charging behaviors. Compared with conventional scheduling problems, the collaborative scheduling of RCs, YCs, QCs, and AGVs under energy constraints requires not only the assignment of tasks, sequencing, and start time decisions, but also the joint optimization of AGV charging timing and flexible charging durations. This significantly increases variable coupling and elevates the complexity of both modeling and solution processes.

(2) Large-scale problem size and high computational complexity. The problem is NP-hard in nature (Ding et al., 2023). As the number of tasks, equipment, and energy-related constraints increases, the solution complexity grows exponentially. Traditional optimization or heuristic approaches tend to suffer from slow convergence and local optima in large-scale instances.

(3) Dynamic operational environment and frequent disturbances. Real-world terminal operations are often affected by disruptions such as scheduling deviations, equipment failures, and energy fluctuations, which render static scheduling plans infeasible. There is a pressing need for scheduling mechanisms with dynamic perception and real-time response capabilities.

Building upon the above, this study proposes a MIP model integrating AGV charging and multi-equipment co-scheduling, develops a Decomposition-Iteration-based Improved Genetic Algorithm (DI-iGA) algorithm for large-scale problem solving, and enhances a DT-based hybrid rescheduling framework to respond to AGV-related disturbances. These developments provide the methodological foundation for the subsequent contributions.

(1) To address the unique operational characteristics of U-shaped SRIACTs, this study develops a unified multi-equipment collaborative scheduling model that integrates the coordinated workflows of RCs, YCs, QCs, and AGVs across the RCS-yard-seaside regions. The model simultaneously captures multi-equipment temporal dependencies as well as AGV energy and fast-charging constraints, while accommodating the generalized double-cycling behavior inherent in sea-rail intermodal operations.

(2) To overcome the high computational complexity of the proposed MIP model and the strong coupling among multi-equipment and energy-related decisions, this study develops a DI-iGA algorithm. By decomposing the problem structure and embedding an improved GA within an iterative coordination framework, the proposed method enhances computational efficiency and solution quality, particularly for large-scale SRIACT scheduling instances.

(3) Building upon the DT-based hybrid rescheduling framework established in our previous research (Li et al., 2025a), this study further develops a disturbance-aware rescheduling mechanism that integrates AGV battery dynamics, charging requirements, and equipment failures. The enhanced DT layer enables real-time perception and rapid rescheduling, thus strengthening the robustness and responsiveness of multi-equipment operations in SRIACTs.

The remainder of this paper is organized as follows: Section 2 reviews the related research; Section 3 analyzes the system characteristics of SRIACTs, formulates the optimization model, and defines the associated constraints; Section 4 presents the solution algorithm for the model and the extended DT-based hybrid rescheduling mechanism; Section 5 validates the proposed model, algorithm, and DT-based rescheduling method through simulation experiments and case studies; Section 6 concludes the study and outlines future research directions.

2. Literature review

Based on the research background and objectives, this section systematically reviews relevant literature from three key perspectives: the multi-equipment co-scheduling in terminals, the scheduling of AGVs with energy consumption and replenishment considerations, and the handling of uncertainty and dynamic disturbances in terminal operations. This comprehensive review aims to clarify existing achievements and limitations and to provide a solid foundation for the proposed research framework.

2.1. Multi-equipment co-scheduling for terminals

In recent years, the coordinated scheduling of AGVs and handling equipment in automated container terminals has become a critical research focus for improving overall operational efficiency and energy performance.

Regarding AGV coordination with single equipment, (Xia and Zhu, 2023) optimized the collaborative scheduling of AGVs and YCs by introducing a space-time network model and heuristic rules, improving scalability and solution efficiency for large-scale terminals. Building on this, Zhang et al. (2024b) addressed twin YC interference by formulating a MIP model and designing a heuristic method based on the branch-and-bound principle to achieve integrated AGV-YC scheduling. In addition to AGV-YC coordination, the coordinated scheduling of AGVs and other single-type equipment is also a focus of attention. Zhu and Ma (2024) focused on the synchronized scheduling of automated stacking cranes (ASCs) and AGVs, considering handshake areas and buffer constraints, and adopted a swarm intelligence algorithm to reduce AGV waiting time and improve ASC efficiency. Kong et al. (2024) studied the scheduling of AGVs serving tandem QCs, developing an MIP model combined with a multi-start local search method, incorporating traffic congestion, AGV conflict, and buffer capacity constraints, and demonstrating the importance of efficient QC and AGV coordination for improving terminal performance. Furthermore, Wang et al. (2025c) introduced real-world constraints such as gantry interference and vehicle congestion into AGV-QC scheduling and proposed a two-stage framework combining branch-and-bound and column generation, effectively balancing solution quality and computational complexity.

Building on this foundation, scholars have progressively expanded research towards multi-equipment collaborative scheduling, aiming to more realistically capture multi-stage interactions and resource coupling within terminals. Tang et al. (2024a) and Li et al. (2024c) focused on the coordination of QCs, YCs, and AGVs, developing MIP models combined with Benders decomposition

and two-layer coordination strategies to optimize task assignment and operation sequencing across multiple areas. Building on this, Zhong et al. (2024) further extended these models by introducing flexible transshipment paths and multiple routing options, and developed a multi-objective optimization model solved by an enhanced NSGA-II algorithm to improve scheduling flexibility and solution efficiency across multi-equipment and operational zones. Meanwhile, to tackle the computational challenges arising from large-scale multi-equipment coordination, Wang et al. (2025b) proposed a hybrid framework combining MIP and offline-online reinforcement learning to dynamically coordinate QCs, block stations, intersections, and YCs, demonstrating the feasibility of integrating data-driven and optimization approaches to improve solution adaptability and efficiency.

With the growing diversity in ACT spatial layouts, the coordinated scheduling of AGVs and multi-equipment in U-shaped terminals, which involve more complex multi-point loading/unloading and path conflict scenarios, has attracted increasing attention. Zhang et al. (2024a) investigated multi-equipment scheduling for U-shaped ACTs involving dual trolley QCs, AGVs, double cantilever rail cranes, and external trucks, combining an MIP model with an improved cuckoo search algorithm to improve system coordination and throughput. Ma et al. (2024) focused on the trade-off between energy consumption and task completion time for AGVs and YCs in U-shaped terminals, proposing an integrated approach that combines speed adjustment strategies with a time-energy coordinated scheduling model, aiming to achieve a balance between task completion time and energy consumption. Peng et al. (2025) further studied conflict-free path planning and scheduling for double-side cantilever YCs, AGVs, and external trucks in U-shaped yards, using a bi-objective MIP model and introducing an enhanced particle swarm optimization (PSO) algorithm tailored for multi-objective scenarios, aiming to improve both task completion time and energy efficiency.

Furthermore, with the expansion of sea-rail intermodal transportation, multi-equipment scheduling has increasingly evolved from traditional terminal operations to the integrated coordination of QCs, yards, horizontal transport, and railway connections. Yu et al. (2023) developed a bi-directional hybrid flow-shop scheduling model for QCs, automated straddle carrier, and automated rail mounted gantry crane, using a PSO with Adaptive Tent Chaos Mapping to improve solution quality, although the yard buffer and horizontal transport were not fully modeled. Zhao et al. (2025) proposed a multi-equipment scheduling model for a stereo container yard, coordinating QCs, YCs, AGVs, ASCs, and double-stack trains. Their work centers on the unique three-dimensional yard structure and large-scale cooperative scheduling, but does not consider AGV energy consumption or charging decisions, and the operational setting differs fundamentally from sea-rail intermodal terminals. For the U-shaped SRIACT, Wang and Jin (2025) proposed a bi-objective scheduling and intersection allocation model for AYCs, AGVs, and internal trucks, considering direct and indirect transshipment modes with energy and conflict balancing. Furthermore, Li et al. (2025b) coordinated QCs, AGVs, YCs, and RCs through a multi-objective model with flexible transshipment routes, but did not consider AGV battery levels, charging decisions, or their coupling with multi-equipment scheduling.

In summary, although existing studies have extensively explored AGV and multi-equipment co-scheduling, including some investigations in U-shaped terminal layouts, most of them still focus on a single operational area or local processes, lacking comprehensive coordination models that integrate the RCS, terminal yards, and seaside operations.

2.2. AGV scheduling with energy consumption and replenishment considerations

In recent years, with the growing demand for energy efficiency and sustainability in automated container terminals, research on AGV scheduling has gradually expanded from traditional makespan minimization to integrated consideration of energy consumption constraints and energy replenishment strategies.

Regarding models that explicitly consider energy consumption, Gong et al. (2024) constructed a multi-AGV scheduling framework based on multi-agent deep reinforcement learning, formulating the problem as a Markov decision process to jointly optimize total energy consumption and task completion time.

Building on this, recent studies have increasingly focused on optimizing AGV energy replenishment strategies, including battery swapping, charging, and hybrid schemes. For battery swapping scenarios, Yang et al. (2023a) developed a multi-objective MIP model under limited swapping capacity and proposed a flexible pooling strategy to balance operational efficiency and energy costs. Zhou et al. (2024) integrated battery swapping into a co-optimization framework and adopted a discrete whale optimization algorithm to reduce energy and maintenance costs, while Li et al. (2025c) combined reinforcement learning and hybrid genetic algorithms to manage battery swapping scheduling under uncertain electricity prices and waiting times. For hybrid strategies combining charging and swapping, Zhen et al. further developed a column generation-based framework with a label-setting algorithm for the mixed-mode scenario, validating its practicality in real terminal conditions. In the context of pure charging optimization, Wang et al. (2025a) designed a multi-agent simulation framework to explore the optimal combination of charging frequency and battery thresholds for B-IGV energy management, while Zhao and Liang (2025) focused on a shallow charge and shallow discharge charging strategy, formulating a bi-objective model to minimize makespan and battery life loss.

Notably, some studies have begun to address the integration of AGV charging strategies with multi-equipment collaborative scheduling. For instance, Yang et al. (2025) investigated the joint scheduling of QCs, AGVs, and YCs in automated container terminals, incorporating both charging and fast battery-swapping modes. However, their study is restricted to ACT operations with buffer-assisted AGV-YC interactions and does not involve the multi-stage coordination among RCs, YCs, QCs, and AGVs required in SRIACT. Moreover, detailed battery degradation and the coupling between charging decisions and transport task scheduling were not fully considered.

2.3. Uncertainty handling and dynamic disturbance response in terminal scheduling

In recent years, multi-source uncertainties, such as vessel arrival deviations, equipment availability fluctuations, and handling time variability, have posed significant challenges to the feasibility and robustness of terminal operation schedules. To address these typical disturbances, researchers have explored various methods covering forecasting, robust modeling, and DT-based strategies.

In terms of prediction and simulation methods, data-driven forecasting, machine learning, and interactive simulation are widely applied to estimate key disturbance information in advance, providing more reliable input parameters and reducing execution deviations. For example, Yu et al. (2018) used data-driven methods to predict vessel arrival deviations and analyzed their impact on berth and QCs allocation. Wang et al. (2023b) combined simulation-based interaction models to examine container arrival times and yard operation coordination. Park et al. (2024) further enhanced feed-forward prediction accuracy for concurrent multi-equipment operations by integrating support vector machine algorithms with discrete event simulation, effectively improving the reliability and precision of input data.

Directly embedding uncertainty into scheduling models is another widely adopted approach to mitigate operational disruptions. Many studies focus on typical uncertainty scenarios, such as handling time fluctuations, vessel arrival deviations, and external energy price volatility, employing scenario generation, chance-constrained programming, or robust optimization frameworks to improve feasibility and stability. For example, Ji et al. (2023) addressed vessel arrival uncertainty in berth allocation and QC assignment by combining scenario-based simulation with a dual-objective optimization model and an improved genetic algorithm, aiming to reduce the total port stay time and mitigate resource conflicts. Wang et al. (2024) investigated berth and QC resource fluctuations caused by uncertain arrival times using distributionally robust chance constraints and branch-and-bound methods. Chargui et al. (2023) focused on the electricity price uncertainty and proposed a robust decomposition algorithm to balance energy costs and delay penalties. Li et al. (2024b) developed a two-stage robust optimization model with a hybrid decomposition approach to handle handling-time uncertainty in unidirectional QC operations. Moreover, Cai et al. (2024) emphasized handling time variability and cascading effects in multi-equipment scheduling for U-shaped terminals by proposing a three-stage hybrid flow shop model with bi-objective robust optimization to enhance overall feasibility.

Although these methods improve the adaptability and feasibility of terminal operation schedules from different perspectives, most rely on offline scenario generation or static optimization and fall short of fully addressing multi-source real-time disruptions and cross-linkage effects during execution. In this context, DT-based disturbance detection and response have emerged as a new trend for uncertainty handling in terminal operations. Lou et al. (2023) developed a DT-driven framework for AGV scheduling and routing, combining virtual-physical interaction with swarm intelligence algorithms to significantly improve real-time conflict detection and dynamic adjustment under environmental disturbances. Gao et al. (2024) integrated DT with Q-learning reinforcement learning to validate the flexibility and battery utilization of AGV operations in large-scale scenarios. Li et al. (2024a) further constructed a DT-based hybrid scheduling framework for multi-equipment, multi-stage operations, enhancing the adaptability of operations under equipment failure and resource fluctuations through state awareness and rolling rescheduling.

Overall, DT-based disturbance detection and dynamic response mechanisms have been preliminarily validated in some terminal operation scenarios. However, existing literature primarily focuses on either single equipment or localized stages and lacks a comprehensive framework that addresses multi-source uncertainties as well as cross-equipment and cross-area integration. Therefore, in complex scenarios such as SRIACTs with multi-point handling and multi-container flows, DT-based multi-equipment collaborative scheduling considering AGV charging and dynamic response still requires further in-depth research.

2.4. Research overview

Based on the above analysis, although existing studies have made significant progress in AGV and multi-equipment collaborative scheduling, energy consumption and replenishment strategies, and uncertainty handling, there remain several limitations. First, most multi-equipment scheduling studies mainly focus on single operational stages or local areas and lack comprehensive optimization models that integrate multiple areas, such as the RCS, the terminal yard, and the seaside operation. Second, research on AGV energy consumption and replenishment scheduling predominantly adopts single-mode or static scenarios, making it difficult to fully couple with multi-equipment operational processes. Third, under multi-source uncertainties, DT-based disturbance detection and dynamic response mechanisms have been preliminarily validated in local scenarios, but their application in integrated multi-stage, multi-equipment scheduling still requires further expansion and in-depth exploration.

To address these limitations, this study focuses on the unique characteristics of the U-shaped SRIACT, which features multi-point loading/unloading and complex multi-equipment interactions. An integrated multi-equipment collaborative scheduling framework is developed, specifically considering AGV fast-charging characteristics. By embedding energy constraints and flexible charging strategies, this framework enables dynamic coupling between AGV energy replenishment and multi-equipment operations. Furthermore, a DT-based mechanism for disturbance detection and dynamic rescheduling is proposed to enhance real-time perception and response capabilities under multi-source uncertainties, thereby improving the feasibility and robustness of terminal operation plans.

3. Problem description and model formulation

This chapter describes the problem and formulates the model from three aspects. First, the collaborative scheduling process for multi-equipment operations in the U-shaped SRIACT is analyzed, focusing on the equipment collaboration characteristics of different container flows. Second, the energy consumption characteristics of AGVs are examined in detail, considering loaded/unloaded travel,

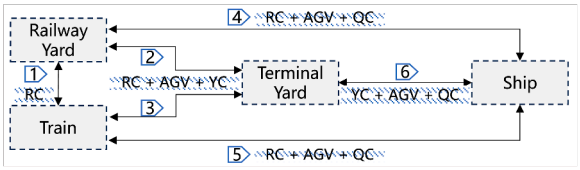

Fig. 2. Multi-equipment cooperative scheduling of six container flows in the SRIACT.

with corresponding calculation methods provided. Finally, an integrated multi-equipment co-scheduling model incorporating AGV charging behavior is developed, with explicit definitions of the objective function, relevant constraints, and variable domains.

3.1. Multi-equipment co-scheduling in the SRIACT with double-cycling mode

The U-shaped SRIACT considered in this study comprises a dedicated railway yard within the RCS, where containers transported by train can be temporarily stored or directly moved to the terminal yard when necessary. Based on practical operational scenarios, six types of bidirectional container flows are defined, as shown in Fig. 2, including: (1) Railway yard-Train, (2) Train-Terminal yard, (3) Railway yard-Terminal yard, (4) Train-Ship, (5) Railway yard-Ship, and (6) Terminal yard-Ship. Let $\mathcal{N}$ denote the set of all containers involved in the SRIACT operations. The six bidirectional container flows characterize different equipment collaboration patterns at the operation-stage level. Accordingly, $c = 1, 2, \ldots, 6$ indexes the flow types, and $\mathcal{N}_c$ denotes the subset of containers associated with the cth bidirectional container flow at a given operation stage. For a given operation stage, each container is associated with exactly one flow type. Thus, the following relations hold: $\cup_{c=1}^{6} \mathcal{N}_c = \mathcal{N}, \mathcal{N}_c \cap \mathcal{N}_{c'} = \varnothing (c \neq c')$.

It is worth noting that, in practical operations, a container may experience multiple transportation stages (e.g., a container being unloaded from a ship, temporarily stored, and subsequently loaded onto a train). Such multi-stage processes often involve different vessels or trains and require consideration of their respective arrival schedules and waiting times. In this study, each container is therefore modeled as a single transportation request with a unique origin-destination pair within the planning horizon, while multi-stage transportation processes involving vessel/train arrival synchronization are beyond the scope of this work and will be investigated in future research.

Specifically, the six bidirectional container flows correspond to different equipment collaboration patterns. For each flow type c, the associated container set $\mathcal{N}_c$ can be further divided into export and import directions, denoted by $\mathcal{N}_c^E$ and $\mathcal{N}_c^I$, respectively. Containers in $\mathcal{N}_1^E$ are transported from the train to the railway yard via RC, while those in $\mathcal{N}_1^I$ follow the reverse direction. Containers in $\mathcal{N}_2^E$ move from the railway yard to the terminal yard through the coordinated operations of RC, AGV, and YC, whereas those in $\mathcal{N}_2^I$ move in the reverse direction. Containers in $\mathcal{N}_3^E$ are transported from the train to the terminal yard involving RC, AGV, and YC, while those in $\mathcal{N}_3^I$ follow the reverse direction. Containers in $\mathcal{N}_4^E$ move from the railway yard to the ship through RC, AGV, and QC, whereas those in $\mathcal{N}_4^I$ follow the reverse operations. Containers in $\mathcal{N}_5^E$ are transferred from the train to the ship via RC, AGV, and QC, while those in $\mathcal{N}_5^I$ move from the ship back to the train. Containers in $\mathcal{N}_6^E$ are transported from the terminal yard to the ship through QC, AGV, and YC, whereas those in $\mathcal{N}_6^I$ move from the ship to the terminal yard.

Collectively, these six bidirectional flows reflect the cooperative relationships among the RCS, terminal yard, and seaside operations, forming the conceptual foundation for subsequent multi-equipment co-scheduling. In SRIACTs, loading and unloading activities may occur simultaneously, forming a circulation pattern that resembles a double-cycling mechanism.

However, unlike the traditional double-cycling adopted in quay-yard automated terminals, where each AGV is forced to execute an import task immediately followed by an export task through strict pairing constraints, SRIACT features a generalized and more flexible form of double-cycling. Because AGVs operate across three functional regions (the seaside, the terminal yard and the RCS), their circulation patterns naturally evolve into sequences such as QC-YC-QC (traditional import-export), QC-YC-RC (import-import), RC-YC-QC (export-export), and similar cross-area combinations.

This generalized double-cycling arises endogenously from spatial availability, task precedence, and energy constraints, rather than from any mandatory import-export pairing. Such flexibility enables AGVs to reduce empty travel and supports the cross-area operation that is essential in sea-rail intermodal terminals.

The following subsections detail the operational logic and temporal coordination of the RC, YC, and AGV, respectively, before integrating them into a unified multi-equipment collaboration mechanism.

For clarity, all indices, sets, parameters and variables related to multi-equipment co-scheduling are unified in advance and summarized in Table 1, which provides the notation system for analyzing the cooperative operations among RCs, YCs, QCs, and AGVs.

3.1.1. Operation analysis of individual equipment

In the SRIACT with a double-cycling mode, the RC transfers containers between the RCS and other subsystems. Since two consecutive container tasks may originate from different container flows, the RC's operation times are analyzed separately. In this paper, the start time of the RC's operation on a container is defined as the moment when the RC is already in position, with its gantry located in the corresponding bay and its trolley positioned on the appropriate line. Based on this definition, the RC's operation processes for containers associated with different flows are analyzed as follows.

Table 1
Definition of indices, sets, parameters and decision variables.

Name	Description
Indices	
(k,g)	The charging activity indexed by (k,g) corresponds to the g*th* operation at charging facility k.
i,j	Indices for container.
$r,y,q,\ a$	Indices for RC, YC, QC, and AGV, respectively.
l,b	Indices for the railway block and the yard block, respectively.
S,F	Virtual start and end containers.
Sets	
R,Y,Q,A	Sets of RCs, YCs, QCs, and AGVs, respectively, where $r\in R, y\in Y, q\in Q$, and $a\in A$.
L,B	Sets of railway blocks in the RCS and yard blocks in the terminal yard, where $l\in L$ and $b\in B$.
R_l,Y_b	Subset of RCs assigned to railway block l and YCs assigned to yard block b, respectively.
$\mathcal{N}$	Set of all containers, $i\in\mathcal{N}$.
$\mathcal{N}_c$	Subset of containers belonging to the c*th* container flow ($\mathcal{N}_c\subset\mathcal{N}, c=\{1,2,\ldots,6\}$); these subsets are mutually exclusive and collectively exhaustive: $\bigcup_{c=1}^{6}\mathcal{N}_c=\mathcal{N}$.
$\mathcal{N}_c^E,\mathcal{N}_c^I$	Subsets of $\mathcal{N}_c$ representing the export and import containers of the c*th* flow, respectively.
$\mathcal{N}_l^{RB},\mathcal{N}_b^{YB}$	Sets of containers allocated to railway block l and yard block b, respectively.
$\mathcal{N}_q^{QC}$	Sets of containers handled by QC q.
$\mathcal{N}^S,\mathcal{N}^F$	Complete container set augmented with a virtual start container ($\mathcal{N}^S=\mathcal{N}\cup\{S\}$) and a virtual end container ($\mathcal{N}^F=\mathcal{N}\cup\{F\}$), respectively.
H^{RC},H^{YC}	Pre-processed sets of container pairs that cannot be handled simultaneously by RCs/ YCs due to insufficient bay separation based on their initial or final yard positions.
K	Set of all charging facilities, where $k\in K$.
G	Set of charging activities for each charging facility, where $g\in G$.
Ch	Set of all charging activities, represented by pairs (k,g) where $k\in K$ and $g\in G$.
Parameters	
λ_i	$=1$, if container i is first handled by RC/YC/QC and then transferred to an AGV; $=0$, otherwise.
μ_i	$=1$, if container i is an import container; $=0$, otherwise.
$\sigma_{(q,i)}^{QC}$	$=1$, if container i is assigned to QC q; $=0$, otherwise.
$\delta_{(q,i,j)}^{QC}$	$=1$, if containers i and j are handled successively by QC q; $=0$, otherwise.
$s_{(i,j)}^{RC},s_{(i,j)}^{YC}$	Setup time required for the RC and YC to move from completing container i to executing container j, unit: min.
s^{QC}	Fixed setup time for the QC between two consecutive container tasks, unit: min.
p_i^{RC},p_i^{YC}	Processing time of the RC and YC for container i, unit: min.
p^{QC}	Fixed processing time of the QC for a single container, unit: min.
$\theta^{RC},\theta^{YC},\theta^{QC}$	Interaction time between RC/YC/QC and AGV during container handling, unit: min.
t_1^{RC},t_1^{YC}	Time required for the RC's and YC's gantry to move one bay,respectively, unit: min.
$h_{saf}^{RC},h_{saf}^{YC}$	Safe separation distance (in bays) that must be maintained between two RCs / two YCs, respectively, unit: bay.
$t_i^{AGV},t_{(i,j)}^{AGV},t_{(i,k)}^{V\_Ch},t_{(k,i)}^{Ch\_V}$	Time for AGV to (i) transport container i, (ii) travel from container i to the next container j, (iii) travel from container i to charging facility k , and (iv) return from charging facility k to container i, respectively, unit: min.
$e_i^{AGV},e_{(i,j)}^{AGV},e_{(i,k)}^{V\_Ch},e_{(k,i)}^{Ch\_V}$	Derived AGV energy consumptions for the four travel scenarios above, corresponding respectively to the time $t_i^{AGV},t_{(i,j)}^{AGV},t_{(i,k)}^{V\_Ch},t_{(k,i)}^{Ch\_V}$, unit: kWh.
E^{All}	Battery capacity of the AGV, unit: kWh.
E_a^{Ini}	Initial battery capacity of the AGV a, unit: kWh.
$O_{\min},O_{\max}$	Minimum and maximum energy thresholds for AGV battery capacity.
η_{wait}^{AGV}	Energy consumption rate of the AGV in waiting state, unit: kWh/h.
η_{Ch}	Charging rate of the AGV battery, unit: kWh/h.
M_T,M_E	A sufficiently large constant for time-related and energy-related constraints, respectively.
α	A weighting coefficient used in the objective function.
Decision variables	
0–1 variables	
$\alpha_{(r,i)}^{RC},\alpha_{(y,i)}^{YC},\alpha_{(a,i)}^{AGV}$	$=1$, if container i is assigned to RC r, YC y, or AGV a, respectively; $=0$, otherwise.
$\alpha_{(a,(k,g))}^{Ch}$	$=1$, if AGV a performs the g*th* charging activity at charge facility k; $=0$, otherwise.
$\beta_{(r,i,j)}^{RC},\beta_{(y,i,j)}^{YC}$	$=1$, if containers i and j are handled sequentially by RC r or YC y, respectively; $=0$, otherwise.
$\chi_{(a,i,j)}^{V\_V}$	$=1$, if AGV a transports containers i and j sequentially; $=0$, otherwise.
$\chi_{(a,i,(k,g))}^{V\_Ch}$	$=1$, if AGV a performs charging activity (k,g) immediately after transporting container i; $=0$, otherwise.
$\chi_{(a,(k,g),i)}^{Ch\_V}$	$=1$, if AGV a finishes charging activity (k,g) and subsequently transports container i; $=0$, otherwise.
Time-related variables	
$\overline{\tau}_{(r,i)}^{RC},\underline{\tau}_{(r,i)}^{RC}$	Start and completion times of RC r handling container i, respectively, unit: min.
$\overline{\tau}_{(y,i)}^{YC},\underline{\tau}_{(y,i)}^{YC}$	Start and completion times of YC y handling container i, respectively, unit: min.
$\overline{\tau}_{(q,i)}^{QC},\underline{\tau}_{(q,i)}^{QC}$	Start and completion times of QC q handling container i, respectively, unit: min.
$\overline{\tau}_{(a,i)}^{AGV},\underline{\tau}_{(a,i)}^{AGV}$	Start and completion times of AGV a transporting container i, respectively, unit: min.
$\overline{\tau}_{(a,(k,g))}^{Ch},\tau_{(k,g)}^{Ch\_dur}$	Start time of AGV a performing the charging activity (k,g), and duration of the charging activity (k,g), unit: min.
Energy-related variables	
$\overline{\varepsilon}_{(a,i)}^{AGV},\underline{\varepsilon}_{(a,i)}^{AGV}$	Battery level of AGV a at start and completion of transporting container i, unit: kWh.
$\overline{\varepsilon}_{(a,(k,g))}^{Ch}$	Battery level of AGV a at the start of charging activity (k,g), unit: kWh.

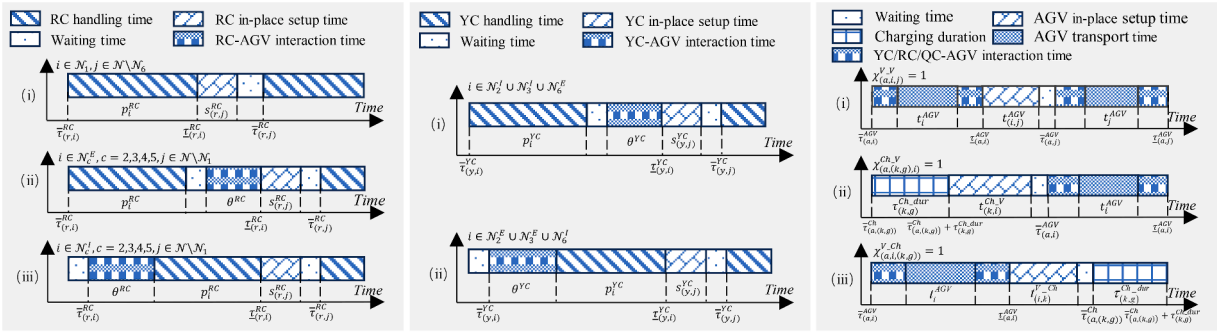

(a). RC (b). YC (c). AGV

Fig. 3. Time relationships of RC, YC, and AGV operations.

When container i belongs to the 1st container flow, the RC transfers the container between the train and the railway yard, as illustrated in Fig. 3(a)(i). The operation includes lowering the spreader, lifting the container, moving the gantry to the target bay, and positioning the trolley along the designated line.

When container i is an export container from the 2nd to 5th flows, the temporal relationships among the RC's actions are shown in Fig. 3(a)(ii). After picking up the container, the RC moves the trolley to the AGV operation lane, waits for the AGV to be in position, and then lowers the spreader to load the container onto the AGV.

When container i is an import container from the 2nd to 5th flows, the corresponding process is illustrated in Fig. 3(a)(iii). The RC starts handling when the AGV is in position, unloads the container from the AGV, and then moves the trolley to the designated bay to place the container.

Detailed calculation formulas for these handling times are provided in Appendix A.1.

In addition to the handling time of individual tasks, the RC requires a certain preparation period between two consecutive operations to reposition its gantry and trolley. This setup process ensures that the RC is properly aligned for the next container task. The duration depends on the relative positions of the containers and the types of container flows. Considering all possible combinations of same-flow and cross-flow transitions, a total of 100 possible scenarios exist for a single RC handling two consecutive containers. The detailed mathematical formulations and parameter definitions for calculating the setup times in each scenario are presented in Appendix A.1.

Following the RC, the YC's operation logic is analyzed in a similar manner. The relationship between the time parameters for the interaction between the YC and the AGV during storage is illustrated in Fig. 3(b)(i). Meanwhile, the time relationships involved in ship or train loading operations are shown in Fig. 3(b)(ii). The detailed calculation formulas for the YC's handling time and the in-place setup time between two consecutive container tasks are provided in Appendix A.2.

For the AGV, in the double-cycling mode, three possible scenarios occur when an AGV consecutively performs two tasks: (1) performing two transportation tasks successively, i.e., $\chi^{V\_V}_{(a,i,j)} = 1$; (2) performing a transportation task followed by a charging activity, i.e., $\chi^{V\_Ch}_{(a,i,(k,g))} = 1$; and (3) performing a charging activity followed by a transportation task, i.e., $\chi^{V\_Ch}_{(a,(k,g),i)} = 1$. The temporal relationships among these operations are illustrated in Fig. 3(c). The detailed calculation formulas for the AGV's transportation time and in-place setup time under various operational scenarios are provided in Appendix A.3.

These analyses of individual equipment operations lay the foundation for establishing cooperative time relationships among the RC, YC, QC, and AGV in Section 3.1.2.

3.1.2. Operation analysis of multi-equipment collaboration

For containers in the 2nd to 6th container flows, the co-scheduling of RC, YC, QC and AGV is required. Through analysis, six possible scenarios can be identified. The relationships between the corresponding time parameters are illustrated in Fig. 4.

3.2. Energy consumption of AGVs

The AGV, a driverless transport vehicle, operates through an electric-drive system powered by batteries and uses electric motors to achieve precise positioning and efficient container transportation. According to the China Energy Data Report (2025), in 2024, China's thermal power generation reached 6374.26 billion kilowatt-hours, accounting for 63.19% of the total power generation. Although the share of thermal power has slightly decreased, its dominant position in electricity generation is expected to remain unchanged for a long time, making energy consumption a critical factor in AGV scheduling decisions.

Let e_{mn} denote the energy consumption of an AGV traveling between nodes m and n. To characterize AGV energy consumption at the scheduling level, two energy-consumption coefficients, κ^L and κ^E, are introduced to represent the energy consumption per unit distance for loaded and empty travel, respectively. These coefficients aggregate the effects of vehicle characteristics and operating conditions and are treated as constants in this study. The detailed physical formulation of e_{mn} and the corresponding parameter definitions are provided in Appendix B.

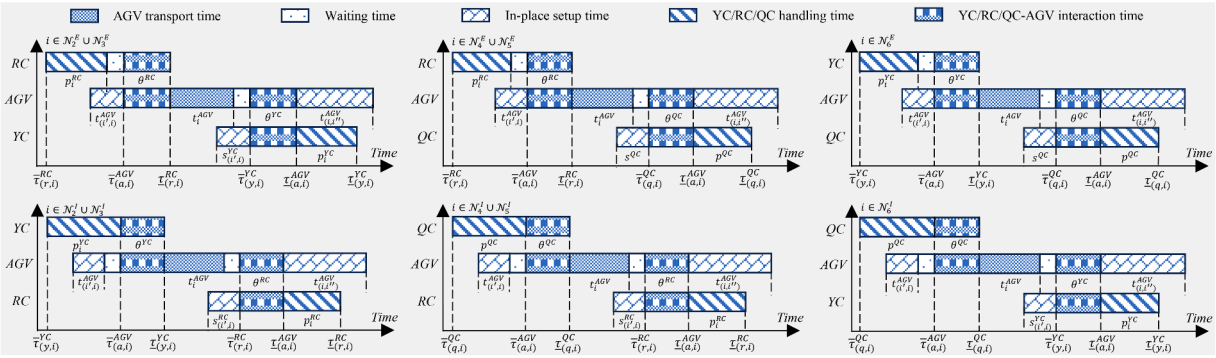

Fig. 4. Time relationship for multi-equipment collaborative operation.

In this study, four AGV travel scenarios are considered in the scheduling process: (1) loaded travel to transport container i, (2) unloaded travel to transport container j after container i is transported, (3) unloaded travel to charging facility k after container i is transported, and (4) unloaded travel to transport container i after charging is complete at charging facility k. The corresponding AGV energy consumptions are expressed as:

$$\begin{cases} e_i^{AGV} = \kappa^L \cdot d_i^{AGV}, \\ e_{(i,j)}^{AGV} = \kappa^E \cdot d_{(i,j)}^{AGV}, \\ e_{(i,k)}^{V\_Ch} = \kappa^E \cdot d_{(i,k)}^{V\_Ch}, \\ e_{(k,i)}^{Ch\_V} = \kappa^E \cdot d_{(k,i)}^{Ch\_V}, \end{cases} \tag{1}$$

where $d(\cdot)$ denotes the corresponding travel distance. In the scheduling model, travel distances are determined by routing decisions, while the selection among the above travel scenarios depends on task sequencing and charging decisions. Consequently, AGV energy consumption is directly linked to the decision variables of the scheduling problem.

3.3. Multi-equipment co-scheduling model

Section 3.3.1 presents the basic assumptions. Section 3.3.2 introduces a mixed-integer programming model aimed at balancing AGV energy consumption and maximum completion time, thereby optimizing the scheduling and AGV charging plans.

3.3.1. Model assumptions

To simplify the model formulation and ensure the solvability of the integrated problem, the following assumptions are proposed.

(1) All containers are forty-foot containers, and each AGV, YC, QC, and RC can handle only one container at a time.

(2) The operation sequence of QCs is predefined based on the double-cycle handling strategy.

(3) Potential conflicts or collisions among AGVs within the road network are disregarded.

(4) The battery charging function of the AGV is linear.

(5) The handling duration of containers by QCs is treated as known, and the interaction times between AGVs and RCs, YCs, and QCs are assumed to be fixed.

3.3.2. Mathematical model

This section presents a mathematical formulation for the joint optimization of AGV charging and coordinated equipment scheduling.

(1) Objective function

The primary goal of this study is to reduce the maximum completion time and the energy consumption of the AGV, where the energy consumption is translated into the charging duration of the AGV. Therefore, the objective function of the model can be formulated as shown in Eq. (2) below.

$$\min T_0 = \alpha \cdot T_F + (1-\alpha) T_{Ch} \tag{2}$$

$$T_F = \max_{r\in R, y\in Y, q\in Q, i\in\mathcal{N}} \left\{ \underline{\tau}_{(r,i)}^{RC}, \underline{\tau}_{(y,i)}^{YC}, \underline{\tau}_{(q,i)}^{QC} \right\} \tag{3}$$

$$T_{Ch} = \sum_{a\in A} \sum_{(k,g)\in Ch} \tau_{(a,(k,g))}^{Ch\_dur} \tag{4}$$

where T_F represents the maximum completion time and its calculation formula is given in Eq. (3), T_{Ch} denotes the total charging duration of all AGVs and its calculation is provided in Eq. (4).

(2) Sequence-related constraints

These constraints are used to restrict 0–1 decision variables, including $\alpha^{RC}_{(r,i)}$, $\beta^{RC}_{(r,i,j)}$, $\alpha^{YC}_{(y,i)}$, $\beta^{YC}_{(y,i,j)}$, $\alpha^{AGV}_{(a,i)}$,$\chi^{V\_V}_{(a,i,j)}$, $\chi^{V\_Ch}_{(a,i,(k,g))}$, $\chi^{Ch\_V}_{(a,(k,g),i)}$, and $\alpha^{Ch}_{(a,(k,g))}$, to ensure the operating sequence of RCs, YCs, AGVs and charging facilities.

$$\sum_{r\in R_l} \alpha^{RC}_{(r,i)} = 1, \forall i \in \mathcal{N}^{RB}_l, l \in L \tag{5}$$

$$\sum_{j\in\mathcal{N}^{RB}_l\cup\{F\}, j\neq i} \beta^{RC}_{(r,i,j)} = \alpha^{RC}_{(r,i)}, \sum_{j\in\mathcal{N}^{RB}_l\cup\{S\}, j\neq i} \beta^{RC}_{(r,j,i)} = \alpha^{RC}_{(r,i)}, \forall r \in R_l, i \in \mathcal{N}^{RB}_l, l \in L \tag{6}$$

$$\sum_{i\in\mathcal{N}^{RB}_l} \beta^{RC}_{(r,S,i)} \le 1, \sum_{i\in\mathcal{N}^{RB}_l} \beta^{RC}_{(r,i,F)} \le 1, \forall r \in R_l, l \in L \tag{7}$$

Eqs. (5)–(7) specify the assignment and sequencing of RC operations. Eq. (5) ensures that each container i in railway block l is assigned to exactly one RC. Eq. (6) enforces sequence continuity by requiring each assigned container to have exactly one predecessor and one successor. Eq. (7) restricts the outgoing arc from the dummy start node S and the incoming arc to the dummy end node F to at most one, preventing multiple disjoint task chains on the same RC.

$$\sum_{y\in Y_b} \alpha^{YC}_{(y,i)} = 1, \forall i \in \mathcal{N}^{YB}_b, b \in B \tag{8}$$

$$\sum_{j\in\mathcal{N}^{YB}_b\cup\{F\}, j\neq i} \beta^{YC}_{(y,i,j)} = \alpha^{YC}_{(y,i)}, \sum_{j\in\mathcal{N}^{YB}_b\cup\{S\}, j\neq i} \beta^{YC}_{(y,j,i)} = \alpha^{YC}_{(y,i)}, \forall y \in Y_b, i \in \mathcal{N}^{YB}_b, b \in B \tag{9}$$

$$\sum_{i\in\mathcal{N}^{YB}_b} \beta^{YC}_{(y,S,i)} \le 1, \sum_{i\in\mathcal{N}^{YB}_b} \beta^{YC}_{(y,i,F)} \le 1, \forall y \in Y_b, b \in B \tag{10}$$

Eqs. (8)–(10) specify the assignment and sequencing of YC operations. Their structure is identical to Eqs. (5)–(7) for RC, ensuring that each container in yard block b is assigned to exactly one YC and that the processing sequence on each YC contains only one predecessor and one successor, with at most one arc connected to the dummy start and end nodes.

$$\sum_{a\in A} \alpha^{AGV}_{(a,i)} = 1, \forall i \in \mathcal{N}\backslash\mathcal{N}_1 \tag{11}$$

$$\begin{cases} \sum_{j\in\mathcal{N}^F\backslash\mathcal{N}_1, j\neq i} \chi^{V\_V}_{(a,i,j)} + \sum_{(k,g)\in Ch} \chi^{V\_Ch}_{(a,i,(k,g))} = \alpha^{AGV}_{(a,i)} \\ \sum_{j\in\mathcal{N}^S\backslash\mathcal{N}_1, j\neq i} \chi^{V\_V}_{(a,j,i)} + \sum_{(k,g)\in Ch} \chi^{Ch\_V}_{(a,(k,g),i)} = \alpha^{AGV}_{(a,i)} \end{cases}, \forall a \in A, i \in C\backslash\mathcal{N}_1 \tag{12}$$

$$\sum_{i\in\mathcal{N}\backslash\mathcal{N}_1} \chi^{V\_V}_{(a,S,i)} \le 1, \sum_{i\in\mathcal{N}\backslash\mathcal{N}_1} \chi^{V\_V}_{(a,i,F)} \le 1, \forall a \in A \tag{13}$$

$$\sum_{i\in\mathcal{N}\backslash\mathcal{N}_1} \chi^{V\_Ch}_{(a,i,(k,g))} = \alpha^{Ch}_{(a,(k,g))}, \sum_{i\in\mathcal{N}\backslash\mathcal{N}_1} \chi^{Ch\_V}_{(a,(k,g),i)} = \alpha^{Ch}_{(a,(k,g))}, \forall a \in A, (k,g) \in Ch \tag{14}$$

$$\sum_{a\in A} \alpha^{Ch}_{(a,(k,g))} \le 1, \forall (k,g) \in Ch \tag{15}$$

$$\sum_{a\in A} \alpha^{Ch}_{(a,(k,g))} \le \sum_{a\in A} \alpha^{Ch}_{(a,(k,g-1))}, \forall k \in K, g \in G\backslash\{1\}, \tag{16}$$

Eqs. (11)–(16) characterize the assignment and sequencing of AGV transportation tasks and charging activities. Eq. (11) requires that each container i must be transported by exactly one AGV. Eq. (12) ensures the continuity of the operational sequence by requiring each container assigned to an AGV to have exactly one predecessor and one successor. Eq. (13) further restricts the task chain of each AGV to be continuous and unique. Eq. (14) ensures that an AGV is allowed to access a charging activity (k, g) only when it chooses that activity. Eqs. (15) and (16) further ensure that each charging activity is used uniquely and sequentially.

(3) Time-related constraints

These constraints involve temporal factors and define the scheduling relationships between container operations and AGV charging tasks to avoid potential conflicts or time overlaps.

$$\overline{\tau}^{RC}_{(r',j)} + M_T(2 - \alpha^{RC}_{(r,i)} - \alpha^{RC}_{(r',j)}) \geq \underline{\tau}^{RC}_{(r,i)} + h^{RC}_{saf} \cdot t^{RC}_1, \forall r, r' \in R_l, r \neq r', l \in L, (i,j) \in H^{RC} \tag{17}$$

$$\overline{\tau}^{RC}_{(r,j)} + M_T\left(1 - \beta^{RC}_{(r,i,j)}\right) \geq \underline{\tau}^{RC}_{(r,i)} + s^{RC}_{(i,j)}, \forall r \in R_l, i, j \in \mathcal{N}^{RB}_l, i \neq j, l \in L \tag{18}$$

$$\overline{\tau}^{YC}_{(y',j)} + M_T(2 - \alpha^{YC}_{(y,i)} - \alpha^{YC}_{(y',j)}) \geq \underline{\tau}^{YC}_{(y,i)} + h^{YC}_{saf} \cdot t^{YC}_1, \forall y, y' \in Y_b, y \neq y', b \in B, (i,j) \in H^{YC} \tag{19}$$

$$\overline{\tau}^{YC}_{(y,j)} + M_T\left(1 - \beta^{YC}_{(y,i,j)}\right) \geq \underline{\tau}^{YC}_{(y,i)} + s^{YC}_{(i,j)}, \forall y \in Y_b, i, j \in \mathcal{N}^{YB}_b, i \neq j, b \in B \tag{20}$$

$$\overline{\tau}^{QC}_{(q,j)} + M_T\left(1 - \delta^{QC}_{(q,i,j)}\right) \geq \underline{\tau}^{QC}_{(q,i)} + s^{QC}, \forall i, j \in \mathcal{N}^{QC}_q, i \neq j, q \in Q \tag{21}$$

For RC operations, Eq. (17) ensures that RCs working in the same railway block satisfy the required safety separation (measured in bay units). Eq. (18) guarantees that when the same RC consecutively handles two containers, the time interval between the tasks must satisfy the required movement and setup time. For YC operations, Eqs. (19) and (20) enforce temporal requirements that are analogous to the safety-distance and sequencing rules described in Eqs. (17) and (18). For QC operations, Eq. (21) ensures that two consecutive container tasks handled by the same QC have sufficient repositioning and setup time.

$$\overline{\tau}^{AGV}_{(a,j)} + M_T\left(3 - \delta^{QC}_{(q,i,j)} - \alpha^{AGV}_{(a,i)} - \alpha^{AGV}_{(a,j)}\right) \geq \underline{\tau}^{AGV}_{(a,i)}, \forall i, j \in \mathcal{N}^{QC}_q, i \neq j, q \in Q, a \in A \tag{22}$$

$$\overline{\tau}^{AGV}_{(a,j)} + M_T\left(1 - \chi^{V\_V}_{(a,i,j)}\right) \geq \underline{\tau}^{AGV}_{(a,i)} + t^{AGV}_{(i,j)}, \forall i, j \in \mathcal{N} \backslash \mathcal{N}_1, i \neq j, a \in A \tag{23}$$

$$\overline{\tau}^{Ch}_{(a,(k,g))} + M_T\left(1 - \chi^{V\_Ch}_{(a,i,(k,g))}\right) \geq \underline{\tau}^{AGV}_{(a,i)} + t^{V\_Ch}_{(i,k)}, \forall i \in \mathcal{N} \backslash \mathcal{N}_1, (k,g) \in Ch, a \in A \tag{24}$$

$$\overline{\tau}^{AGV}_{(a,i)} + M_T\left(1 - \chi^{Ch\_V}_{(a,(k,g),i)}\right) \geq \overline{\tau}^{Ch}_{(a,(k,g))} + \tau^{Ch\_dur}_{(k,g)} + t^{Ch\_V}_{(k,i)}, \forall i \in \mathcal{N} \backslash \mathcal{N}_1, (k,g) \in Ch, a \in A \tag{25}$$

For AGV transport and charging operations, Eq. (22) ensures that AGV transportation tasks must follow the QC processing sequence. Eqs. (23)–(25) collectively ensure the temporal continuity of AGV operations by enforcing the required time intervals between any two consecutive tasks. Specifically, Eq. (23) handles the case of two consecutive transport tasks, Eq. (24) covers a transport task followed by a charging activity, and Eq. (25) addresses a charging activity followed by a transport task.

$$\overline{\tau}^{Ch}_{(a,(k,g))} + M_T(2 - \alpha^{Ch}_{(a',(k,g-1))} - \alpha^{Ch}_{(a,(k,g))}) \geq \overline{\tau}^{Ch}_{(a',(k,g-1))} + \tau^{Ch\_dur}_{(k,g)}, \forall k \in K, g \in G \backslash \{1\}, a, a' \in A \tag{26}$$

Eq. (26) enforces the temporal ordering of charging events at the same charging facility.

$$\begin{cases} \overline{\tau}^{AGV}_{(a,i)} \lambda_i + \underline{\tau}^{AGV}_{(a,i)}(1 - \lambda_i) + M_T(2 - \alpha^{AGV}_{(a,i)} - \alpha^{RC}_{(r,i)}) \geq \overline{\tau}^{RC}_{(r,i)} + p^{RC}_i \lambda_i + \theta^{RC}(1 - \lambda_i) \\ \underline{\tau}^{RC}_{(r,i)} + M_T(2 - \alpha^{AGV}_{(a,i)} - \alpha^{RC}_{(r,i)}) \geq (\overline{\tau}^{AGV}_{(a,i)} + \theta^{RC})\lambda_i + (\underline{\tau}^{AGV}_{(v,i)} + p^{RC}_i)(1 - \lambda_i) \end{cases}, \begin{matrix} \forall i \in \mathcal{N} \setminus (\mathcal{N}_1 \cup \mathcal{N}_6) \\ a \in A,\ r \in R \end{matrix} \tag{27}$$

$$\begin{cases} \overline{\tau}^{AGV}_{(a,i)} \lambda_i + \underline{\tau}^{AGV}_{(a,i)}(1 - \lambda_i) + M_T(2 - \alpha^{AGV}_{(a,i)} - \alpha^{YC}_{(y,i)}) \geq \overline{\tau}^{YC}_{(y,i)} + p^{YC}_i \lambda_i + \theta^{YC}(1 - \lambda_i) \\ \underline{\tau}^{YC}_{(y,i)} + M_T(2 - \alpha^{AGV}_{(a,i)} - \alpha^{YC}_{(y,i)}) \geq (\overline{\tau}^{AGV}_{(a,i)} + \theta^{YC})\lambda_i + (\underline{\tau}^{AGV}_{(v,i)} + p^{YC}_i)(1 - \lambda_i) \end{cases}, \begin{matrix} \forall i \in \mathcal{N}_2 \cup \mathcal{N}_3 \cup \mathcal{N}_6 \\ a \in A,\ y \in Y \end{matrix} \tag{28}$$

$$\begin{cases} \overline{\tau}^{AGV}_{(a,i)} \lambda_i + \underline{\tau}^{AGV}_{(a,i)}(1 - \lambda_i) + M_T(2 - \alpha^{AGV}_{(a,i)} - \sigma^{QC}_{(q,i)}) \geq \overline{\tau}^{QC}_{(q,i)} + p^{QC} \lambda_i + \theta^{QC}(1 - \lambda_i) \\ \underline{\tau}^{QC}_{(q,i)} + M_T(2 - \alpha^{AGV}_{(a,i)} - \sigma^{QC}_{(q,i)}) \geq (\overline{\tau}^{AGV}_{(a,i)} + \theta^{QC})\lambda_i + (\underline{\tau}^{AGV}_{(a,i)} + p^{QC})(1 - \lambda_i) \end{cases}, \begin{matrix} \forall i \in \mathcal{N}_4 \cup \mathcal{N}_5 \cup \mathcal{N}_6 \\ a \in A,\ q \in Q \end{matrix} \tag{29}$$

Eqs. (27)–(29) characterize the temporal coupling between RC/YC/QC operations and AGV transportation. Following the unification strategy adopted by Xing et al. (2025), the parameter λ_i serves to distinguish whether a container operation is followed by an AGV task ($\lambda_i = 1$) or preceded by one ($\lambda_i = 0$), which enables a unified representation of the temporal interaction among RC/YC/QC equipment and AGVs.

$$\overline{\tau}^{RC}_{(r,i)}\mu_i + \overline{\tau}^{YC}_{(y,i)}(1-\mu_i) + M_T(3-\alpha^{AGV}_{(a,i)} - \alpha^{RC}_{(r,i)} - \alpha^{YC}_{(y,i)}) \geq \underline{\tau}^{YC}_{(y,i)}\mu_i + \underline{\tau}^{RC}_{(r,i)}(1-\mu_i) + t^{AGV}_i, \quad \forall i \in \mathcal{N}_2 \cup \mathcal{N}_3, a \in A, y \in Y, r \in R \tag{30}$$

$$\overline{\tau}^{RC}_{(r,i)}\mu_i + \overline{\tau}^{QC}_{(q,i)}(1-\mu_i) + M_T(3-\alpha^{AGV}_{(a,i)} - \alpha^{RC}_{(r,i)} - \sigma^{QC}_{(q,i)}) \geq \underline{\tau}^{QC}_{(q,i)}\mu_i + \underline{\tau}^{RC}_{(r,i)}(1-\mu_i) + t^{AGV}_i, \quad \forall i \in \mathcal{N}_4 \cup \mathcal{N}_5, a \in A, q \in Q, r \in R \tag{31}$$

$$\overline{\tau}^{YC}_{(y,i)}\mu_i + \overline{\tau}^{QC}_{(q,i)}(1-\mu_i) + M_T(3-\alpha^{AGV}_{(a,i)} - \alpha^{YC}_{(y,i)} - \sigma^{QC}_{(q,i)}) \geq \underline{\tau}^{QC}_{(q,i)}\mu_i + \underline{\tau}^{YC}_{(y,i)}(1-\mu_i) + t^{AGV}_i, \quad \forall i \in \mathcal{N}_6, a \in A, q \in Q, y \in Y \tag{32}$$

Eqs. (30)–(32) further describe the coordinated sequencing of multiple facilities under the import and export flows. The parameter μ_i distinguishes import containers ($\mu_i = 1$) from export containers ($\mu_i = 0$), enabling these constraints to consistently enforce the temporal coordination among RC, YC, QC, and AGV operations within a unified framework for different container flows.

(4) Energy-related constraints

The following constraints characterize the battery update dynamics of the AGVs.

$$\overline{\varepsilon}^{AGV}_{(a,i)} + M_E\left(\chi^{V\_V}_{(a,S,i)} - 1\right) \leq E^{Ini}_a, \forall a \in A, i \in \mathcal{N}\backslash\mathcal{N}_1 \tag{33}$$

$$\underline{\varepsilon}^{AGV}_{(a,i)} + M_E(\alpha^{AGV}_{(a,i)} - 1) \leq \overline{\varepsilon}^{AGV}_{(a,i)} - e^{AGV}_i - \eta^{AGV}_{wait}\left(\underline{\tau}^{AGV}_{(a,i)} - \overline{\tau}^{AGV}_{(a,i)} - t^{AGV}_i\right), \forall a \in A, i \in \mathcal{N} \setminus \mathcal{N}_1 \tag{34}$$

$$\underline{\varepsilon}^{AGV}_{(a,i)} + M_E(1-\alpha^{AGV}_{(a,i)}) \geq O_{min}E^{All}, \forall a \in A, i \in \mathcal{N} \setminus \mathcal{N}_1 \tag{35}$$

$$\overline{\varepsilon}^{Ch}_{(a,(k,g))} + \eta_{Ch}\tau^{Ch\_dur}_{(k,g)} + M_E(1-\alpha^{Ch}_{(a,(k,g))}) \geq O_{min}E^{All}, \forall a \in A, (k,g) \in Ch \tag{36}$$

$$\overline{\varepsilon}^{Ch}_{(a,(k,g))} + \eta_{Ch}\tau^{Ch\_dur}_{(k,g)} + M_E(\alpha^{Ch}_{(a,(k,g))} - 1) \leq O_{max}E^{All}, \forall a \in A, (k,g) \in Ch \tag{37}$$

Eq. (33) specifies the available initial battery level of each AGV. Eqs. (34) and (35) characterize the remaining battery level after an AGV completes a transport task and ensure that the minimum energy requirement is satisfied. Eqs. (36) and (37) impose that the battery level after a charging activity fall within the allowable range.

$$\overline{\varepsilon}^{AGV}_{(a,j)} + M_E(\chi^{V\_V}_{(a,i,j)} - 1) \leq \underline{\varepsilon}^{AGV}_{(a,i)} - e^{AGV}_{(i,j)}, \forall a \in A, i, j \in \mathcal{N} \setminus \mathcal{N}_1, i \neq j \tag{38}$$

$$\overline{\varepsilon}^{Ch}_{(a,(k,g))} + M_E(\chi^{V\_Ch}_{(a,i,(k,g))} - 1) \leq \underline{\varepsilon}_{(a,i)} - e^{V\_Ch}_{(i,k)}, \forall a \in A, i \in \mathcal{N} \setminus \mathcal{N}_1, (k,g) \in Ch \tag{39}$$

$$\overline{\varepsilon}^{AGV}_{(a,i)} + M_E(\chi^{Ch\_V}_{(a,(k,g),i)} - 1) \leq \overline{\varepsilon}^{Ch}_{(a,(k,g))} + \eta_{Ch}\tau^{Ch\_dur}_{(k,g)} - e^{Ch\_V}_{(k,i)}, \forall a \in A, i \in \mathcal{N} \setminus \mathcal{N}_1, (k,g) \in Ch \tag{40}$$

Eqs. (38)–(40) further ensure that, when an AGV performs consecutive tasks or moves from a charging point to the next task location, the update of its remaining battery level correctly reflects both the travel energy consumption and the charging gain.

(5) Domain of variables

$$\alpha^{RC}_{(r,i)}, \alpha^{YC}_{(y,i)}, \alpha^{AGV}_{(a,i)}, \alpha^{Ch}_{(a,(k,g))}, \beta^{RC}_{(r,i,j)}, \beta^{YC}_{(y,i,j)}, \chi^{V\_V}_{(a,i,j)}, \chi^{V\_Ch}_{(a,i,(k,g))}, \chi^{Ch\_V}_{(a,(k,g),i)} \in [0,1], \quad \forall i, j \in \mathcal{N}, r \in R, y \in Y, a \in A, (k,g) \in Ch \tag{41}$$

$$\overline{\tau}^{RC}_{(r,i,)}, \underline{\tau}^{RC}_{(r,i)}, \overline{\tau}^{YC}_{(y,i)}, \underline{\tau}^{YC}_{(y,i)}, \overline{\tau}^{QC}_{(q,i)}, \underline{\tau}^{QC}_{(q,i)}, \overline{\tau}^{AGV}_{(v,i)}, \underline{\tau}^{AGV}_{(a,i)}, \overline{\tau}^{Ch}_{(a,(k,g))}, \tau^{Ch\_dur}_{(k,g)} \geq 0, \quad \forall i \in \mathcal{N}, r \in R, y \in Y, q \in Q, a \in A, (k,g) \in Ch \tag{42}$$

$$\overline{\varepsilon}^{AGV}_{(a,i)}, \underline{\varepsilon}^{AGV}_{(a,i)}, \overline{\varepsilon}^{Ch}_{(a,(k,g))} \in \left[0, E^{All}\right], \forall a \in A, i \in \mathcal{N}, (k,g) \in Ch \tag{43}$$

In this model, sequence-related variables are formulated as binary, while variables associated with time and energy consumption are treated as continuous. The corresponding constraints are specified in Eqs. (41)–(43).

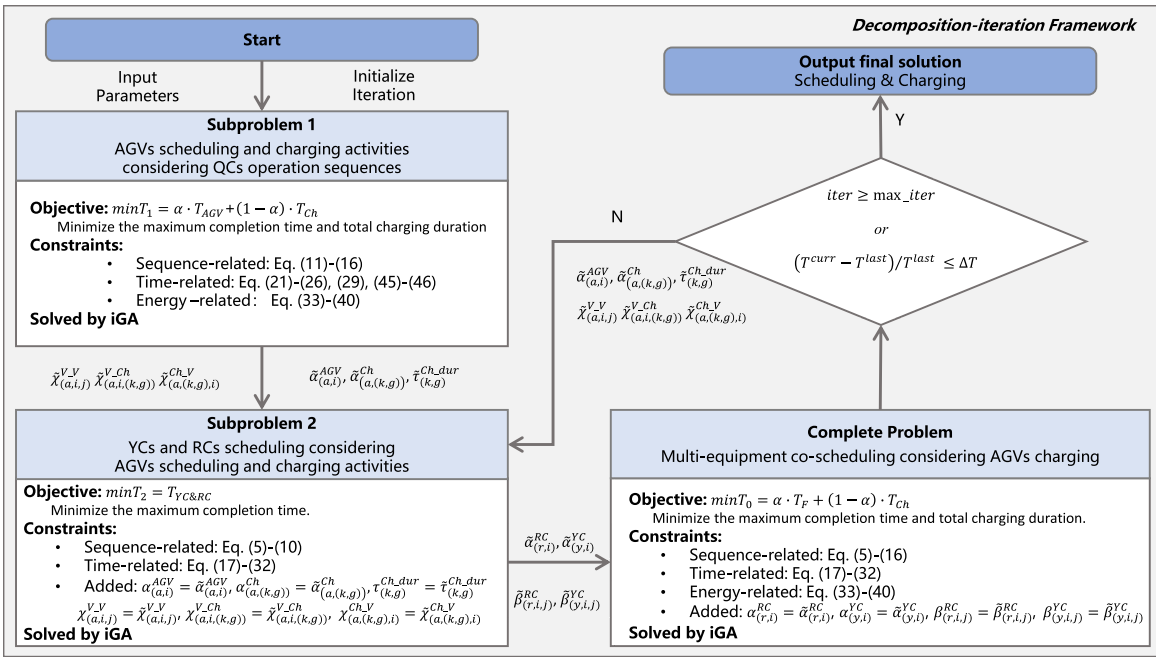

Fig. 5. Logical diagram of the decomposition-iteration framework operation.

4. Solution approach

As described in Section 3.3, the proposed mathematical model is formulated as a MIP model incorporating sequence-, time-, and energy-related constraints. The decision variables involve not only multi-equipment co-scheduling but also the timing, location, and duration of AGV charging, resulting in many strongly coupled variables and making the problem difficult to solve directly. Drawing inspiration from a related study (Wang et al., 2023a), where a bi-level optimization framework is applied to coordinate logistics and energy management through problem decomposition, this study adopts a similar strategy. Specifically, the original integrated scheduling problem with AGV charging is decomposed into two inter-related subproblems within a Decomposition-Iteration framework, and a Decomposition-Iteration-based Improved Genetic Algorithm (DI-iGA) is formulated to effectively address the problem.

Accordingly, Section 4.1 introduces the Decomposition-Iteration framework, including the design of Subproblem 1, Subproblem 2, and the iteration and termination conditions. Section 4.2 elaborates on the Improved Genetic Algorithm. Section 4.3 describes the design of a DT-based hybrid rescheduling mechanism for dynamic disturbance response, which supports the real-time adaptability of the overall scheduling framework.

4.1. Decomposition-iteration framework

For small-scale instances, this problem can be directly solved using Gurobi. However, for large-scale instances, owing to the complex and computation-intensive nature of the problem, Gurobi often cannot obtain a feasible solution within the limited solution time (1 h). Therefore, to enhance solution efficiency, this study adopts a decomposition-iteration framework that divides the overall model into two interconnected subproblems, which are optimized in an alternating fashion until near-optimality is reached.

The core decision variables in this study include task allocation and its operation sequence, operation time arrangements, and AGV charging decisions (including the timing of AGV charging, the selection of a charging facility, the start time of charging and its duration). Overall, this paper addresses multi-equipment task allocation, operation sequencing, operation time coordination, and AGV charging optimization. Due to the complex coupling relationships among these decision variables, directly solving for the global near-optimal solution entails extremely high computational complexity. Therefore, as shown in Fig. 5, a decomposition-iteration framework is employed to reduce computational complexity and improve solution efficiency.

First, subproblem 1 is constructed with the objective of minimizing the makespan and AGV charging duration. AGV task allocation, transport sequencing, charging timing, charging facility selection, and charging duration are optimized while satisfying the AGV transport order, operating time, and energy consumption constraints. The solution of Subproblem 1 is then used as input for Subproblem 2. In Subproblem 2, the task allocation and operating sequence of RCs and YCs are optimized based on the AGV transport sequence and charging decisions. However, at this point, Subproblem 2 does not consider the energy consumption of the AGV, while Subproblem 1 overlooks the AGV's energy usage during idle periods. Therefore, the task assignment and operation sequence of RCs and YCs obtained by Subproblem 2 need to be used as an input to re-optimize the complete model, incorporating energy consumption constraints and further optimizing the AGV transport sequence and charging decisions. The updated AGV transport sequence and

charging decisions are then fed back into Subproblem 2 for further iterative optimization. This iterative process continues until the iterative termination condition is satisfied, ultimately converging to a global near-optimal solution. The following sections provide detailed descriptions of Subproblem 1, Subproblem 2, and the iterative termination condition of the iterative process.

4.1.1. Subproblem 1

Subproblem 1 aims to minimize the maximum completion time and the AGV charging duration by optimizing the AGV task allocation, transportation sequence, charging timing, charging facility selection, and charging duration. In addition to considering the constraints related to the AGV and charging facilities, the container operation sequence determined by QC must also be considered to ensure the rationality of task connection. Therefore, the objective function, constraints, and decision variables of Subproblem 1 are defined as follows.

Objective function:

$$\min T_1 = \alpha \cdot T_{AGV} + (1-\alpha) \cdot T_{Ch} \tag{44}$$

where $T_{AGV} = \max_{i \in \mathcal{N} \setminus \mathcal{N}_1, a \in A} \underline{\tau}^{AGV}_{(a,i)}$ represents the makespan of AGV operations, $T_{Ch} = \sum_{(k,g) \in Ch} \tau^{Ch\_dur}_{(k,g)}$ denotes the total AGV charging time.

Constraints:

(1) Sequence-related constraints:

Eqs. (11)–(16) ensure that AGV transportation and charging activities meet the relevant sequence constraints.

(2) Time-related constraints:

In Subproblem 1, only AGV transport tasks are considered, and the constraints on the start and completion times ensure that the AGV operations match the QC operation sequence. However, in the complete model, the start and completion times of AGV operations must also satisfy synchronization constraints with RC and YC operations. Thus, the constraints of the complete model cannot be directly used in Subproblem 1, and the time-related constraints need to be redefined to ensure computational efficiency. The specific time-related constraints are formulated as follows:

$$\underline{\tau}^{AGV}_{(a,i)} + M_T(1-\alpha^{AGV}_{(a,i)}) \geq \overline{\tau}^{AGV}_{(a,i)} + t^{AGV}_i, \forall a \in A, i \in \mathcal{N}_2 \cup \mathcal{N}_3 \tag{45}$$

$$\underline{\tau}^{AGV}_{(a,i)}\mu_i + \overline{\tau}^{QC}_{(q,i)}(1-\mu_i) + M_T(2-\alpha^{AGV}_{(a,i)} - \sigma^{QC}_{(q,i)}) \geq \underline{\tau}^{QC}_{(q,i)}\mu_i + \overline{\tau}^{AGV}_{(a,i)}(1-\mu_i) + t^{AGV}_i, \forall a \in A, q \in Q, i \in \mathcal{N}_4 \cup \mathcal{N}_5 \cup \mathcal{N}_6 \tag{46}$$

For containers belonging to the 2nd and 3rd container flows, the AGV transportation process only involves interactive operations with RCs and YCs. Since Subproblem 1 does not consider the scheduling of RCs and YCs, Eq. (45) is applied to constrain the start and completion times of the AGV transportation task for these flows. For containers in the 4th, 5th, and 6th container flows, their AGV transportation process require interactive operations with both RC/YC and QC. Accordingly, in addition to the original QC-AGV synchronization constraint (Eq. (29)) in the complete model, Subproblem 1 introduces the supplementary constraint (Eq. (46)) to exclude the influence of RC/YC interaction that are not modeled in this subproblem. Together, these two constraints determine the feasible start and completion times of AGV transportation for the 4th-6th container flows.

In addition, Subproblem 1 also retains the time-related constraints in Eqs. (21)–(26) from the complete model. Among them, Eq. (21) ensures that the time constraints for two consecutive QC loading and unloading tasks are satisfied, while Eqs. (22)–(26) ensure that the AGV transportation and charging activities meet the time constraints, and ensure alignment with the QC operation sequence.

(3) Energy-related constraints: Eqs. (33)–(40)

Decision Variables:

$$\alpha^{AGV}_{(a,i)}, \alpha^{Ch}_{(a,(k,g))}, \chi^{V\_V}_{(a,i,j)}, \chi^{V\_Ch}_{(a,i,(k,g))}, \chi^{Ch\_V}_{(a,(k,g),i)} \in [0,1], \forall i,j \in \mathcal{N} \setminus \mathcal{N}_1, a \in A, (k,g) \in Ch \tag{47}$$

$$\overline{\tau}^{QC}_{(q,i)}, \underline{\tau}^{QC}_{(q,i)}, \overline{\tau}^{AGV}_{(a,i)}, \underline{\tau}^{AGV}_{(a,i)}, \overline{\tau}^{Ch}_{(a,(k,g))}, \tau^{Ch\_dur}_{(k,g)} \geq 0, \forall i \in \mathcal{N} \setminus \mathcal{N}_1, q \in Q, a \in A, (k,g) \in Ch \tag{48}$$

$$\overline{\varepsilon}^{AGV}_{(a,i)}, \underline{\varepsilon}^{AGV}_{(a,i)}, \overline{\varepsilon}^{Ch}_{(a,(k,g))} \in [0, E^{All}], \forall i \in \mathcal{N} \setminus \mathcal{N}_1, a \in A, (k,g) \in Ch \tag{49}$$

The optimal solutions $\tilde{\alpha}^{AGV}_{(a,i)}, \tilde{\alpha}^{Ch}_{(a,(k,g))}, \tilde{\chi}^{V\_V}_{(a,i,j)}, \tilde{\chi}^{V\_Ch}_{(a,i,(k,g))}, \tilde{\chi}^{Ch\_V}_{(a,(k,g),i)}$ and $\tilde{\tau}^{Ch\_dur}_{(k,g)}$ obtained from the solution will be used as input data for Subproblem 2 to further optimize the task scheduling of RCs and YCs.

4.1.2. Subproblem 2

Given the pre-determined AGV task allocation, transport sequencing, and charging decisions, Subproblem 2 aims to optimize the task allocation and scheduling of RCs and YCs. The objective is to minimize the maximum completion time to enhance overall scheduling efficiency. The mathematical model is formulated as follows:

Objective function:

$$\min T_2 = T_{YC\&RC} \tag{50}$$

where $T_{YC\&RC} = \max_{i\in\mathcal{N}, r\in R, y\in Y} \left\{ \underline{\tau}^{RC}_{(r,i)}, \underline{\tau}^{YC}_{(y,i)} \right\}$ denotes the makespan, i.e., the maximum completion time among all RCs' and YCs' tasks.

Constraints:

(1) Sequence-related constraints: Eqs. (5)–(10).

(2) Time-related constraints: Eqs. (17)–(32).

(3) Added constraints:

To ensure consistency between Subproblem 1 and Subproblem 2, the following constraints are introduced:

$$\begin{aligned} &\alpha^{AGV}_{(a,i)} = \tilde{\alpha}^{AGV}_{(a,i)}, \alpha^{Ch}_{(a,(k,g))} = \tilde{\alpha}^{Ch}_{(a,(k,g))}, \tau^{Ch\_dur}_{(k,g)} = \tilde{\tau}^{Ch\_dur}_{(k,g)}, \\ &\chi^{V\_V}_{(a,i,j)} = \tilde{\chi}^{V\_V}_{(a,i,j)}, \chi^{V\_Ch}_{(a,i,(k,g))} = \tilde{\chi}^{V\_Ch}_{(a,i,(k,g))}, \chi^{Ch\_V}_{(a,(k,g),i)} = \tilde{\chi}^{Ch\_V}_{(a,(k,g),i)} \end{aligned} \quad ,\forall a \in A, i, j \in \mathcal{N} \setminus \mathcal{N}_1, (k,g) \in Ch \tag{51}$$

Decision Variables:

$$\alpha^{RC}_{(r,i)}, \alpha^{YC}_{(y,i)}, \beta^{RC}_{(r,i,j)}, \beta^{YC}_{(y,i,j)}, \forall i, j \in \mathcal{N}, r \in R, y \in Y \tag{52}$$

$$\overline{\tau}^{RC}_{(r,it)}, \underline{\tau}^{RC}_{(r,i)}, \overline{\tau}^{YC}_{(y,i)}, \underline{\tau}^{YC}_{(y,i)}, \overline{\tau}^{QC}_{(q,i)}, \underline{\tau}^{QC}_{(q,i)}, \overline{\tau}^{AGV}_{(a,i)}, \underline{\tau}^{AGV}_{(a,i)}, \overline{\tau}^{Ch}_{(a,(k,g))} \geq 0, \forall i \in \mathcal{N}, r \in R, y \in Y, q \in Q, a \in A, (k,g) \in Ch \tag{53}$$

The optimal solutions obtained for $\tilde{\alpha}^{RC}_{(r,i)}, \tilde{\alpha}^{YC}_{(y,i)}, \tilde{\beta}^{RC}_{(r,i,j)}$ and $\tilde{\beta}^{YC}_{(y,i,j)}$ serve as input data for the complete model, facilitating further optimization of the overall scheduling strategy.

4.1.3. Iteration and termination criteria

After solving Subproblem 2 and obtaining the optimized solutions $\tilde{\alpha}^{RC}_{(r,i)}, \tilde{\alpha}^{YC}_{(y,i)}, \tilde{\beta}^{RC}_{(r,i,j)}$ and $\tilde{\beta}^{YC}_{(y,i,j)}$, these results are incorporated into the complete mathematical model, where energy constraints are reintroduced for further optimization. If the termination condition is satisfied, the equipment scheduling plan and AGV charging plan are outputted. Otherwise, the complete model results $\tilde{\alpha}^{AGV}_{(a,i)}, \tilde{\alpha}^{Ch}_{(a,(k,g))}, \tilde{\chi}^{V\_V}_{(a,i,j)}, \tilde{\chi}^{V\_Ch}_{(a,i,(k,g))}, \tilde{\chi}^{Ch\_V}_{(a,(k,g),i)}$ and $\tilde{\tau}^{Ch\_dur}_{(k,g)}$ are fed back into Subproblem 2 for the next iteration.

In each iteration, the task allocation and scheduling variables of Subproblem 2 (i.e. $\tilde{\alpha}^{RC}_{(r,i)}, \tilde{\alpha}^{YC}_{(y,i)}, \tilde{\beta}^{RC}_{(r,i,j)}$ and $\tilde{\beta}^{YC}_{(y,i,j)}$) are updated based on the latest optimization results and used as inputs for the complete model. This iterative process continues until the termination condition is met.

To enhance the computational efficiency of the decomposition-iteration framework, an additional termination criterion is introduced alongside the maximum iteration limit. Specifically, the optimization process terminates when the changes in the objective function decrease to a preset threshold, i.e. $\left|T^{Curr\_iter} - T^{Last\_iter}\right| / T^{Last\_iter} \leq \Delta T$. For clarity, the overall decomposition-iteration solution process is summarized in Algorithm 1.

4.2. Improved genetic algorithm

Building upon the decomposition-iteration framework introduced in Section 4.1, this study develops an improved genetic algorithm (iGA) and embeds it as the inner evolutionary engine within the DI framework (forming the DI-iGA structure). The outer DI framework updates the coupling decisions and feasible region across subproblems, while the inner iGA performs evolutionary search within the feasible space defined by the current DI iteration and the DT-synchronized system state.

Traditional GA often suffers from slow convergence and local optimality issues when dealing with multi-objective, large-scale, and tightly constrained scheduling problems. To overcome these limitations, this study introduces several enhancements in fitness evaluation and parent selection, crossover and mutation operators, and chromosome repair mechanisms. In addition, real-time system information synchronized through the DT layer, such as AGV battery levels, equipment availability, and task execution states, is used to perform feasibility checks on the solution candidates. This ensures that individuals violating essential energy or equipment constraints are filtered out without involving DT simulation in the fitness evaluation process.

Specifically, the improvements introduced in the proposed DI-iGA can be summarized in three aspects:

First, the fitness evaluation and selection mechanisms are optimized to balance the weight of multiple objectives during optimization. This improvement enhances the algorithm's efficiency and accuracy, better handling complex scheduling constraints and avoiding the conflicts and poor convergence typically encountered in traditional GA. In addition, the DT-synchronized operational information, such as AGV battery status, equipment availability, and task feasibility, is used to validate whether each individual satisfies essential operational constraints, ensuring that infeasible solutions are removed during evolution.

Second, two key improvements are proposed for the crossover and mutation. (1) The use of a combination of ordered and structural alignment crossovers is used to ensure diversity in the scheduling sequence while enhancing local search capabilities. (2) An adaptive mechanism is introduced, where cosine and sine functions are used to dynamically adjust the crossover probability and mutation probability. This mechanism ensures extensive exploration in the early stages of the algorithm and enhances local search during the search process, thereby improving convergence and efficiency.

Algorithm 1 Decomposition-iteration framework.

Input: Parameters about container tasks, RCs, YCs, QCs, AGVs, charging facilities and layout of the SRIACT; maximum iteration limit ($\max\_iter$) thresholds for the objective function (ΔT)

Output: Optimized scheduling plan and AGV charging activities, maximum completion time, AGVs charging duration and computational time

Initialize the iteration count $iter = 0$, the termination flag $iter\_stop = Fales$, the objective function $T^{last\_iter} = 0$.
(Subproblem 1) Solve Subproblem 1 to obtain the initial AGVs task allocation, transport sequence, and charging activities ($\tilde{\alpha}^{AGV}_{(a,i)}$, $\tilde{\alpha}^{Ch}_{(a,(k,g))}$, $\tilde{\chi}^{V\_V}_{(a,i,j)}$, $\tilde{\chi}^{V\_Ch}_{(a,i,(k,g))}$, $\tilde{\chi}^{Ch\_V}_{(a,(k,g),i)}$ and $\tilde{\tau}^{Ch\_dur}_{(k,g)}$).
(Subproblem 2) Solve Subproblem 2 based on the results of Subproblem 1 and obtain the optimized task allocation and sequencing of RCs and YCs ($\tilde{\alpha}^{RC}_{(r,i)}$, $\tilde{\alpha}^{YC}_{(y,i)}$, $\tilde{\beta}^{RC}_{(r,i,j)}$ and $\tilde{\beta}^{YC}_{(y,i,j)}$).
while $iter < \max\_iter$ and $iter\_stop = Fales$ **do**
  (Complete Model) Solve the complete model based on the results from Subproblem 2.
  Obtain updated AGV decisions: ($\tilde{\alpha}^{AGV}_{(a,i)}$, $\tilde{\alpha}^{Ch}_{(a,(k,g))}$, $\tilde{\chi}^{V\_V}_{(a,i,j)}$, $\tilde{\chi}^{V\_Ch}_{(a,i,(k,g))}$, $\tilde{\chi}^{Ch\_V}_{(a,(k,g),i)}$ and $\tilde{\tau}^{Ch\_dur}_{(k,g)}$), the maximum completion time T_F, the charging time T_{Ch} and the objective function T.
  if $\left|T - T^{last\_iter}\right| / T^{last\_iter} \le \Delta T$ **then**
    $iter\_stop = True$
  end if
  if $iter \ge \max\_iter$ or $iter\_stop = True$ **then**
    Output final scheduling plan and AGV charging activities.
    Break
  else
    $iter += 1$ and $T^{last\_iter} = T$
    (Subproblem 2 update) Update Subproblem2's input according to the latest AGV decisions.
    Solve Subproblem 2 again to obtain the updated RC/YC allocations ($\tilde{\alpha}^{RC}_{(r,i)}$, $\tilde{\alpha}^{YC}_{(y,i)}$, $\tilde{\beta}^{RC}_{(r,i,j)}$ and $\tilde{\beta}^{YC}_{(y,i,j)}$).
    Continue iteration.
  end if
end while
return Final optimized solution (scheduling plan & AGV charging activities)

Finally, two types of chromosome repair mechanisms are designed: one for charging facilities and times to satisfy energy constraints, and the other for equipment allocation and task sequencing to meet operational order constraints. These mechanisms effectively prevent the generation of infeasible solutions, ensuring that the offspring remain within the feasible solution space. Together, these repair procedures effectively eliminate infeasible individuals and ensure that the offspring remain within the feasible solution space defined by the DI iteration, with their feasibility validated against the DT-synchronized system state.

With these improvements, the proposed iGA efficiently finds better solutions for the complex multi-equipment collaborative scheduling problem, while avoiding the slow convergence and local optimality issues typical of traditional GA in high-dimensional solution spaces. At the same time, embedding iGA into the DI framework enables the algorithm to adapt to the dynamically updated feasible region and virtual-physical system state.

4.2.1. Encoding and decoding

Based on the characteristics of Subproblem 1, Subproblem 2, and the complete problem, different chromosome structures are designed in this study to ensure that the solutions for each subproblem and the complete problem meet the corresponding operational constraints and task requirements. These problem-structured encodings provide the basis for enforcing the multi-equipment coupling embedded in the mathematical model. Moreover, unlike traditional quay-yard automated terminals in which each AGV is required to follow a strict double-cycling constraint (i.e., executing an import task immediately followed by an export task), the SRIACT considered in this study operates across three functional regions. As a result, AGVs naturally exhibit more flexible multi-stage circulation patterns. To accommodate this operational characteristic, no mandatory import-export pairing is imposed in the encoding design. Instead, the chromosome directly follows the transport sequence produced by the DI framework, ensuring that AGV operations remain feasible with respect to equipment precedence and energy constraints without restricting the feasible region by forced double-cycling.

(1) Encoding and decoding for Subproblem 1

For Subproblem 1, a four-row chromosome with $|\mathcal{N}|$-column is designed, where $|\mathcal{N}|$ denotes the total number of containers. The first row represents the sequence of container tasks; the second row assigns an AGV to each container, specifying the transportation task and its execution order; the third row indicates whether the AGV requires charging after completing the transportation task for the corresponding container, where 0 denotes no charging and a positive integer corresponds to the assigned charging facility; the fourth row specifies the charging duration, with values in the range $(0, 1]$, where 1 represents the time required to fully charge the battery from 0% to 100%.

Considering that the QC has a fixed operational sequence, the AGV task assignment must account for these constraints to improve efficiency. Specifically, containers handled by the same AGV must be scheduled in a way that the transportation sequence aligns with the QC's operational order.

Fig. 6 illustrates an example of the chromosome representation, which contains 10 containers, 2 AGVs and 1 charging facility. Assume the operational sequences of QC 1 and QC 2 are $\{8, 9, 7\}$ and $\{6, 10\}$, respectively. As shown in Fig. 6(a), the initial assignment assigns containers 7 and 8 to AGV 2, but their transportation order does not satisfy the operation order of QC 1. Therefore, the positions

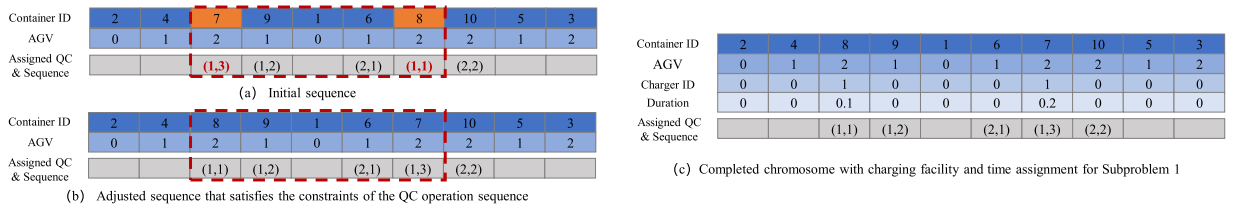

Fig. 6. Chromosome representation for Subproblem 1.

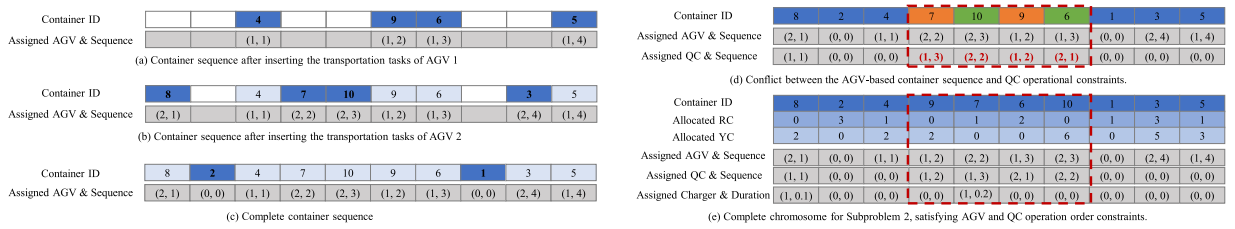

Fig. 7. Chromosome representation for Subproblem 2.

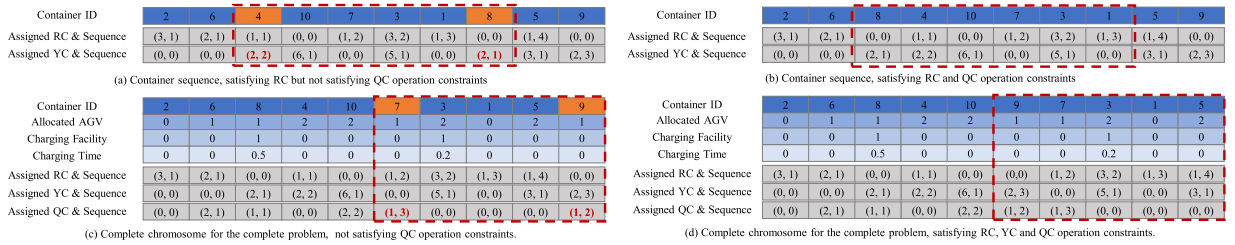

Fig. 8. Chromosome representation for complete problem.

of these containers need to be adjusted to meet the operation constraints, as shown in Fig. 6(b). After supplementing the chromosome with charging facility assignments and charging durations, a complete chromosome structure is formed, as illustrated in Fig. 6(c).

A detailed example based on AGV 2 is as follows: it first transports Container 8, then proceeds to Charging Facility 1 for charging, with a charging duration of $0.1 \times \tau^{Ch}_{0-100\%}$. After charging, AGV 2 continues with the transportation of Container 7, followed by Container 10. After completing Container 10, AGV 2 returns to Charging Facility 1 for another charging lasting $0.2 \times \tau^{Ch}_{0-100\%}$. Finally, it executes the transportation task for Container 3. The same process applies to other AGVs.

The entire initial population is generated by repeatedly constructing chromosomes following the above procedure, where chromosomes are created based on the attributes of containers until the predefined population size is reached.

(2) Encoding and decoding for Subproblem 2

For Subproblem 2, a three-row and $|\mathcal{N}|$-column chromosome is structured. The first row represents the randomly generated container task sequence, which dictates the order of transportation tasks. The second row assigns the RC to each container, where a value of 0 corresponds to containers in the 4th, 5th or 6th flow that do not require RC operations. The third row represents the YC assignment, in which 0 indicates containers from 1st, 4th or 5th flow that do not require YC operations.

Because AGV task assignments and execution sequences are predetermined by Subproblem 1 (or the complete model), the chromosome for Subproblem 2 is initialized by inserting container tasks according to the AGV execution order. Assume that Fig. 6(c) represents the solution to Subproblem 1; the corresponding construction process for Subproblem 2 is illustrated in Fig. 7(a)–(c).

However, as shown in Fig. 7(d), the initial sequence may violate the processing sequence constraints of QCs. To ensure feasibility, the container sequence is adjusted to match the predefined QC processing requirements. After this alignment and equipment assignment correction, the final feasible chromosome for Subproblem 2 is obtained, as illustrated in Fig. 7(e).

(3) Encoding and decoding of the complete problem

The chromosome for the complete problem adopts the same four-row structure as in Subproblem 1, while incorporating the RC and YC task sequences extracted from Subproblem 2. As shown in Fig. 10, the RC-based container sequences are first inserted into the chromosome according to the order of RC 1 to RC $|R|$, after which the remaining containers (those not requiring RC operations) are placed in the remaining positions.

Because the RC and YC sequences jointly constrain the feasible container order, the initial chromosome may violate YC precedence constraints. Therefore, an adjustment step is applied to realign the container sequence with the YC operational order obtained from Subproblem 2. This produces the intermediate chromosome shown in Fig. 8(b).

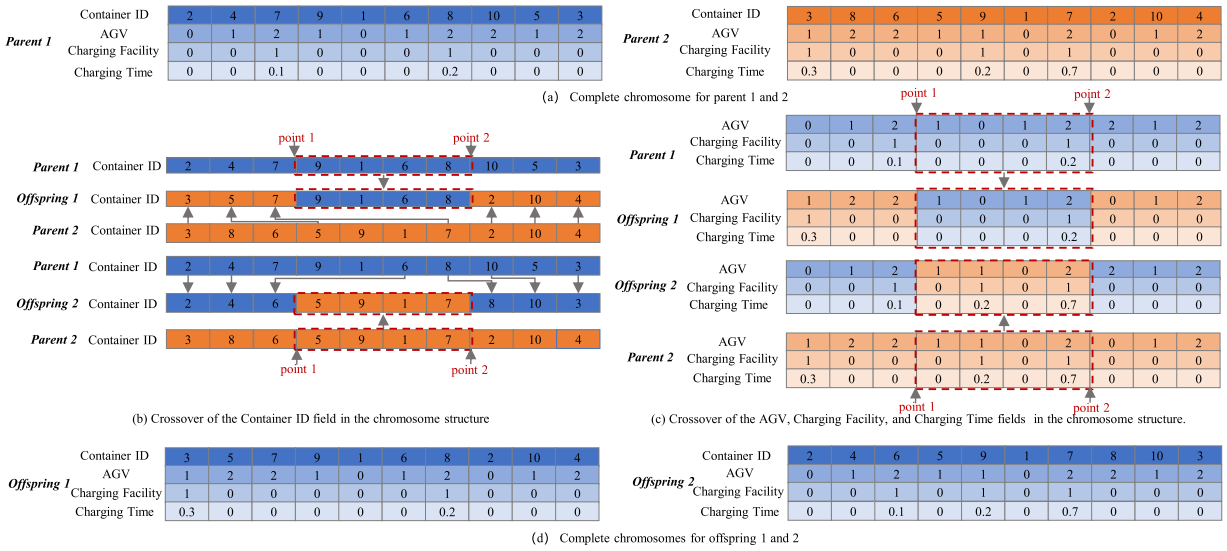

Fig. 9. An illustration of the crossover operator.

Next, AGV assignments, charging equipment and duration are filled in according to the type of container flow, generating the structure shown in Fig. 8(c). Since QC sequencing constraints must also be satisfied at the complete-model level, a final correction is performed to ensure that the container sequence simultaneously respects RC, YC, and QC task-precedence rules, resulting in the feasible chromosome shown in Fig. 8(d).

After these adjustments, each container has a consistent assignment of RC/YC equipment, AGV transport sequence, and charging strategy. The resulting chromosome satisfies all sequencing and energy-related constraints defined in Eqs. (5)–(35). During initial population generation, the same encoding logic is applied, followed by a charging-field repair step to guarantee the feasibility of charging-facility choices and durations (see Section 4.2.4).

4.2.2. Fitness evaluation and parent select operation

For each individual p, the fitness value is determined by a fitness evaluation function that reflects how well the individual aligns with the optimization objectives. Since the goal of this study is to minimize the maximum completion time and AGVs' total charging time, the fitness value is inversely related to the objective function. Therefore, the fitness function is defined as $f_p = 1/T_p$, ensuring that individuals with lower T (i.e. better performance) receive higher fitness values, thereby guiding the evolutionary process toward optimal solutions.

A parent selection mechanism identifies candidate individuals from the existing population to produce the offspring of the next generation. In this study, a tournament selection strategy with an embedded elimination mechanism is adopted. Compared to standard tournament selection, the proposed method enhances global search capability and avoids premature convergence by excluding the bottom 10% of low-quality individuals based on fitness values. The remaining individuals are then included in the tournament selection process.

4.2.3. Crossover and mutation operations

In the crossover operation, a differentiated strategy is applied to maintain the structural diversity of chromosomes while ensuring the consistency of coupled fields. Specifically, for all chromosome structures, whether for Subproblem 1, Subproblem 2, or the complete problem, the first row, representing the operation sequence (i.e., Container ID), is processed using Order Crossover (OX). This ensures diversity in transportation task sequences and the uniqueness of genes. For the remaining fields, such as equipment allocation (AGV, RC, YC), charging facility assignment, and charging time, a two-point crossover strategy is employed. The overall logic of the crossover operation is illustrated in Fig. 9, with the chromosome structure of Subproblem 1 used as an example to demonstrate the integration of order crossover and two-point crossover.

In the mutation operation, a mutation operator based on the 2-opt strategy (Slama et al., 2021) is adopted to enhance population diversity and avoid premature convergence. Specifically, a pair of positions is randomly selected from the chromosome, and the corresponding segment is reversed to generate a new gene sequence. This mutation operation helps to explore the solution space more effectively and prevents the algorithm from getting trapped in local optima. The mutation procedure is illustrated in Fig. 10.

To maintain population diversity in the early stage and promote solution refinement in the later stage, this study employs a triangular adaptive strategy to dynamically adjust the crossover probability (ϖ_c), and the mutation probability (ϖ_m), inspired by Chai et al. (2022) and Gupta and Deep (2019). This approach utilizes cosine and sine functions to adaptively adjust the probabilities according to the difference between the average fitness of an individual and that of the population, allowing the algorithm to explore broadly during early iterations and intensify local exploitation as the search progresses.

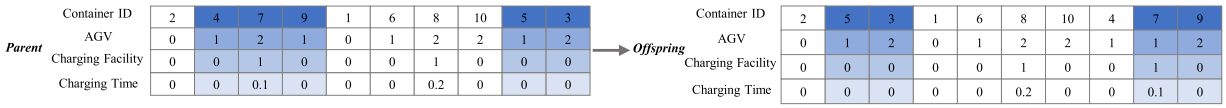

Fig. 10. An illustration of the mutation operator.

Let $\varpi_c^{'}$and $\varpi_m^{'}$ represent the baseline crossover and mutation probabilities, f_p denote the fitness value of the current individual, and f_{avg}, $f_{\max}$, and $f_{\min}$ represent the average, maximum, and minimum fitness of the current population, respectively. Both crossover and mutation probabilities vary within specified intervals, namely $\left[\varpi_{c\_\min}, \varpi_{c\_\max}\right]$ and $\left[\varpi_{m\_\min}, \varpi_{m\_\max}\right]$, respectively. The crossover probability is adjusted as follows:

If the individual's fitness $f_p < f_{avg}$, the crossover probability is increased using a cosine function: =

$$\varpi_c = \varpi_c^{'} + \left(\varpi_{c\_\max} - \varpi_c^{'}\right) \cdot \cos\left(\frac{f_{agv} - f_p}{f_{agv} - f_{\min}} \cdot \frac{\pi}{2}\right) \tag{54}$$

If $f_p \geq f_{avg}$, the crossover probability is increased using a cosine function:

$$\varpi_c = \varpi_c^{'} - \left(\varpi_c^{'} - \varpi_{c\_\min}^{'}\right) \cdot \sin\left(\frac{f_p - f_{agv}}{f_{\max} - f_{avg}} \cdot \frac{\pi}{2}\right) \tag{55}$$

A similar symmetrical structure is applied to the mutation probability ϖ_m, ensuring that both operators adapt to the evolving population dynamics.

This adaptive mechanism effectively prevents premature convergence and improves local search performance in the later stages. As a result, it strengthens the robustness and global optimization capability of the algorithm in solving the multi-equipment scheduling and AGV charging coordination problem.

4.2.4. Chromosome repair

To ensure the generated chromosomes meet energy constraints and the rationality of charging requirements, several chromosome repair mechanisms are designed. After the initial population is generated for Subproblem 1 and the complete problem, as well as following crossover and mutation operations, the charging facility and charging time fields in the chromosomes must be repaired. This repair process ensures the validity of the chromosome's charging facility assignment and charging time settings while satisfying the battery charging-related constraints.

Moreover, regarding the task order constraints, repair methods have been designed for different subproblems. Specifically, for Subproblem 1, the repair process after crossover and mutation follows the adjustment logic described in Section 4.2.1 (1); for Subproblem 2, it follows the logic presented in Section 4.2.1 (2); and for the complete problem, task order adjustments are made based on the integrated logic in Section 4.2.1 (3). These mechanisms guarantee the validity of device allocation and task order, ensuring that the generated individuals adhere to all constraints within the feasible solution space.

4.2.5. Algorithm stopping rules

The stopping criteria for the algorithm in this paper are based on two conditions, and the algorithm stopping when either condition is met: first, the iteration limit, where the algorithm terminates upon reaching the preset maximum number of iterations; second, the convergence condition, where the algorithm stops once the improvement in the objective value becomes negligible relative to the preset threshold.

4.3. A DT-based hybrid rescheduling framework with integrated AGV status and charging conflict resolution

The operating environment of the SRIACT is highly complex, where scheduling systems are frequently disrupted by transportation delays, equipment state fluctuations, and uncertainties in AGV charging behavior. While the multi-equipment cooperative scheduling model presented in Section 3 and the DI-iGA introduced in Sections 4.1 and 4.2 exhibit strong optimization performance under static conditions, they are not inherently capable of handling real-time disturbances arising in actual terminal operations. These dynamics necessitate an enhanced mechanism capable of continuously sensing operational states and adapting scheduling decisions accordingly.

To this end, this study embeds the scheduling model and DI-iGA algorithm within a DT-enhanced hybrid rescheduling framework, which provides the necessary virtual-physical linkage and dynamic adaptiveness. The fundamental DT modeling mechanisms, including virtual-physical operation mapping, state synchronization, and disturbance-detection workflow, have been comprehensively established in our previous DT research (Li et al., 2025a). Building upon this foundation, the present study extends the DT architecture by embedding AGV status monitoring, battery-level tracking, and charging-conflict resolution into the rescheduling workflow. This framework combines global and local as well as proactive and reactive rescheduling strategies, enabling flexible scheduling responses under virtual-physical fusion.

To operationalize this DT-based framework, the virtual model must first remain consistently aligned with the physical terminal through real-time data synchronization. Accordingly, before disturbance monitoring and rescheduling are performed, the DT layer remains continuously synchronized with the physical terminal through a two-way data pipeline. Operational data, including AGV positions, battery SoC, YC/RC/QC task progress, and equipment availability, are transmitted to the DT model at fixed update intervals.

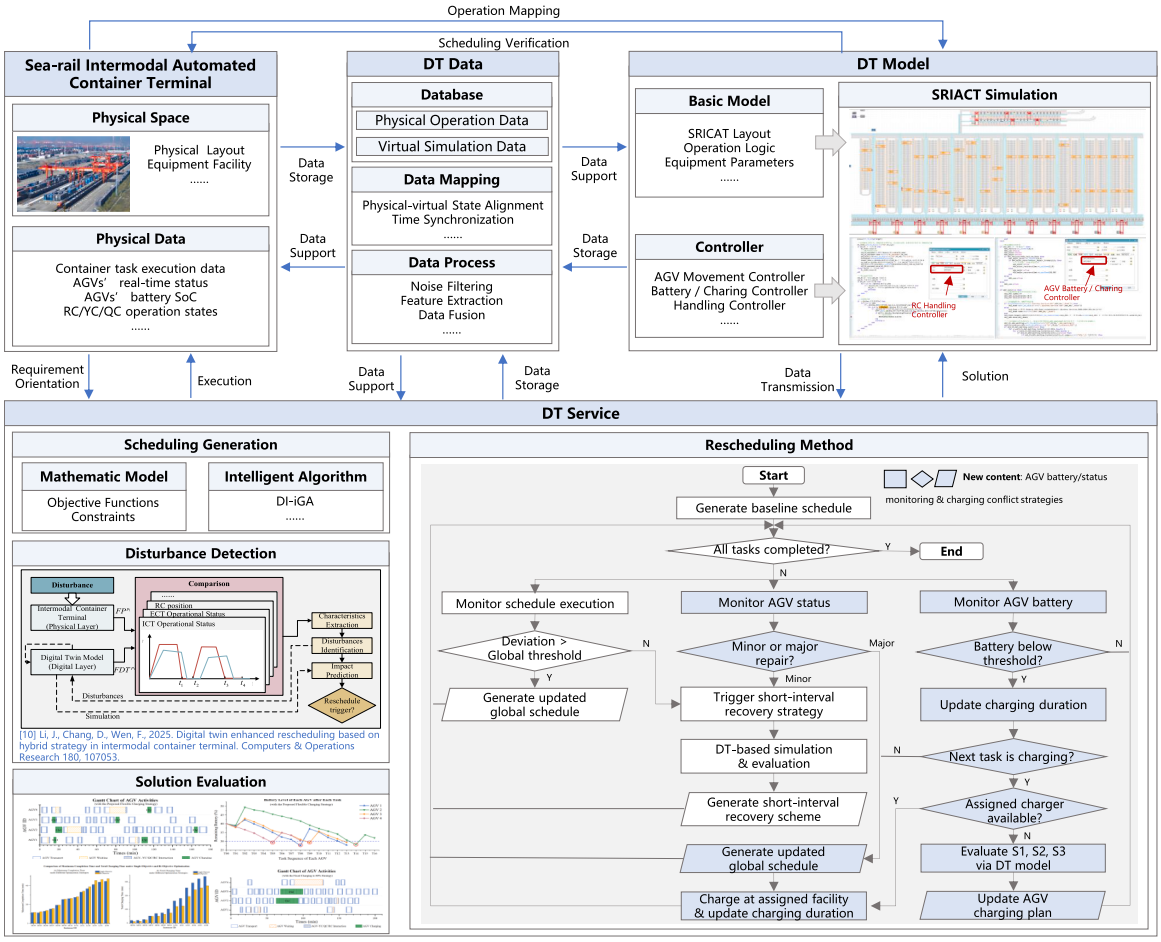

Fig. 11. DT-based rescheduling decision flow under AGV status monitoring, battery management, and charging disturbances.

These data are mapped to virtual entities using time-alignment and state-matching rules developed in Li et al. (2025a), ensuring that the virtual system faithfully mirrors current physical operations. This synchronized state provides the basis for AGV-status monitoring, battery-level assessment, and subsequent disturbance detection.

Building upon this foundation, the rescheduling mechanism is enhanced by introducing a dynamic AGV monitoring module that integrates real-time battery status and equipment condition monitoring, thereby broadening disturbance detection. The rescheduling logic is categorized into proactive and reactive mechanisms, as illustrated in Fig. 11, which presents the overall decision-making process integrating AGV status monitoring, battery management, and charging conflict resolution. Proactive rescheduling, as a form of global rescheduling, is periodically triggered based on preset time intervals to enable regular updates of the scheduling plan. Reactive rescheduling, in contrast, is activated in real time based on deviations from planned operations, and is further classified into global and local responses. Global reactive rescheduling is initiated when one of the following situations occurs: (1) the actual start or completion time of a task deviates beyond a predefined threshold; (2) the remaining battery capacity of an AGV falls below the critical threshold while its next assigned task still requires transportation; or (3) an AGV experiences a major repair, which is characterized by a long and uncertain recovery duration that renders it temporarily unavailable for operations. Local reactive rescheduling handles sub-threshold disturbances that may disrupt schedule continuity, such as AGV minor repairs with short recovery times, unreleased equipment, incomplete predecessor tasks, or occupied charging stations.

Focusing on local disturbances arising from AGV charging conflicts, this study develops three response strategies. These are simulated and evaluated within a dedicated lightweight DT model tailored to AGV-level transport and charging behavior. The strategies include: **S1**, waiting in queue at the originally assigned charge facility; **S2**, switching to an idle charge facility and completing the original charging plan; **S3**, partially charging at an alternative facility and returning to the originally assigned facility to complete the task. These strategies represent typical AGV responses under constrained charging resources and can be independently resolved through local rescheduling without interfering with other equipment or task sequences. While alternative approaches such as postponing charging or prioritizing transport tasks theoretically exist, they involve coordination with other resources (e.g., QCs, YCs and RCs) and may lead to system-wide ripple effects. Therefore, such strategies are excluded from the current scope of evaluation.

To systematically compare the impact of each charging conflict strategy, this study introduces the concept of a closed-loop evaluation interval for charging behavior. Unlike prior approaches that evaluated local rescheduling performance within fixed windows between two global rescheduling points, the closed-loop interval focuses on the self-contained impact of charging disturbance responses. This interval begins when the AGV enters a strategy execution decision (e.g., due to charger occupation) and ends upon the completion of the charging process and resumption of the transport task. Within this interval, key performance indicators, including makespan, scheduling deviation, and number of charging interruptions, are collected to provide a more precise and bounded assessment.

For instance, under strategy S2, suppose an AGV plans to go to Charging Facility 1 after completing a transport task, but Charging Facility 1 is occupied. The AGV is then reassigned to Charging Facility 2, beginning execution of the strategy at time T_0, starting to charge at T_1, finishing charging at T_2, and resuming transport at T_3. Accordingly, the interval $[T_0, T_3]$ is defined as the evaluation interval for this round of strategy execution. Notably, this interval not only captures the behavioral changes of the triggering AGV itself, but also includes the chain reaction effects of the chosen strategy on other AGVs' charging and task execution, thereby ensuring the comprehensiveness and objectivity of the simulation-based evaluation.

In the strategy selection mechanism, this paper employs a multi-criteria prioritization approach. First, the strategy with the lowest total task completion time is preferred. In the event of a tie, the strategy with the smallest total deviation from the plan is selected. If both are still equal, the one with the fewest charging interruptions is chosen. If all indicators are equivalent, the simplest strategy with the lowest execution cost is prioritized, following the order S1 > S2 > S3. This decision-making mechanism balances scheduling efficiency and stability, enhancing the system's adaptability and resilience to charging disturbances.

In the proposed framework, the DT does not merely serve as a data-collection or visualization tool. Instead, it acts as the decision-support backbone of the rescheduling mechanism. Specifically: (1) it determines rescheduling triggers by evaluating physical-virtual deviations in real time; (2) it simulates and evaluates DI-iGA candidate schedules, ensuring feasibility under actual equipment states and AGV battery levels; and (3) it continuously feeds updated system states back into the optimization model, enabling each newly generated schedule to operate on consistent virtual-physical information. Through this integration of sensing, evaluation, optimization, and execution, the DT framework substantially enhances the system's adaptability to dynamic disturbances and supports robust decision-making under realistic operational conditions.

Although the current DT system at Qinzhou Port is primarily designed for existing operational conditions, where ICT-based transport between the RCS and the terminal yard remains dominant, the proposed framework is not restricted to a specific transport mode. As AGVs are gradually introduced with the automation upgrade of the RCS, the DT architecture can naturally incorporate their operational data, enabling full-area transport automation in future scenarios. Accordingly, the framework proposed in this study provides methodological and technical support for the long-term deployment of intelligent terminal scheduling systems.

5. Numerical experiments

To verify the rationality of the proposed mathematical models, the effectiveness and performance of the DI-iGA algorithm, and the validity of the DT-based rescheduling framework, extensive numerical experiments and simulation studies are conducted. The MIP model is solved using the GUROBI solver (Version 11.3.0) with the concert interface of Python 3.12. The DI-iGA algorithm is also implemented in Python 3.12. To evaluate the effectiveness of the proposed DT-based rescheduling method, a simulation model is developed using Plant Simulation (Version 16.0). All experiments are executed on a personal computer with an Intel(R) Core(TM) i7-13800H CPU @ 2.50 GHz, 64 GB RAM, and a 12 GB GPU.

5.1. Parameter settings

This study focuses on Qinzhou Port, located in southwestern China, which features a U-shaped layout. The port comprises a total of 21 yard blocks, with each block equipped with two double-cantilever YCs. It is connected to the RCS situated behind the port. The RCS consists of two railway blocks, each equipped with three RCs. The layout diagram is presented in Fig. 1. Input parameters employed in this study are detailed in Table 2.

In this study, four algorithms are designed for comparative analysis to evaluate the performance and applicability of the proposed decomposition-iteration framework: the Decomposition-Iteration Improved Genetic Algorithm (DI-iGA), the Decomposition-Iteration Genetic Algorithm (DI-GA), the Improved Genetic Algorithm based on the full model (iGA), and the Traditional Genetic Algorithm based on the full model (GA). Among them, DI-iGA represents the proposed method of this study, while DI-GA, iGA, and GA serve as baseline methods for comparison. The key parameter settings for these algorithms are summarized in Table 3. It is noted that for the complete problem-solving approaches (iGA and GA), a larger initial population size and a higher number of generations are employed to address the increased problem complexity, whereas the decomposition-iteration-based methods (DI-iGA and DI-GA) adopt smaller values to ensure computational efficiency.

5.2. Performance of the proposed algorithm

To evaluate the performance of the proposed algorithm, three types of test cases, small-scale case, middle-scale case and large-scale case, are designed, as shown in Tables 4–6. Six primary elements define each case, including the number of containers, QCs, AGVs, YCs, RCs, and charging facilities. For algorithmic comparison, the proposed DI-iGA is compared with four other methods: the commercial solver GUROBI, GA, iGA, and DI-GA. The GUROBI solver is configured with a time limit of 3600 s, while each metaheuristic algorithm

Table 2
Input parameters.

Parameters	Numerical Values
$p_i^{RC}, s_{(i,j)}^{RC}$	Calculated by Eqs. (A.1)-(A.5), where $t_1^{RC} = 80m/\min$, $t_2^{RC} = 85m/\min$ and $s_t^{RC} = 30m/\min$ (Yang et al., 2023b).
$p_i^{YC}, s_{(i,j)}^{YC}$	Calculated by Eqs. (A.6)-(A.7), where $t_1^{YC} = 80m/\min$, $t_2^{YC} = 85m/\min$ and $s_t^{YC} = 30m/\min$ (Yang et al., 2023b).
p^{QC}, s^{QC}	The handling time at QCs is represented by random numbers within the interval [1.5, 2.5], and the setup time of QCs is random, ranging from 0.5 to 1.5 min.
$\theta^{QC}, \theta^{YC}, \theta^{RC}$	Both of them are assumed as 0.5 min (Xing et al., 2025).
$h_{saf}^{RC}, h_{saf}^{YC}$	1 carriage.
$E^{All}, \eta_{Ch}, O_{\min}, O_{\max}, E_a^{Ini}$	The battery capacity is 89 kWh, which takes approximately 1 h to fully charge, consistent with the battery configuration at Qinzhou Port. And $O_{\min} = 0.3, O_{\max} = 0.8, E_a^{Ini} = 0.4$ (He et al., 2019).
$e_i^{AGV}, e_{(i,j)}^{AGV}, e_{(i,k)}^{V\_Ch}, e_{(k,i)}^{Ch\_V}$	Calculated by Eq. (B.2), where $\phi = 1.1847, \varphi = 1.1124, \varsigma = 0.0981, \rho_{air} = 1.2kg/m^3$, $g = 9.81m/s^2, \varrho_r = 0.01, \varrho_d = 0.7$ (Murakami, 2017), $v_{em}^{AGV} = 4m/s, v_{load}^{AGV} = 3m/s$ (Gao et al., 2024), $F_{em} = 1.06m^2$, $F_{load} = 6.59m^2, w_{self} = 24ton$, consistent with the AGV parameters of Qinzhou Port, and w_{load} is a variable, selected from the operational data of Qinzhou Port.
$d_i^{AGV}, d_{(i,j)}^{AGV}, d_{(i,k)}^{V\_Ch}, d_{(k,i)}^{Ch\_V} t_i^{AGV}, t_{(i,j)}^{AGV}, t_{(i,k)}^{V\_Ch}, t_{(k,i)}^{Ch\_V}$	All variables are determined by the layout of Qinzhou Port, the starting and ending positions of containers i and j, and the location information of charging facility k.
$\sigma_{(q,i)}^{QC}, \delta_{(q,i,j)}^{QC}$	Determined by the sequence of container loading and unloading ships and QC allocation information.
M_T, M_E	$M_T = 100\min$ (time-related Big-M, larger than the maximum completion time in all small instances); $M_E = 100kWh$ (energy-related Big-M, slightly above the AGV battery capacity 89 kWh).

Table 3
Parameter settings for the compared algorithms.

Algorithm	Population Size	Maximum Iterations	Crossover Probability	Mutation Probability	Adaptivity
DI-iGA	50	100	[0.4,0.9]	[0.01,1]	Yes
DI-GA	50	100	0.8	0.05	No
iGA	100	200	[0.4,0.9]	[0.01,1]	Yes
GA	100	200	0.8	0.05	No

is executed 10 times, with the average objective value and CPU time reported. Regarding performance metrics, the objective integrates the makespan and total charging time through a weighted sum formulation, and CPU time is used to assess the overall computational efficiency. To further compare algorithmic performance, the relative percentage deviations of objective values between methods are also calculated.

As shown in Table 4, five algorithms are compared on small-scale cases: GUROBI, GA, iGA, DI-GA, and DI-iGA. The results are evaluated using GUROBI as the baseline reference. Under the time limit of 3600 s, GUROBI is able to obtain optimal solutions for instances SC01 to SC05, but can only return feasible solutions for SC06 to SC10. The objective values obtained by all algorithms remain relatively close to the GUROBI results, with deviations within 10% across all instances. In particular, iGA outperforms the standard GA both in terms of solution quality and computational efficiency. Similarly, DI-iGA shows noticeable improvement over DI-GA in both aspects, indicating that the improved genetic algorithm provides better convergence performance. It is also observed that DI-GA and DI-iGA require slightly more CPU time than GA and iGA in small-scale cases.

Table 5 further compares the four metaheuristic algorithms (GA, iGA, DI-GA, DI-iGA) on middle-scale instances, using GA as the baseline. It can be observed that iGA consistently improves upon GA in both objective value and runtime. DI-GA also achieves comparable or slightly better solution quality than GA, while significantly reducing CPU time, especially as the instance size increases. Furthermore, DI-iGA achieves the best overall performance, delivering lower objective values across most instances and demonstrating better scalability in terms of runtime.

As shown in Table 6, large-scale cases are used to further assess the scalability and robustness of the algorithms. Due to the significantly increased problem size, both GA and iGA fail to complete the solution process within the time limit of 3600 s in instance MC10 and are thus excluded from the comparison. Therefore, only DI-GA and DI-iGA are evaluated in this context. The results demonstrate that DI-iGA consistently outperforms DI-GA in both solution quality and runtime across all large-scale instances. While DI-GA still maintains a reasonable performance, its computational time increases significantly as the problem size grows. In contrast, DI-iGA achieves lower objective values with substantially reduced CPU time, confirming its superior capability to handle large and complex scheduling scenarios efficiently.

To verify the effectiveness of the proposed scheduling and charging strategy, instance MC07 (50/3/4/8/3/2) is selected for analysis. In this case, four AGVs are jointly scheduled to perform container transport and charging activities. Fig. 12 illustrates the Gantt chart of AGV operations. It not only visualizes the transport and charging activities of each AGV, but also depicts the waiting times after AGV arrival and the interaction durations with YCs, QCs, and RCs, as defined in the model formulation in Section 3.1. The Gantt chart provides a detailed temporal representation of AGV behavior, highlighting the coordination between transport, waiting, interaction, and charging.

Further insights are revealed by examining the task execution sequences and container flow types shown in Table 7. It is evident that the transport tasks exhibit cross-flow characteristics, which reduce unnecessary unloaded driving time and improve resource

Table 4
Result comparisons for small-scale cases.

NO.	Equipment Configuration	MIP		GA			iGA			DI-GA			DI-iGA		
		Obj_1	CPU/s	Obj_2	CPU/s	$Diff_2$(%)	Obj_3	CPU/s	$Diff_3$(%)	Obj_4	CPU/s	$Diff_4$(%)	Obj_5	CPU/s	$Diff_5$(%)
SC01	6/1/1/2/3/1	18.34	1.74	18.34	6.13	0.00	18.34	4.30	0.00	18.35	12.77	0.03	18.35	16.92	0.03
SC02	8/2/1/2/3/1	28.33	11.27	28.63	24.71	1.06	28.63	19.81	1.06	28.33	20.50	0.00	28.33	30.90	0.00
SC03	10/2/1/4/3/1	35.99	178.14	38.49	73.19	6.95	38.46	40.96	6.86	38.09	36.39	5.83	36.30	35.37	0.85
SC04	10/2/2/4/3/1	17.58	402.51	18.50	12.09	5.23	18.41	8.63	4.72	18.55	25.79	5.52	18.49	22.43	5.18
SC05	11/2/2/4/3/1	20.63	1338.89	21.48	13.71	4.11	21.24	11.14	2.95	21.40	29.64	3.70	20.72	33.54	0.40
SC06	12/3/2/4/3/1	22.89	3600.00	23.85	18.33	4.19	24.02	16.74	4.94	23.80	34.71	3.98	24.03	53.19	4.96
SC07	13/3/2/4/3/1	26.47	3600.00	28.08	34.49	6.06	26.49	38.89	0.06	27.73	45.65	4.74	28.09	51.98	6.08
SC08	13/3/3/4/3/1	18.45	3600.00	19.75	16.68	7.08	19.71	15.34	6.86	19.03	40.91	3.14	19.33	46.64	4.77
SC09	14/3/3/4/3/1	20.37	3600.00	22.26	28.29	9.31	21.53	24.19	5.72	21.96	46.05	7.83	21.08	54.99	3.49
SC10	15/3/3/4/3/2	21.76	3600.00	23.59	31.99	8.43	22.96	29.19	5.54	22.89	56.76	5.22	21.85	66.41	0.44

Note: Equipment configuration is listed in the order of Containers/QCs/AGVs/YCs/RCs/Charging facilities.
MIP results are obtained using the Gurobi solver (Version 11.3.0).
$Diff_2(\%) = (Obj_2 - Obj_1) / Obj_1 * 100$;
$Diff_3(\%) = (Obj_3 - Obj_1) / Obj_1 * 100$;
$Diff_4(\%) = (Obj_4 - Obj_1) / Obj_1 * 100$;
$Diff_5(\%) = (Obj_5 - Obj_1) / Obj_1 * 100$.
Obj represents the objective value (unit: min).

Table 5
Result comparisons for middle-scale cases.

NO.	Equipment Configuration	GA		iGA			DI-GA			DI-iGA		
		Obj_1	CPU/s	Obj_2	CPU/s	$Diff_2$(%)	Obj_3	CPU/s	$Diff_3$(%)	Obj_4	CPU/s	$Diff_4$(%)
MC01	20/3/4/6/3/2	25.37	47.86	25.45	50.39	0.32	25.17	82.82	-0.81	24.16	87.81	-4.77
MC02	25/3/4/6/3/2	31.39	77.74	30.66	65.98	−2.33	31.90	131.65	1.61	31.86	126.40	1.48
MC03	30/3/4/6/3/2	36.44	160.17	36.60	148.72	0.44	35.80	218.10	-1.77	35.70	196.59	−2.04
MC04	35/3/4/6/3/2	65.54	373.37	63.52	276.27	−3.08	64.57	308.04	-1.49	63.79	266.77	−2.67
MC05	40/3/4/8/3/2	72.32	585.06	72.52	431.14	0.28	73.09	396.29	1.06	68.34	310.14	−5.50
MC06	45/3/4/8/3/2	87.18	875.32	88.31	433.39	1.30	88.78	770.20	1.84	79.70	555.91	−8.59
MC07	50/3/4/8/3/2	104.29	1123.15	103.41	615.07	−0.84	105.93	631.12	1.57	103.38	555.52	−0.88
MC08	60/4/5/8/3/2	125.75	1670.90	123.87	934.39	−1.50	125.99	1108.27	0.19	122.62	844.60	−2.49
MC09	70/4/5/8/3/2	157.64	3550.22	152.61	2479.53	−3.19	159.99	1477.61	1.49	160.72	1014.55	1.95
MC10	80/4/5/10/3/3	172.29	5280.10	171.97	4113.04	−0.19	174.26	1931.22	1.14	169.43	1387.52	−1.66

Note: Equipment configuration is listed in the order of Containers/QCs/AGVs/YCs/RCs/Charging facilities.
$Diff_2(\%) = (Obj_2 - Obj_1) / Obj_1 * 100$;
$Diff_3(\%) = (Obj_3 - Obj_1) / Obj_1 * 100$;
$Diff_4(\%) = (Obj_4 - Obj_1) / Obj_1 * 100$.
Obj represents the objective value (unit: min).

utilization. For instance, considering AGV 1, its first five tasks clearly demonstrate how the scheduling algorithm takes advantage of container flow directions to reduce idle movements. AGV 1 first transports Container 37 from the yard to the QC, and then proceeds to Charging Facility 1, which is located on the seaside of the yard, to perform a charging operation. After recharging, it transports Container 38 from the QC back to the yard. It then continues by picking up Container 16 from the yard and delivering it to the RCS. Subsequently, AGV 1 moves Container 35 from the yard to the QC. This sequence of operations reflects how the algorithm efficiently coordinates inbound and outbound flows to minimize unloaded driving time and improve overall transport efficiency.

To assess energy management performance, Fig. 13 presents the battery level of each AGV after completing individual tasks, with an initial battery level of 40% for all AGVs. Taking AGV 1 as an example, its battery drops below the minimum charging threshold (30%) after the eighth task (T08). Consequently, a charging activity is inserted as the ninth task (T09), ensuring compliance with the lower limit constraint. Across all AGVs, the battery level after charging operations remains below the upper limit of 80%, satisfying the charging constraints defined in the model. This confirms that the proposed algorithm effectively enforces the conditional charging rules by ensuring that charging is triggered when the battery level falls below the lower bound, and that the battery level after charging does not exceed the specified upper threshold.

These results validate the practicality of the proposed scheduling model in coordinating AGV operations and managing energy consumption under operational constraints.

5.3. Comparative and sensitivity analysis of single-objective and bi-objective optimization

To assess the performance of the developed bi-objective optimization approach, this section selects medium- to large-scale instances (MC04 to LC06) for comparison with the single-objective optimization strategy. Small-scale instances (SC01 to MC03) are not

Table 6
Result comparisons for large-scale cases.

NO.	Equipment Configuration	DI-GA		DI-iGA		
		Obj_1	CPU/s	Obj_2	CPU/s	$Diff_2$(%)
LC01	100/5/6/10/3/3	218.93	2074.12	202.64	1520.32	−7.44
LC02	120/5/6/12/6/4	246.97	2687.52	233.98	1831.11	−5.26
LC03	140/5/7/12/6/5	331.23	3265.58	291.86	2221.78	−11.89
LC04	160/6/8/14/6/6	379.65	3714.78	349.38	2556.94	−7.97
LC05	180/6/9/14/6/7	384.90	4286.04	361.50	2941.37	−6.08
LC06	200/6/10/16/6/8	413.61	5460.01	373.00	3424.19	−9.82

Note: Equipment configuration is listed in the order of Containers/QCs/AGVs/YCs/RCs/Charging facilities.
$Diff_2(\%) = (Obj_2 - Obj_1) / Obj_1 * 100$.
Obj represents the objective value (unit: min).

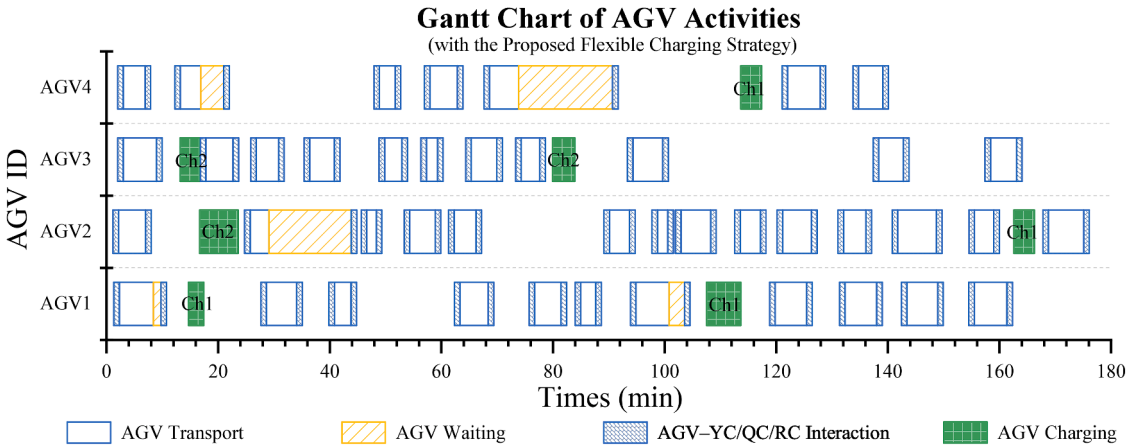

Fig. 12. Gantt chart of AGV activities with the proposed flexible charging strategy in instance MC07.

Table 7
Task sequence and container flow for each AGV.

AGV ID	Task Sequence (with Container Flow)
AGV 1	37(-6)-Ch1-38(+4)-16(-2)-35(-6)-44(-6)-41(-6)-22(-6)-Ch1-20(+2)-46(+6)-11(+3)-13(+3)
AGV 2	15(-6)-Ch2-29(+6)-40(+2)-42(-6)-10(+3)-19(-2)-49(-6)-28(+6)-25(-6)-17(+2)-18(-4)-26(+6)-30(-6)-Ch1-12(+5)
AGV 3	36(-6)-Ch 2-45(+6)-27(-6)-31(+6)-23(-6)-43(-6)-50(-6)-33(-6)-Ch 2-8(+4)-39(-6)-21(+5)
AGV 4	34(-6)-14(+2)-32(-6) 24(+6)-47(-6)-Ch1-9(+3)-48(-6)

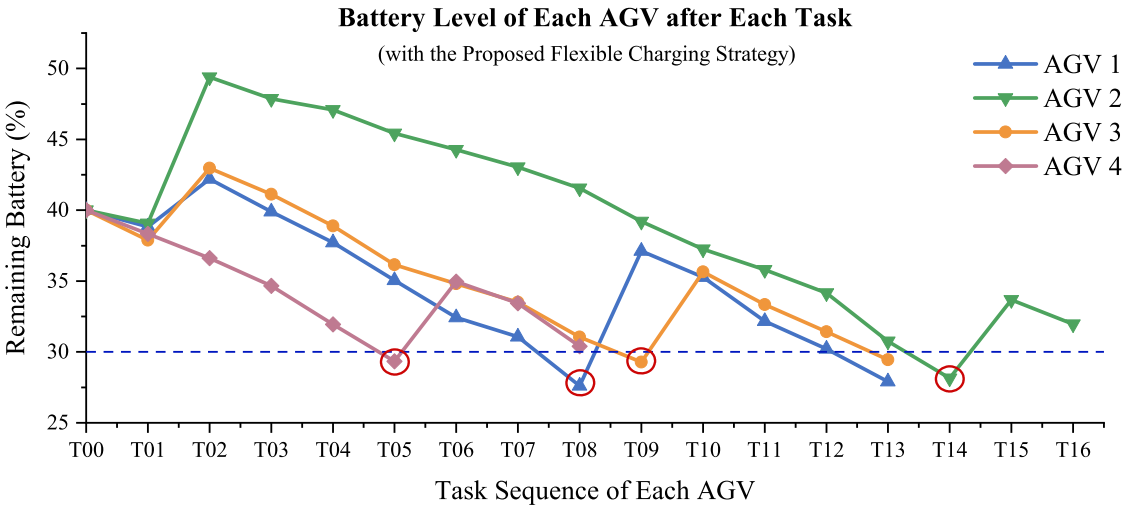

Fig. 13. Battery level of each AGV after each task in instance MC07 under the proposed flexible charging strategy.

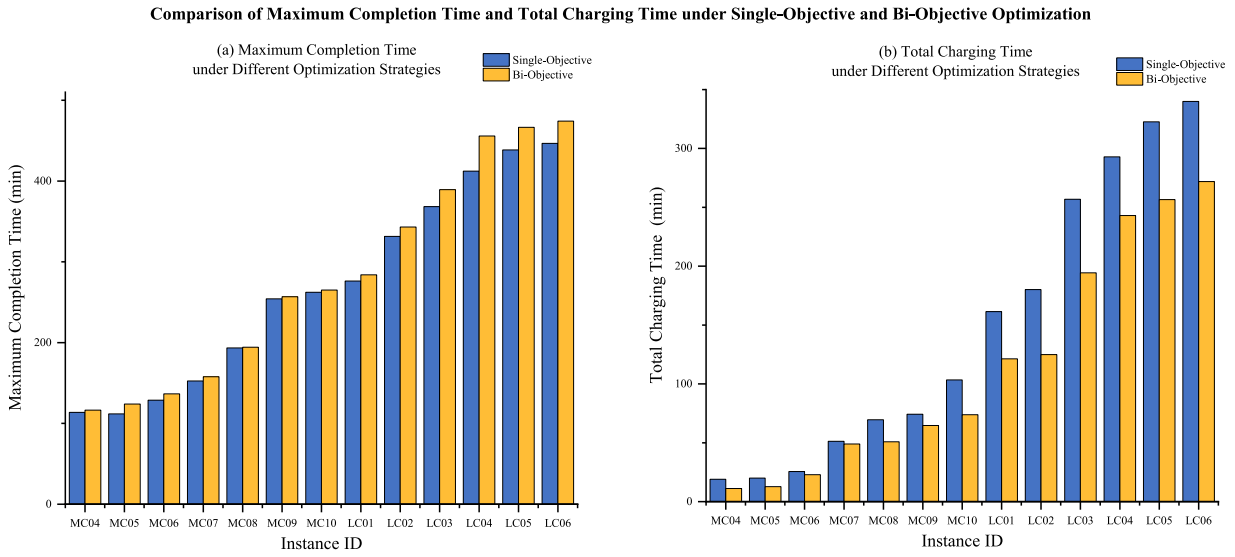

Fig. 14. Comparison of maximum completion time and total charging time under single- and bi-objective optimization.

included in this comparison because, in these cases, AGVs do not require charging under either optimization strategy. As a result, the total charging time remains zero, making it impossible to assess the impact of different objective settings on charging behavior and scheduling performance. Therefore, only 13 instances from MC04 to LC06 are considered in this section, with each instance being executed 10 times and the average results used for comparison.

As shown in Fig. 14, the comparison focuses on two key metrics: maximum completion time and total charging time. A comparison reveals that the bi-objective optimization strategy, relative to the single-objective one, the bi-objective optimization strategy slightly increases the maximum completion time in most cases, but significantly reduces the total charging time. This result demonstrates that incorporating energy consumption into the optimization process effectively balances the trade-off between scheduling efficiency and energy utilization, leading to a more energy-efficient scheduling solution at the cost of a minor increase in completion time.

To further analyze the impact of the objective function's weight parameter settings on the scheduling results, four instances (MC04, MC07, LC01, and LC06) were selected. The weight coefficient was adjusted incrementally from 0 to 1 with a step size of 0.1 to conduct a sensitivity analysis of the bi-objective optimization results.

Although both the maximum completion time and the total charging time are expressed in minutes, their scales differ significantly in practical scenarios. To ensure the comparability of the results and to intuitively reflect the effects of different weight settings, the two indicators were normalized using the Min-Max method, as shown below:

$$N_{T_F} = \frac{T_F - \min(T_F)}{\max(T_F) - \min(T_F)} \tag{56}$$

$$N_{T_{Ch}} = \frac{T_{Ch} - \min(T_{Ch})}{\max(T_{Ch}) - \min(T_{Ch})} \tag{57}$$

The normalized results are presented in Fig. 15. It can be observed that as the weight coefficient α for the maximum completion time gradually increases, the normalized value of makespan generally shows a decreasing trend, while the normalized total charging time increases correspondingly. This indicates a clear trade-off relationship between the two objectives: when more emphasis is placed on minimizing the makespan, the scheduling strategy tends to prioritize compressing task durations, which may lead to more frequent AGV charging operations and relatively higher energy consumption. Conversely, when more attention is paid to reducing charging time, the makespan may increase to some extent. Additionally, the slopes and inflection points of the curves vary slightly across different instances, suggesting that the influence of the weight parameter depends on the scale and operational characteristics of each scenario. Overall, a reasonable setting of α can help achieve a practical balance between time efficiency and energy consumption.

5.4. Analysis of charging strategy and thresholds

To evaluate the effectiveness of the proposed flexible charging strategy, it is compared with a fixed charging strategy. Under this fixed-charging scheme, once charging is initiated, the AGV must be charged up to a preset level of 80%, regardless of its current remaining battery level. In contrast, the proposed flexible charging strategy determines the charging duration dynamically based on the AGV's task scheduling requirements and current battery status, thereby improving overall scheduling efficiency and energy utilization. Both strategies adopt the same minimum battery threshold (30%), meaning that charging is mandatory when the battery level falls below this value.

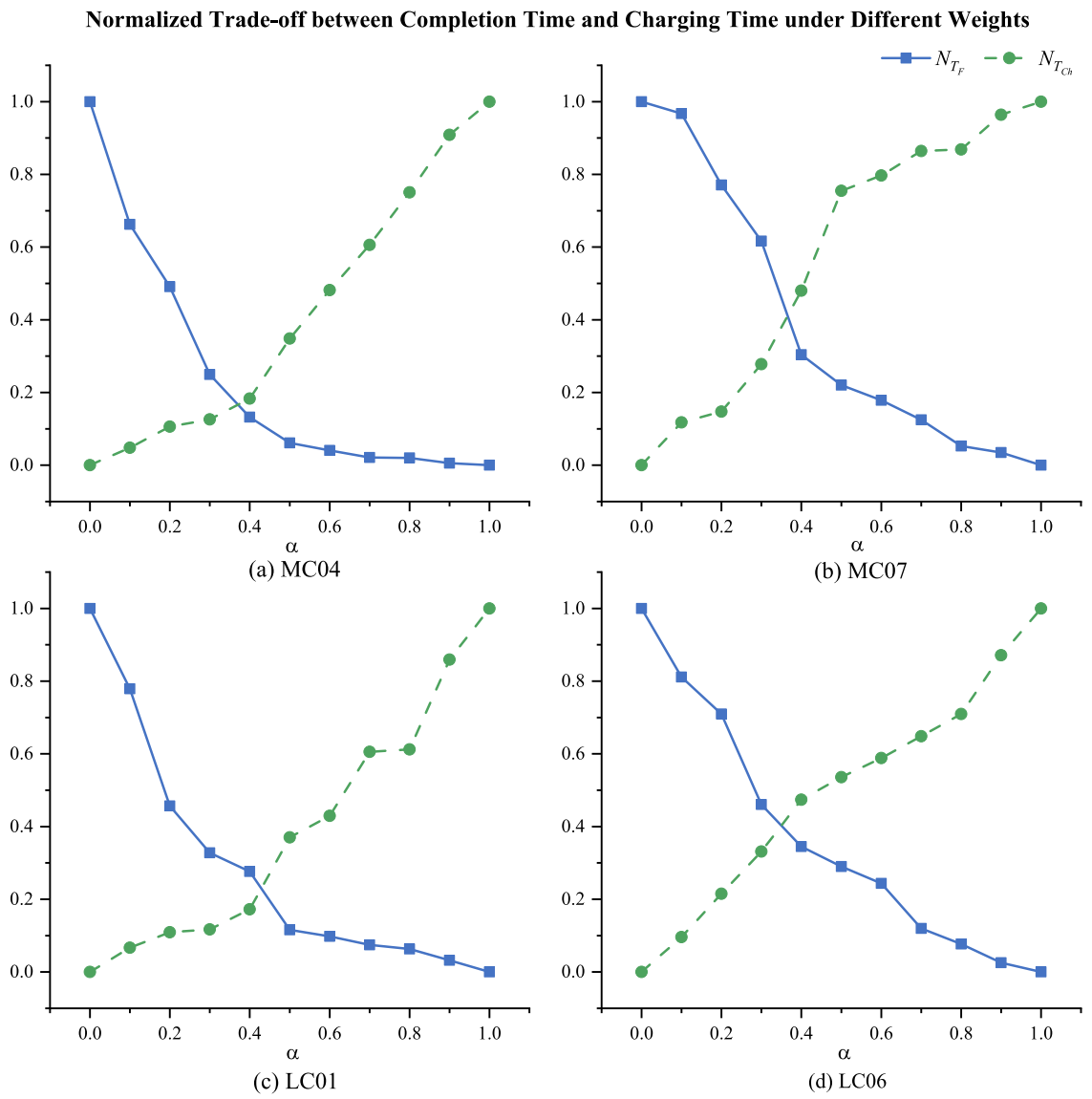

Fig. 15. Normalized comparison of makespan and total charging time under different weight settings.

Table 8
Performance comparison between fixed and flexible charging strategies.

Metric	Fixed Charging to 80%	Proposed Flexible Charging	Improvement (%)
Maximum Completion Time (min)	204.61	177.26	13.37%
Total Charging Time (min)	61.62	30.63	50.28%

A detailed evaluation based on the MC07 instance, as summarized in Table 8, shows that the flexible charging strategy delivers notable improvements over the fixed scheme in both completion time and charging duration. Specifically, the flexible strategy improves scheduling efficiency by shortening the longest task's completion time by 13.37% and cutting total charging demand nearly in half, demonstrating significant advantages in operational efficiency and energy consumption.

Furthermore, as shown in the Gantt charts (Fig. 12 for the flexible strategy and Fig. 16 for the fixed strategy), under the fixed strategy, due to the longer duration required for each charging operation, only two AGVs are assigned charging tasks to reduce the total charging time. As a result, a large number of transport tasks are concentrated on these two AGVs, leading to imbalanced task allocation and reduced equipment utilization. In contrast, the flexible charging strategy maintains battery constraints while achieving a more balanced distribution of tasks, improving overall operational efficiency.

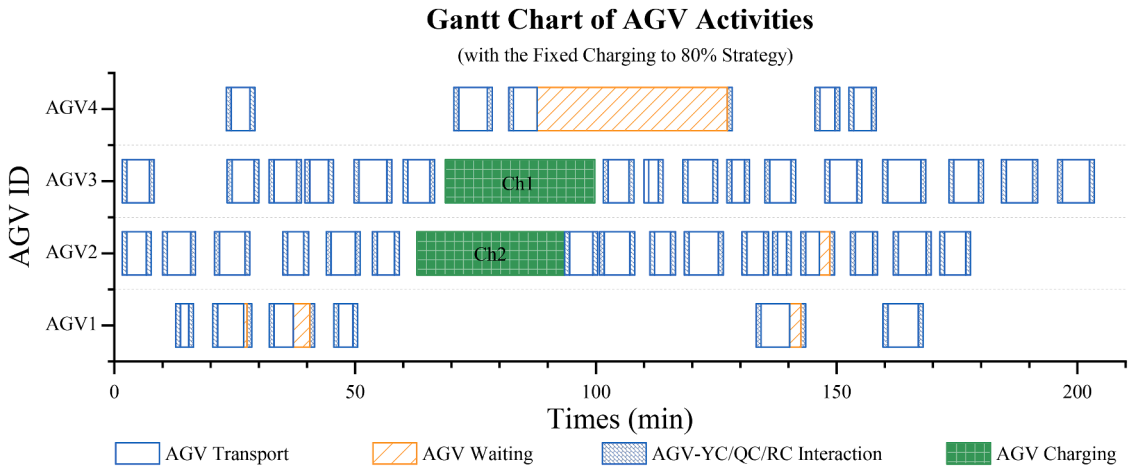

Fig. 16. Gantt chart of AGV activities with the proposed charging strategy in instance MC07.

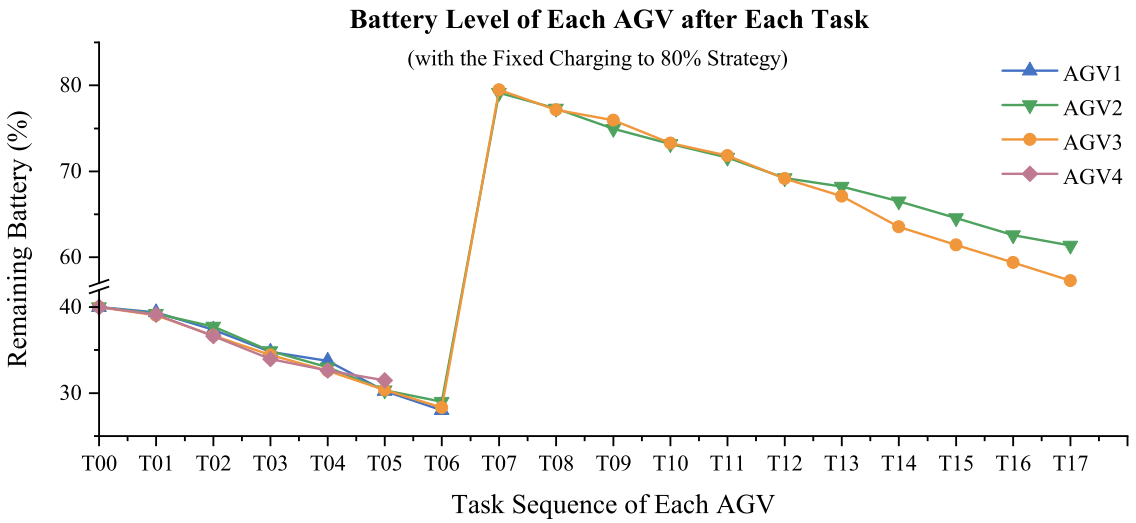

Fig. 17. Battery level of each AGV after each task in instance MC07 with the fixed charging to 80% strategy.

In addition, the AGV battery level trends (illustrated in Figs. 13 and 17) further validate these conclusions. Under the fixed strategy, although battery levels quickly recover to 80% after each charge, some AGVs remain underutilized due to long waiting times or insufficient scheduling. Meanwhile, under the flexible charging strategy, battery levels exhibit smoother depletion and replenishment curves, with more continuous and rational scheduling, leading to more effective resource utilization.

To further validate the effectiveness of the proposed flexible charging strategy, the following section conducts a sensitivity analysis of its key parameters, the lower and upper charging thresholds, to investigate how different settings affect scheduling performance. Fig. 18 presents the detailed comparison results.

As shown in Fig. 18, four instances (MC04, MC07, LC01, and LC06) are selected to conduct a sensitivity analysis of different charging threshold settings under the proposed flexible charging strategy. The results indicate that, with the flexible charging mechanism, reducing the minimum charging threshold, from 30% to 20%, can significantly shorten the total charging time while also contributing to a certain degree of reduction in the makespan. This finding suggests that allowing AGVs to reach a lower battery level before recharging reduces the frequency of charging operations, thereby improving overall scheduling efficiency and resource utilization.

In addition, varying the maximum charging threshold, from 80% to 100%, has relatively limited effects on both makespan and total charging time, with only slight fluctuations observed. This phenomenon demonstrates that, under the flexible charging strategy, AGV charging behaviors rely more on actual task demands and the dynamic status of battery levels, rather than the preset upper threshold alone. Overall, appropriately lowering the minimum charging threshold can further enhance the advantages of the flexible charging strategy in achieving a better trade-off between energy consumption and scheduling performance.

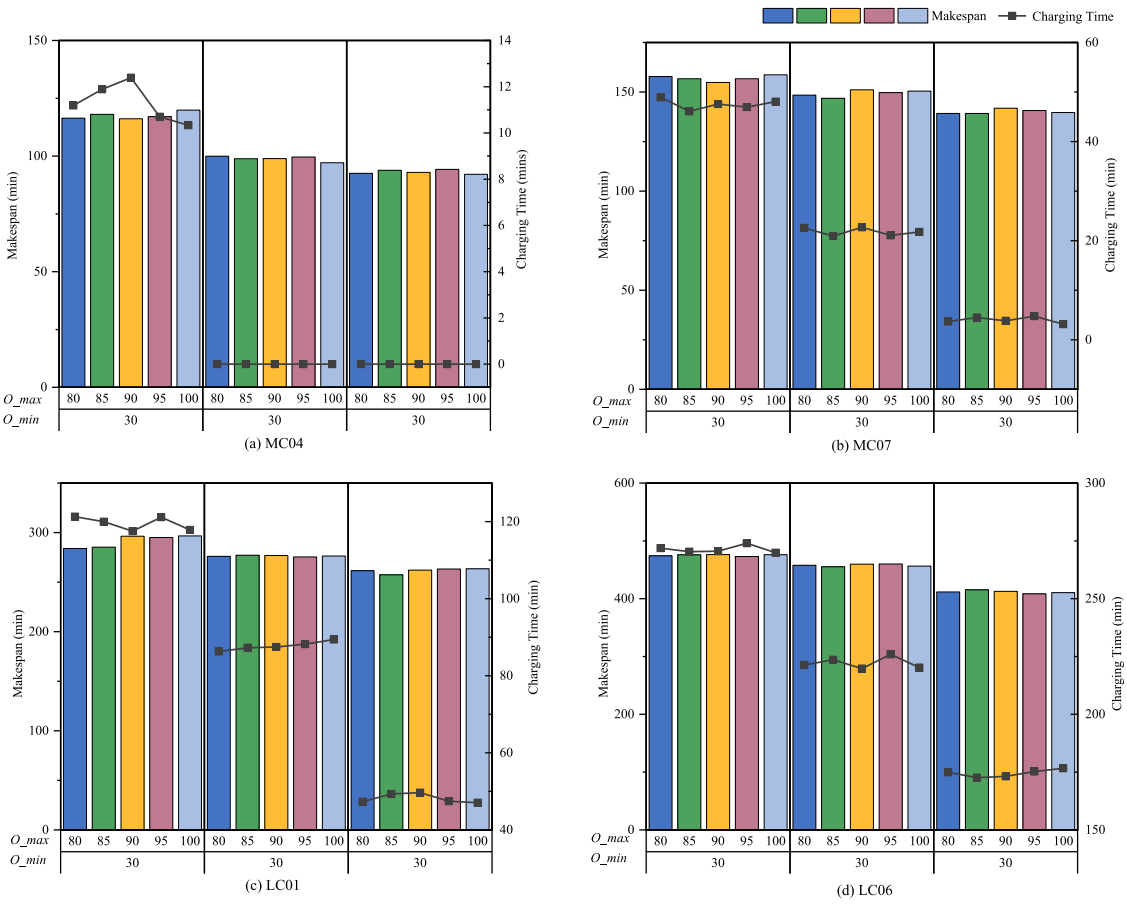

Fig. 18. Comparison of makespan and charging time for four instances under different threshold settings.

5.5. *Validation of the proposed DT-based hybrid rescheduling framework*

In our previous study (Li et al., 2025a), a DT-enhanced hybrid rescheduling method has been verified to effectively perceive and respond to disturbances in terminal operations. This method mitigated the adverse impact on overall operational efficiency by enabling dynamic rescheduling.

Building upon this foundation, the current study further extends the DT-enhanced rescheduling framework by introducing additional functional modules, including AGV fault response, battery level monitoring, and charging activity tracking. The aim is to develop a scheduling optimization system aligned with the automation needs of sea-rail intermodal transportation, thereby enhancing its adaptability and practicality in complex terminal environments.

Since the automation upgrade and AGV system of the RCS at Qinzhou Port are still in the planning phase, a simulation-based experimental environment is developed to simulate task disturbances, resource status feedback, and scheduling trigger processes. This enables a systematic evaluation of the proposed DT-enhanced rescheduling method that integrates AGV energy consumption and operational status awareness.

To emulate potential disruptions in the experimental setup, a failure rate of 10% is assigned to AGVs. Given a failure, there is a 10% probability of a major repair with a repair duration randomly drawn from a uniform distribution between 30 and 90 min, and a 90% probability of a minor repair with a repair duration randomly drawn from a uniform distribution between 2 and 8 min. To accurately capture the nonlinear characteristics of lithium battery charging, this study adopts the function $FucSOC(SOC_0, t)$ from Xu and Meng (2019), which models charging behavior across different phases. This allows the estimation of the SOC level at the end of charging based on the initial SOC (SOC_0) and charging duration (t), thereby improving the model's ability to characterize realistic charging behavior.

As shown in Fig. 19, in the absence of real-time monitoring and response mechanisms enabled by the DT, the actual makespan is significantly prolonged. In contrast, after introducing the DT-based rescheduling method, such delays are noticeably alleviated, and the makespan gradually decreases as the global rescheduling threshold becomes smaller. This improvement indicates that timely task adjustments help mitigate the uncertainty caused by operational disruptions. One important reason for the prolonged makespan in

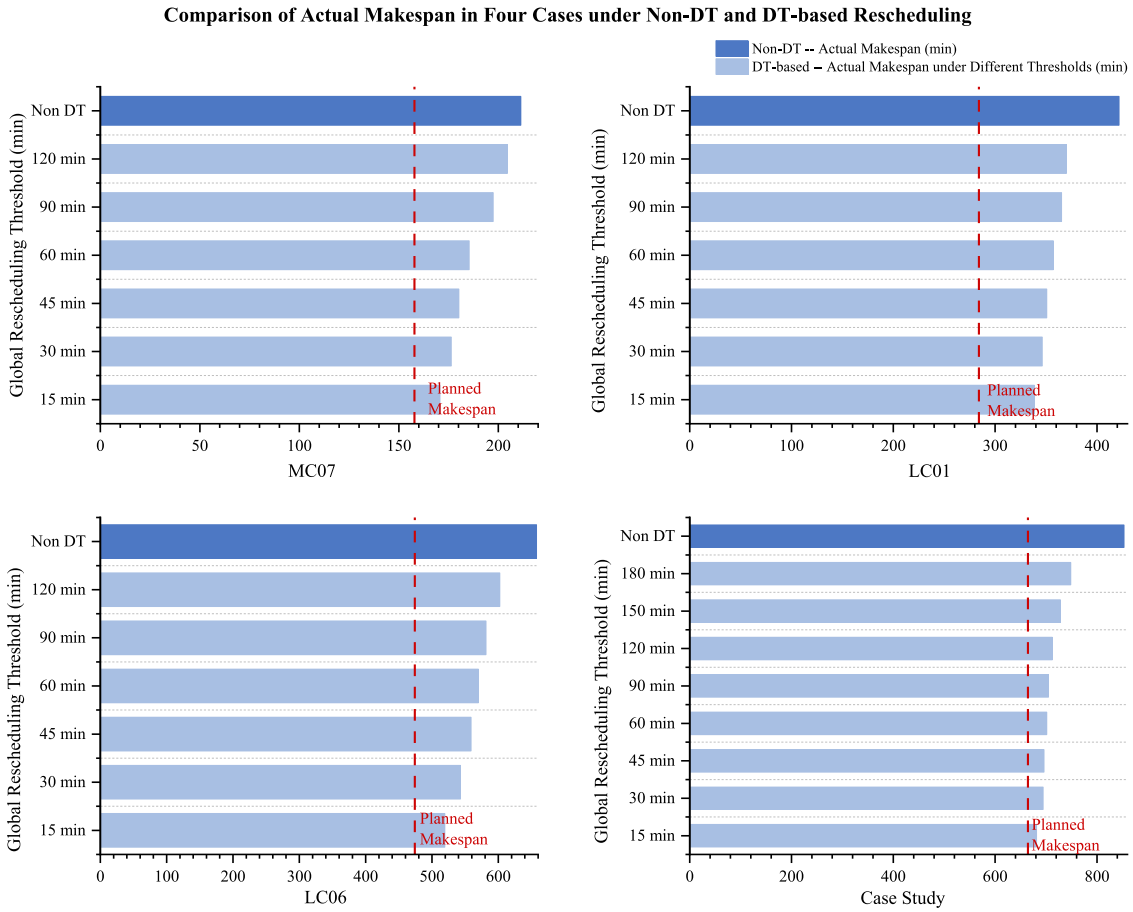

Fig. 19. Comparison of actual makespan in four cases under Non-DT and DT-based rescheduling.

the non-DT scenario is AGV failures, which not only directly delay task execution but also create cascading effects on subsequent operations. As indicated by the statistics in Table 9, since the AGV failure rate is fixed in the simulation model, the number of failures is primarily related to the task volume, remaining relatively stable within the same case but increasing markedly with larger case scales. For example, in the MC07 case, where 43 containers were transported by four AGVs, the AGVs experienced a total of five failures, including four minor repairs and one major repair. In the LC06 case, which involved 185 containers handled by ten AGVs, the number of failures increased to 22, comprising 18 minor repairs and four major repairs.

Beyond failures, low-battery events were also observed. In the non-DT scenario, occurrences of AGV battery levels falling below the minimum charging threshold (30%) are primarily due to the absence of real-time monitoring of AGV battery status. In this case, task execution strictly follows the original schedule without dynamically adjusting for the actual battery level. However, during plan execution, AGVs inevitably enter standby states that still consume energy; additionally, queuing, traffic congestion, and other delays further increase energy consumption; and the actual battery discharge process is nonlinear. As a result, strictly following the schedule without considering real-time battery conditions may lead to situations where the battery level drops below 30% without timely charging. With the increase in task volume, such occurrences become more frequent; for example, in the MC07 case, only one such instance was recorded, whereas in the LC06 case, there were four occurrences of the battery level falling below 30% without timely charging. After introducing the DT-based hybrid rescheduling framework, AGV battery levels can be monitored and assessed in real time, enabling timely charging decisions and preventing these occurrences; as shown in Table 9, no low-battery events are observed under the DT-based results. Moreover, in the DT scenario, to accommodate additional power consumption caused by fluctuations in energy usage, standby periods, and power draw during traffic congestion and queuing, the actual total charging duration tends to be slightly higher than the initially planned duration.

The complete elimination of below-threshold battery events in the DT-based scenario is primarily attributed to the framework's capability to dynamically adjust charging plans based on real-time battery information. Such adjustments include the selection of charging facility, the determination of charging time, and the setting of charging durations, which result in multiple modifications to the original charging schedule during execution. As shown in Table 9, the number of charging plan adjustments increases noticeably with the growth of task volume, indicating a clear positive correlation between operational scale and the frequency of charging

Table 9
Comparison of scheduling results with and without DT-based rescheduling.

Instance ID	Avg. Tasks per AGV	DT-based Rescheduling	Global Rescheduling Threshold (min)	Minor repairs	Major repairs	Global Resched.	Low-Battery Events	Charging Plan Adj.	Actual Charging Time (min)	Diff (%)
MC07	10.75	✗	Nan	4	1	Nan	1	Nan	48.93	0
		✓	15	4	0	15	0	0	50.29	2.78
			30	5	0	8	0	0	50.42	3.04
			45	4	1	5	0	0	50.78	3.78
			60	4	0	3	0	2	50.70	3.61
			90	4	1	4	0	3	50.57	3.36
			120	4	0	3	0	2	50.22	2.64
LC01	16.00	✗	Nan	8	3	Nan	2	Nan	121.28	0
		✓	15	8	3	23	0	3	126.34	4.17
			30	7	3	11	0	3	125.94	3.84
			45	8	3	8	0	4	125.16	3.20
			60	8	4	5	0	3	125.80	3.73
			90	8	3	4	0	5	125.60	3.56
			120	8	3	3	0	5	126.71	4.48
LC06	15.6	✗	Nan	18	4	Nan	4	Nan	271.84	0
		✓	15	18	4	37	0	9	291.45	7.22
			30	19	4	18	0	12	289.31	6.43
			45	18	4	11	0	13	290.95	7.03
			60	18	5	9	0	11	287.76	5.86
			90	19	4	6	0	11	289.20	6.39
			120	18	4	4	0	12	286.65	5.45
Case Study	7.22	✗	Nan	51	8	Nan	105	Nan	784.29	0
		✓	15	51	8	44	0	23	858.56	9.47
			30	49	9	22	0	22	854.25	8.92
			45	51	8	15	0	21	855.42	9.07
			60	51	8	12	0	23	862.56	9.98
			90	50	8	7	0	22	865.31	10.33
			120	51	9	5	0	25	868.60	10.75
			150	51	8	4	0	26	858.88	9.51
			180	50	8	4	0	27	869.31	10.84

Note: Diff(%) = ((Total Charging Time (with DT) - Total Charging Time (Non DT)) / Total Charging Time (non DT)) * 100.

schedule modifications. Within the same case, the number of adjustments generally tends to rise with higher rescheduling thresholds, although this increase is not particularly pronounced.

Based on the analysis of the MC07, LC01, and LC06 cases, it can be observed that the introduction of the DT-based hybrid rescheduling framework significantly alleviates makespan delays, while also improving AGV-related performance in terms of eliminating low-battery-without-charging events and optimizing charging plan adjustments. Building on these findings, a case study was conducted to further verify the engineering feasibility and practical value of the proposed method under realistic terminal operating conditions, using real-world container operation data collected from Qinzhou Port on August 1st, 2024 (00:00-12:00). This case involved 544 containers, 10 QCs, 6 RCs, 21 yard blocks, 72 AGVs, and 8 charging facilities, reflecting the current equipment deployment at Qinzhou Port.

As shown in Fig. 19 and Table 9, without the DT-based rescheduling method, the makespan was substantially extended, with a delay magnitude of 28.40%, accompanied by 105 occurrences of AGV battery levels falling below the minimum charging threshold without timely charging-posing a potential operational risk to the entire system. With the introduction of the DT-based hybrid rescheduling framework, these low-battery-without-charging events were completely eliminated, enabling real-time monitoring of AGV battery status and dynamic adjustments to charging plans. In this scenario, the average number of charging plan adjustments reached 23, and the total actual AGV charging duration was slightly longer than the initially planned duration.

It is noteworthy that although the case study involved a much larger task volume than LC06, the delay magnitude did not increase proportionally. A further analysis of AGV workload, as presented in Table 9, shows that when the average workload per AGV is lower (10.75 for MC07, 16.00 for LC01, 15.60 for LC06, and 7.20 for the Case Study), the system can more promptly reassign available AGVs to take over tasks in the event of equipment failures or other disruptions, thereby mitigating overall delays.

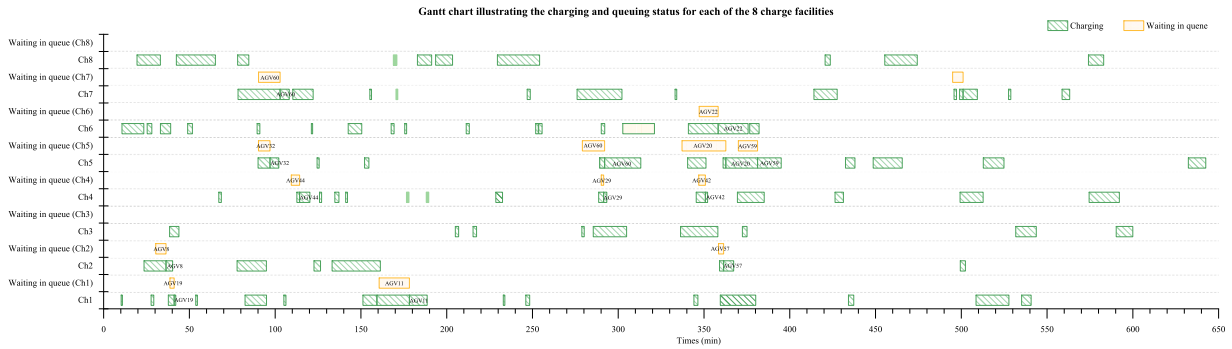

Fig. 20. Gantt chart illustrating the charging and queuing status for each of the 8 charge facilities.

Table 10
Comparative analysis of scheduling performance under different charging facility numbers and locations.

No. of Charging Facilities	Newly Added Charging Facility ID Unloaded Travel Distance (km)	Makespan (min) $Diff_{un}$ (%)	$Diff_{ms}$ (%) Waiting time in queue (min)	$Diff_{w}$ (%)			
8	–	664.46	–	357.41	–	124.00	–
9	RC01_01	607.76	8.53	347.50	2.77	99.75	21.98
	RC02_01	610.95	8.05	348.30	2.55	101.45	20.65
	B02_02	654.75	1.46	355.46	0.55	102.76	19.63
	B12_02	633.02	4.73	349.38	2.25	101.53	20.59
	B20_02	659.64	0.73	350.46	1.94	100.64	21.29

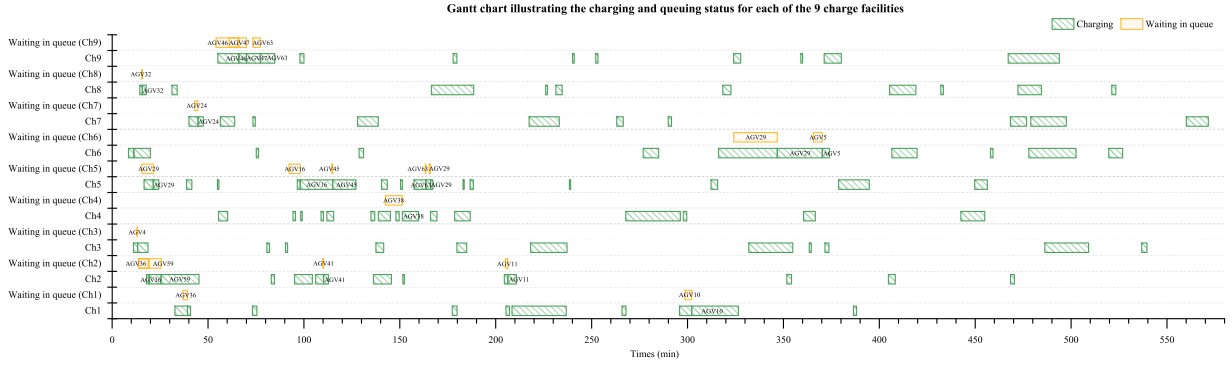

Fig. 21. Gantt chart illustrating the charging and queuing status for each of the 9 charge facilities.

5.6. Analysis of the quantity and location of charging facilities

At present, Qinzhou Port operates 72 AGVs supported by 8 charging facilities, which are primarily located along the seaside area of the yard blocks. Once the railway central station achieves a higher level of automation, AGVs will be able to enter and exit the railway area for operational tasks, thereby expanding their operational scope and routing flexibility. Consequently, it is necessary to further examine whether the current charging facility configuration can adequately meet operational demands under this scenario, and whether additional charging facilities are required, along with their preferred deployment locations.

First, based on the Gantt chart shown in Fig. 20, the current workload of the 8 charging facilities and the queuing status of AGVs can be intuitively observed. Overall, the workload among the facilities is relatively balanced, with no indications of excessively dense or overloaded operation periods, and the AGV queuing time remains generally manageable without significant congestion. This suggests that the existing configuration and layout of the charging facilities are capable of supporting the current operational intensity. However, as AGV operations extend to the RCS, cross-area operations may increase the energy supply pressure in certain regions, potentially affecting operational continuity and scheduling flexibility. Therefore, it is necessary to explore the feasibility of adding one additional charging facility and determining its optimal location, rather than pursuing large-scale capacity expansion.

Accordingly, this study further selects two candidate locations within the RCS and three alternative sites along the seaside yard blocks as potential deployment options for the additional charging facility. A comparative analysis is conducted focusing on key performance indicators, including makespan, AGVs' unloaded travel distance, and AGVs' queuing time for charging. The analysis results are presented in Table 10 and Fig. 21. The results indicate that installing an additional charging facility at any of these

locations can help reduce makespan, shorten AGV unloaded travel distance, and lower queuing times to varying degrees; however, the optimization effects differ significantly across locations. Compared with adding a facility along the seaside yard blocks, deploying the new charging facility near the RCS, particularly adjacent to Railway Yard Block 1, achieves more substantial improvements: the makespan can be reduced by up to 8.53%, AGV unloaded travel distance by 2.77%, and queuing time for charging by 19.56%.

These findings demonstrate that strategically deploying cross-area charging facilities can effectively reduce cross-region unloaded travel distances, enhance the timeliness of energy replenishment, and improve operational continuity, thereby further boosting overall scheduling efficiency and resource utilization.

6. Conclusions

This paper investigates the multi-equipment collaborative scheduling problem in a SRIACT, with a particular focus on AGV charging. A MIP model is developed to minimize the total operation completion time and the total charging time, incorporating task sequencing, time, and energy consumption constraints. Based on the problem characteristics, an improved genetic algorithm embedded within a decomposition-iteration framework is designed to solve for the optimal scheduling plans of multiple equipment and the AGV charging activities.

Furthermore, considering the operational complexity and dynamic nature of SRIACTs and the multi-source uncertainties during operations, this paper builds upon previous research (Li et al., 2025a) by further extending a DT-based hybrid rescheduling framework. This framework enables real-time monitoring of AGV operational status and battery levels, disturbance detection, and timely rescheduling responses.

On this basis, a series of comparative experiments and sensitivity analyses are conducted to validate the necessity of the bi-objective model and the weight settings, and to demonstrate the advantages of adopting a flexible charging strategy. Moreover, the impacts of minimum charging thresholds, global rescheduling thresholds, the number of charging facilities, and their spatial layout on scheduling and charging performance are discussed. The results indicate that the proposed methods and findings can provide practical decision support and valuable guidance for terminal managers in charging facility siting, scheduling plan development, and AGV charging activities.

As for future research, the following aspects could be further studied. As the RCS is located on the landside of the terminal, once the RCS becomes operational for AGV tasks, mixed traffic at road intersections between AGVs and manually driven external container trucks will be inevitable. Therefore, future research can further explore optimization and control methods for mixed traffic at intersections to enhance driving safety and traffic efficiency. In addition, the integration of dynamic wireless charging technologies could be considered to further improve scheduling flexibility and enhance the continuity of terminal operations and overall throughput capacity.

CRediT authorship contribution statement

Jiaqi Li: Writing – original draft, Software, Methodology, Conceptualization; **Daofang Chang:** Supervision, Resources, Investigation; **Furong Wen:** Resources, Investigation; **Ilkyeong Moon:** Writing – review & editing, Supervision.

Declaration of interest

The authors declare that they have no known competing financial interests or personal relationships that could have appeared to influence the work reported in this paper

Data availability

The authors do not have permission to share data.

Acknowledgements

The authors are grateful to the associate editor and anonymous reviewers for their valuable comments which improve the manuscript significantly. This work was supported by Shanghai Maritime University Graduate Outstanding Creative Talent Training Program (No.2024YBR017), the China Scholarship Council (No.202408310290), and the National Research Foundation of Korea (NRF) grant funded by the Korean government (MSIT) (No. RS-2023-00218913).

Appendix A. Supplementary calculation formulas for section 3.1

The parameters listed in Table A.1 are those not included in Table 1 of the main text but used in the supplementary formulations presented in this appendix.

Table A.1
Parameters and derived energy terms related to AGV energy consumption.

Name	Description
t_2^{RC}, t_2^{YC}	Time required for the RC's and YC's spreader to rise or fall, respectively.
$v_{tro}^{RC}, v_{tro}^{YC}$	Moving speed of the RC's and YC's trolleys, respectively.
$v_{load}^{AGV}, v_{em}^{AGV}$	Travel speed of the AGV when loaded and when empty, respectively.
x_i^s, y_i^s	Initial line and bay position of container i.
x_i^f, y_i^f	Target line and bay position of container i.
x_{RV}, x_{YV}	Line position of AGV operating lanes in the railway and yard blocks, respectively.
$d_i^{AGV}, d_{(i,j)}^{AGV}\ d_{(i,k)}^{V\_Ch}, d_{(k,i)}^{Ch\_V}$	Distances traveled by the AGV during four travel scenarios: (i) loaded travel for container i, (ii) unloaded travel from container i to the next container j, (iii) unloaded travel from container i to charging facility k, and (iv) un- loaded return travel from charging facility k to container i.

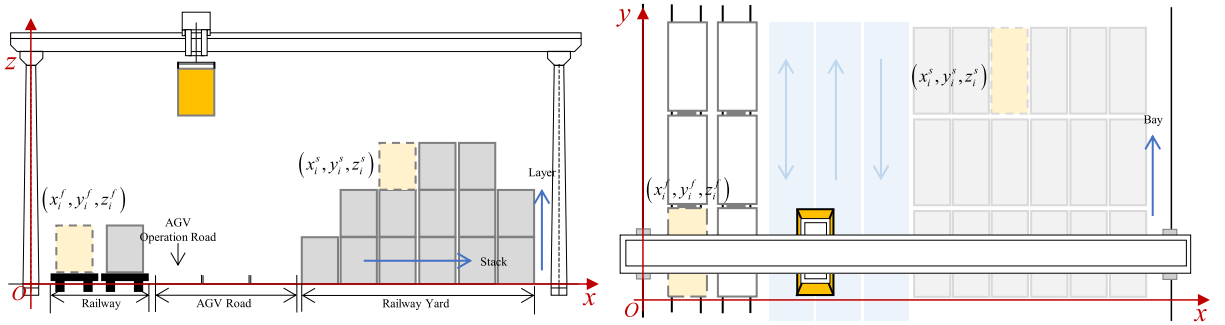

(a). Front view (b). Top view

Fig. A.1. Schematic diagram of the RC at the RCS.

A.1. Calculation of RC handling and setup times

Based on the operational logic described in Section 3.1.1, the handling time and in-place setup time of the RC are derived from the spatial relationships among containers and the operating sequence of the RC.

The handling time for container i (p_i^{RC}) is calculated as:

$$p_i^{RC} = \begin{cases} 3t_2^{RC} + \left|x_i^f - x_i^s\right| / v_{tro}^{RC} + \left|y_i^f - y_i^s\right| \cdot t_1^{RC}, \forall i \in \mathcal{N}_1 \\ 2t_2^{RC} + \left|x_i^s - x_{RV}\right| / v_{tro}^{RC}, \forall i \in \mathcal{N}_c^E, c = 2,3,4,5 \\ 2t_2^{RC} + \left|x_{RV} - x_i^f\right| / v_{tro}^{RC}, \forall i \in \mathcal{N}_c^I, c = 2,3,4,5 \end{cases} \tag{A.1}$$

To illustrate the logic of Eq. (A.1), it should be noted that unlike conventional yards, the RCS layout features an RC that spans multiple functional zones, including the railway tracks, AGV driving and operation lanes, and the railway yard blocks. Consequently, the horizontal movement distance of the RC's trolley cannot be determined solely from the stack index. To address this, a three-dimensional coordinate system is established, as shown in Fig. A.1.

In this system, the x-axis corresponds to the RC's trolley movement direction, determined by the layout information of the RCS and the container's operational position; the y-axis represents the bay position; and the z-axis denotes the stacking tier. By combining the initial and final coordinates of container i, both the horizontal and vertical travel distances of the RC can be determined.

For container i belonging to the 1st container flow, the RC sequentially performs the following actions: (1) spreader lowering, t_2^{RC}; (2) lifting the container, t_2^{RC}; (3) gantry movement across bays, $\left|y_i^f - y_i^s\right| \cdot t_1^{RC}$; (4) trolley movement along the x-axis, $\left|x_i^f - x_i^s\right| / v_{tro}^{RC}$; and (5) lowering the spreader for placement, t_2^{RC}. Hence, the total handling time for the 1st container flow is represented in Eq. (A.1).

For export containers in the 2nd - 5th flows, the RC transfers containers from the railway (or railway yard) to the matched AGV. During this process, the gantry remains stationary since the AGV operates in the bay-aligned lane. The RC's handling time includes: (1) spreader lowering, t_2^{RC}; (2) lifting the container, t_2^{RC}; (3) trolley movement to the AGV operation lane, $\left|x_{RV} - x_i^s\right| / v_{tro}^{RC}$. The subsequent lowering and placement operations are included in the RC-AGV interaction time and thus excluded from the handling duration.

Similarly, for import containers in the 2nd - 5th flows, the RC first lifts the container from the AGV and then places it onto the railway (or railway yard), where the trolley movement distance is calculated as $\left|x_{RV} - x_i^f\right|$.

The in-place setup time for the RC to handle two consecutive tasks is determined according to the relative positions of the containers and the corresponding container flow combination.

In the double-cycling mode, the RC successively handles two container tasks, resulting in a total of $(1 \times 4 + 3 \times 4 + 5 \times 4 + 7 \times 4 + 9 \times 4)$ possible scenarios. Among them, (1×4) represents the four scenarios where only the first container flow is considered, denoted as $(\mathcal{N}_1^E, \mathcal{N}_1^E)$, $(\mathcal{N}_1^E, \mathcal{N}_1^I)$, $(\mathcal{N}_1^I, \mathcal{N}_1^E)$, and $(\mathcal{N}_1^I, \mathcal{N}_1^I)$. The term $(1 \times 4 + 3 \times 4)$ denotes the cases where both the 1st and

2nd container flows are considered simultaneously. By analogy, when all possible combinations of flows are included, a total of 100 scenarios exist for a single RC handling two consecutive containers. The required setup time for each scenario ($s^{RC}_{(i,j)}$) is analyzed as follows.

When two consecutive container tasks (i, j) handled by a single RC satisfy any of the following four conditions: (1) $i, j \in \mathcal{N}_1$, (2) $i \in \mathcal{N}_1, j \in \mathcal{N}^E_c, c = 2,3,4,5$, (3) $i \in \mathcal{N}^I_c, j \in \mathcal{N}_1, c = 2,3,4,5$, or (4) $i \in \mathcal{N}^I_c, j \in \mathcal{N}^E_c, c = 2,3,4,5$, the setup time of the RC is calculated as:

$$s^{RC}_{(i,j)} = t^{RC}_2 + \left|x^f_i - x^s_j\right| / v^{RC}_{tro} + \left|y^f_i - y^s_j\right| \cdot t^{RC}_1 \tag{A.2}$$

When two tasks satisfy either $i \in \mathcal{N}_1, j \in \mathcal{N}^I_c, c = 2,3,4,5$ or $i \in \mathcal{N}^I_c, j \in \mathcal{N}^I_{c'}, c, c' = 2,3,4,5$, the setup time of the RC is given by:

$$s^{RC}_{(i,j)} = t^{RC}_2 + \left|x^f_i - x_{RV}\right| / v^{RC}_{tro} + \left|y^f_i - y^f_j\right| \cdot t^{RC}_1 \tag{A.3}$$

When two tasks satisfy either $i \in \mathcal{N}^E_c, j \in \mathcal{N}_1, c = 2,3,4,5$ or $i \in \mathcal{N}^E_c, j \in \mathcal{N}^E_{c'}, c, c' = 2,3,4,5$, the setup time is calculated as:

$$s^{RC}_{(i,j)} = t^{RC}_2 + \left|x_{RV} - x^s_j\right| / v^{RC}_{tro} + \left|y^s_i - y^s_j\right| \cdot t^{RC}_1 \tag{A.4}$$

When two tasks satisfy $i \in \mathcal{N}^E_c, j \in \mathcal{N}^I_{c'}, c, c' = 2,3,4,5$, the setup time of the RC is determined as:

$$s^{RC}_{(i,j)} = t^{RC}_2 + \left|y^s_i - y^f_j\right| \cdot t^{RC}_1 \tag{A.5}$$

A.2. Calculation of YC handling and setup times

The handling time and in-place setup time of the YC are derived from the spatial relationships between containers and the cooperative operation with AGVs.

The time required for the YC to handle container i (p^{YC}_i) is calculated as shown in Eq. (A.6).

$$p^{YC}_i = \begin{cases} 2t^{YC}_2 + \left|x^s_i - x_{YV}\right| / v^{YC}_{tro}, \forall i \in \mathcal{N}^I_2 \cup \mathcal{N}^I_3 \cup \mathcal{N}^E_6 \\ 2t^{YC}_2 + \left|x_{YV} - x^f_i\right| / v^{YC}_{tro}, \forall i \in \mathcal{N}^E_2 \cup \mathcal{N}^E_3 \cup \mathcal{N}^I_6 \end{cases} \tag{A.6}$$

The in-place setup time ($s^{YC}_{(i,j)}$) between two consecutive YC handling tasks (i, j) depends on the relative positions of the containers and their corresponding flow combinations. Considering all operational cases, the setup time is calculated as follows:

$$s^{YC}_{(i,j)} = \begin{cases} t^{YC}_2 + \left|x^f_i - x_{YV}\right| / v^{YC}_{tro} + \left|y^f_i - y^f_j\right| \cdot t^{YC}_1, i, j \in \mathcal{N}^E_2 \cup \mathcal{N}^E_3 \cup \mathcal{N}^I_6 \\ t^{YC}_2 + \left|x^f_i - x^s_j\right| / v^{YC}_{tro} + \left|y^f_i - y^s_j\right| \cdot t^{YC}_1, i \in \mathcal{N}^E_2 \cup \mathcal{N}^E_3 \cup \mathcal{N}^I_6, j \in \mathcal{N}^I_2 \cup \mathcal{N}^I_3 \cup \mathcal{N}^E_6 \\ t^{YC}_2 + \left|y^s_i - y^f_j\right| \cdot t^{YC}_1, i \in \mathcal{N}2^I \cup \mathcal{N}^I_3 \cup \mathcal{N}^E_6, j \in \mathcal{N}^E_2 \cup \mathcal{N}^E_3 \cup \mathcal{N}^I_6 \\ t^{YC}_2 + \left|x_{YV} - x^s_j\right| / v^{YC}_{tro} + \left|y^s_i - y^s_j\right| \cdot t^{YC}_1, i, j \in \mathcal{N}^I_2 \cup \mathcal{N}^I_3 \cup \mathcal{N}^E_6 \end{cases} \tag{A.7}$$

A.3. Calculation of AGV transportation and setup times

In this study, the AGV is assumed to travel at a constant speed without acceleration or deceleration. Accordingly, the travel time for the AGV to transport container i (t^{AGV}_i), the time for an unloaded AGV to reach the starting point of containe j ($t^{AGV}_{(i,j)}$), the time for an AGV to move to charging facility k after completing container i ($t^{V\_Ch}_{(i,k)}$), and the time for an AGV to move from charging facility k to the starting point of container i ($t^{Ch\_V}_{(k,i)}$) are formulated as follows:

$$t^{AGV}_i = d^{AGV}_i / v^{AGV}_{load}, \forall i \in \mathcal{N} \backslash \mathcal{N}_1 \tag{A.8}$$

$$t^{AGV}_{(i,j)} = d^{AGV}_{(i,j)} / v^{AGV}_{em}, \forall i, j \in \mathcal{N} \backslash \mathcal{N}_1, i \neq j \tag{A.9}$$

$$t^{V\_Ch}_{(i,k)} = d^{V\_Ch}_{(i,k)} / v^{AGV}_{em}, \forall i \in \mathcal{N} \backslash \mathcal{N}_1, k \in K \tag{A.10}$$

$$t^{Ch\_V}_{(k,i)} = d^{Ch\_V}_{(k,i)} / v^{AGV}_{em}, \forall vi \in \mathcal{N} \backslash \mathcal{N}_1, k \in K \tag{A.11}$$

Appendix B. AGV energy consumption analysis

This section provides the detailed derivations and parameter definitions of the AGV energy-consumption model introduced in Section 3.2.The analysis is conducted with reference to the electric-vehicle energy model proposed by Murakami (2017). The energy required for an AGV to travel between nodes (m, n) is expressed as:

$$e_{mn} = \phi\varphi \cdot \left[\varsigma\left(w_{self} + w_{load}\right)v_{mn} + \frac{1}{2}\varrho_d F \rho_{air} v_{mn}^3\right] \cdot t_{mn} \tag{B.1}$$

where e_{mn} denotes the energy consumption of the AGV traveling between nodes (m, n), ϕ is the efficiency parameter of motor mode, φ denotes the efficiency parameter for discharging, ς is the route specific coefficient and calculated as $\varsigma = a_{mn} + g\sin\gamma_{mn} + \varrho_r g\cos\gamma_{mn}$, a_{mn} is the acceleration of the AGV between nodes (m, n), g is the gravitational constant, γ_{mn} is the road angle between nodes (m, n), ϱ_r is the coefficient of rolling resistance, w_{self} is the weight of the AGV, w_{load} denotes the container weight of the AGV load, F is the frontal surface area of the AGV, ρ_{air} denotes air density, ϱ_d is the coefficient of aerodynamic drag, v_{mn} is travel speed of the AGV between nodes (m, n), and t_{mn} is the time needed for the AGV to move between nodes (m, n). In particular, in this paper, it is considered that the AGV is traveling at a constant speed between nodes (m, n), so $t_{mn} = d_{mn}/v_{mn}$.

Based on the above physical formulation, AGV energy consumption depends on the loading state of the vehicle. To maintain a clear and tractable scheduling model in the main text, the detailed physical expressions are abstracted into two energy-consumption coefficients, corresponding to loaded and empty travel, respectively.

Specifically, the energy-consumption coefficient for loaded AGV travel, enoted by κ^L, is derived from Eq. (B.1) by considering the AGV operating with a container load and is expressed as:

$$\kappa^L = \phi\varphi \cdot \left[\varsigma(w_{self} + w_{load}) + \frac{1}{2}\varrho_d F_{load}\rho_{air} v_{load}^{AGV\,2}\right] \tag{B.2}$$

where F_{load} denotes the frontal surface area of the AGV under loaded conditions.

Similarly, the energy-consumption coefficient for empty AGV travel, denoted by κ^E, is computed as:

$$\kappa^E = \phi\varphi \cdot \left[\varsigma w_{self} + \frac{1}{2}\varrho_d F_{em}\rho_{air} v_{em}^{AGV\,2}\right] \tag{B.3}$$

where F_{em} represents the frontal surface area of the AGV in the empty state.

In the scheduling model presented in Section 3.2, AGV energy consumption is calculated as the product of the corresponding energy-consumption coefficient (κ^L or κ^E) and the travel distance.

Appendix C. Model and algorithm validation under a small-scale instance

To further verify the correctness of the proposed mathematical model and the reliability of the DI-iGA implementation, a highly simplified small-scale test instance is constructed and analyzed in this appendix.

C.1. Instance description

The test instance consists of five containers, one AGV, one QC, two YCs, two RCs, and one charging facility. The container flow types, equipment processing times, AGV travel times, and energy-consumption parameters are all treated as known deterministic inputs. Their definitions and value settings are consistent with those adopted in the main model.

Specifically, the container flow types, QC assignment relationships, and the processing times of RCs and YCs are listed in Table C.1. The setup times between consecutive RC and YC operations are given in Tables C.2 and C.3, respectively. The AGV travel times between different container tasks and between container tasks and the charging facility are provided in Table C.4, while the corresponding AGV energy-consumption parameters are summarized in Table C.5. All parameter definitions are consistent with those in Table 1 of the main text and are therefore not repeated here.

Table C.1
Input data for the small-scale validation instance.

Container ID	Container Flow	$\sigma_{(q,i)}^{QC}$	QC Processing Order	p_i^{RC} (min)	p_i^{YC} (min)	t_i^{AGV} (min)	e_i^{RC} (min)
1	1	Nan	Nan	2.77	0.00	0.00	0.00
2	-3	Nan	Nan	1.11	1.59	5.05	0.92
3	5	1	3	1.08	0.00	4.73	0.86
4	6	1	1	0.00	1.48	4.78	1.78
5	6	1	2	0.00	1.30	5.68	2.09

In addition, p^{QC} and s^{QC} are fixed at 2 min and 1 min, respectively, and the interaction times θ^{QC}, θ^{RC}, and θ^{YC} are all set to 1 min.

Table C.2
Setup times between consecutive RC tasks handled by the same RC, $s^{RC}_{(i,j)}$ (min).

	To				
From	Container 1	Container 2	Container 3	Container 4	Container 5
Container 1	0.00	2.02	0.42	Nan	Nan
Container 2	3.24	0.00	1.74	Nan	Nan
Container 3	1.67	1.77	0.00	Nan	Nan
Container 4	Nan	Nan	Nan	Nan	Nan
Container 5	Nan	Nan	Nan	Nan	Nan

Table C.3
Setup times between consecutive YC tasks handled by the same YC, $s^{YC}_{(i,j)}$ (min).

From \ To	Container 1	Container 2	Container 3	Container 4	Container 5
Container 1	Nan	Nan	Nan	Nan	Nan
Container 2	Nan	0.00	Nan	2.71	4.74
Container 3	Nan	Nan	Nan	Nan	Nan
Container 4	Nan	2.59	Nan	0.00	2.59
Container 5	Nan	4.63	Nan	2.59	0.00

Table C.4
AGV travel time, $t^{AGV}_{(i,j)}$, $t^{V\_Ch}_{(i,k)}$, and $t^{Ch\_V}_{(k,i)}$ (min).

From	Container 1	Container 2	Container 3	Container 4	Container 5	Charger 1
Container 1	Nan	Nan	Nan	Nan	Nan	Nan
Container 2	Nan	0.00	3.01	3.01	3.01	0.85
Container 3	Nan	0.47	0.00	3.55	3.55	5.10
Container 4	Nan	3.11	3.69	0.00	3.69	1.52
Container 5	Nan	2.44	4.36	4.36	0.00	2.20
Charger 1	Nan	4.64	2.33	2.33	2.33	0.00

Table C.5
AGV energy consumption, $e^{AGV}_{(i,j)}$, $e^{V\_Ch}_{(i,k)}$, and $e^{Ch\_V}_{(k,i)}$ (kWh).

From \ To	Container 1	Container 2	Container 3	Container 4	Container 5	Charger 1
Container 1	Nan	Nan	Nan	Nan	Nan	Nan
Container 2	Nan	0.00	0.62	0.62	0.62	0.17
Container 3	Nan	0.10	0.00	0.73	0.73	1.06
Container 4	Nan	0.64	0.76	0.00	0.76	0.32
Container 5	Nan	0.50	0.90	0.90	0.00	0.46
Charger 1	Nan	0.96	0.48	0.48	0.48	0.00

C.2. Manual feasibility validation

In this small-scale validation instance, the system is configured with a single AGV, and only four container tasks (Containers 2, 3, 4, and 5) require AGV transportation. Among them, three containers (Containers 3, 4, and 5) must be handled by the same QC according to a predetermined processing sequence. Given the limited number of AGVs and the fixed QC processing order, only a finite number of feasible AGV transportation sequences exist. Considering the above constraints, four feasible AGV transportation sequences can be enumerated, namely: (1) 2-4-5-3, (2) 4-2-5-3, (3) 4-5-2-3, and (4) 4-5-3-2.

Taking the transportation sequence (2-4-5-3) as an illustrative example, the manual derivation process for the first AGV transportation task (Container 2) is presented below. The resulting key time instants and battery level evolution for this transportation sequence are summarized in Table C.6.

Container 2 follows the operation chain RC-AGV-YC. The RC processing time is 1.11 *min*; therefore, the RC can start processing at time 0 and completes the preparation for AGV handover at 1.11 *min*. Considering an RC-AGV interaction time of 1 *min*, the AGV transportation for Container 2 cannot start earlier than 2.11 *min*, and the RC operation completion time is also no earlier than 2.11 *min*. The loaded transportation time of the AGV for Container 2 is 5.05 *min*; thus, the AGV arrival time at the YC position is no earlier than 7.16 *min*, and the YC operation cannot start before that time. Considering an AGV-YC interaction time of 1 *min*, the AGV finishes the transportation task no earlier than 8.16 min. Given the YC processing time of 1.59 *min*, the YC operation for Container 2 is completed no earlier than 9.75 *min*.

For subsequent AGV tasks, the time derivation follows the same temporal connection logic, with the AGV repositioning and interaction times serving as the core reference for task continuity. The start and completion times of RC, YC, and QC operations are

Table C.6
Key time instants and remaining energy for the transportation sequence (2-4-5-3).

Container 2	$\overline{\tau}^{RC}_{(r,2)}$	0.00	$\overline{\tau}^{AGV}_{(1,2)}$	1.11	$\underline{\tau}^{RC}_{(r,2)}$	2.11	$\overline{\tau}^{YC}_{(y,2)}$	7.16	$\underline{\tau}^{AGV}_{(1,2)}$	8.16	$\underline{\tau}^{YC}_{(y,2)}$	9.75	$\overline{\varepsilon}^{AGV}_{(1,2)}$	35.60	$\underline{\varepsilon}^{AGV}_{(1,2)}$	34.38
Container 4	$\overline{\tau}^{QC}_{(1,4)}$	9.17	$\overline{\tau}^{AGV}_{(1,4)}$	11.17	$\underline{\tau}^{QC}_{(1,4)}$	12.17	$\overline{\tau}^{YC}_{(y,4)}$	16.95	$\underline{\tau}^{AGV}_{(1,4)}$	17.95	$\underline{\tau}^{YC}_{(y,4)}$	19.43	$\overline{\varepsilon}^{AGV}_{(1,4)}$	33.76	$\underline{\varepsilon}^{AGV}_{(1,4)}$	31.68
Container 5	$\overline{\tau}^{QC}_{(1,5)}$	19.64	$\overline{\tau}^{AGV}_{(1,5)}$	21.64	$\underline{\tau}^{QC}_{(1,5)}$	22.64	$\overline{\tau}^{YC}_{(y,5)}$	28.32	$\underline{\tau}^{AGV}_{(1,5)}$	29.32	$\underline{\tau}^{YC}_{(y,5)}$	30.62	$\overline{\varepsilon}^{AGV}_{(1,5)}$	30.92	$\underline{\varepsilon}^{AGV}_{(1,5)}$	28.53
Container 3	$\overline{\tau}^{QC}_{(1,3)}$	31.68	$\overline{\tau}^{AGV}_{(1,3)}$	33.68	$\underline{\tau}^{QC}_{(1,3)}$	34.68	$\overline{\tau}^{RC}_{(r,3)}$	39.41	$\underline{\tau}^{AGV}_{(1,3)}$	40.41	$\underline{\tau}^{RC}_{(r,3)}$	41.49	$\overline{\varepsilon}^{AGV}_{(1,3)}$	27.63	$\underline{\varepsilon}^{AGV}_{(1,3)}$	26.47

Note: $\overline{\tau}^{AGV}_{(1,i)}$, $\underline{\tau}^{AGV}_{(1,i)}$, $\overline{\tau}^{RC}_{(r,i)}$, $\underline{\tau}^{RC}_{(r,i)}$, $\overline{\tau}^{QC}_{(q,i)}$, $\underline{\tau}^{QC}_{(q,i)}$, $\overline{\tau}^{YC}_{(y,i)}$, and $\underline{\tau}^{YC}_{(y,i)}$ (unit: *min*); $\overline{\varepsilon}^{AGV}_{(1,i)}$ and $\underline{\varepsilon}^{AGV}_{(1,i)}$ (unit: kWh).

determined accordingly based on their respective processing durations and interaction constraints; therefore, the detailed step-by-step derivations are not repeated. It should be noted that, in this small-scale instance, the assignments of RCs and YCs are selected from feasible combinations permitted by the model, and all inter-equipment continuity, temporal precedence, and safety constraints are satisfied.

From the energy perspective, the initial battery level of the AGV is set to $0.4 \times 89 = 35.60\ kWh$. The loaded transportation energy consumption for Container 2 is $0.92\ kWh$. In addition, considering a waiting energy consumption rate of $0.15\ kWh/min$ per minute, the remaining battery level after completing this task is calculated as $35.6 - 0.92 - 0.15 \times 2 = 34.38\ kWh$, which is higher than the charging threshold of $0.3 \times 89 = 26.7\ kWh$. Therefore, no charging operation is required. The energy consumption calculation for subsequent tasks follows the same logic. It is further noted that, although the remaining battery level after completing the last AGV transportation task (Container 3) is lower than the charging threshold, no charging operation is scheduled since no further transportation tasks remain.

For the remaining three AGV transportation sequences, namely (2) 4-2-5-3, (3) 4-5-2-3, and (4) 4-5-3-2, the corresponding key time instants and energy consumption results are summarized in Tables C.7–C.9, respectively.

Table C.7
Key time instants and remaining energy for the transportation sequence (4-2-5-3).

Container 4	$\overline{\tau}^{QC}_{(1,4)}$	0.00	$\overline{\tau}^{AGV}_{(1,4)}$	2.00	$\underline{\tau}^{QC}_{(1,4)}$	3.00	$\overline{\tau}^{YC}_{(y,4)}$	7.78	$\underline{\tau}^{AGV}_{(1,4)}$	8.78	$\underline{\tau}^{YC}_{(y,4)}$	10.26	$\overline{\varepsilon}^{AGV}_{(1,4)}$	35.60	$\underline{\varepsilon}^{AGV}_{(1,4)}$	33.52
Container 2	$\overline{\tau}^{RC}_{(r,2)}$	10.78	$\overline{\tau}^{AGV}_{(1,2)}$	11.89	$\underline{\tau}^{RC}_{(r,2)}$	12.89	$\overline{\tau}^{YC}_{(y,2)}$	17.94	$\underline{\tau}^{AGV}_{(1,2)}$	18.94	$\underline{\tau}^{YC}_{(y,2)}$	20.53	$\overline{\varepsilon}^{AGV}_{(1,2)}$	32.88	$\underline{\varepsilon}^{AGV}_{(1,2)}$	31.66
Container 5	$\overline{\tau}^{QC}_{(1,5)}$	19.95	$\overline{\tau}^{AGV}_{(1,5)}$	21.95	$\underline{\tau}^{QC}_{(1,5)}$	22.95	$\overline{\tau}^{YC}_{(y,5)}$	28.63	$\underline{\tau}^{AGV}_{(1,5)}$	29.63	$\underline{\tau}^{YC}_{(y,5)}$	30.93	$\overline{\varepsilon}^{AGV}_{(1,5)}$	31.04	$\underline{\varepsilon}^{AGV}_{(1,5)}$	28.65
Container 3	$\overline{\tau}^{QC}_{(1,3)}$	31.99	$\overline{\tau}^{AGV}_{(1,3)}$	33.99	$\underline{\tau}^{QC}_{(1,3)}$	34.99	$\overline{\tau}^{RC}_{(r,3)}$	39.72	$\underline{\tau}^{AGV}_{(1,3)}$	40.72	$\underline{\tau}^{RC}_{(r,3)}$	41.80	$\overline{\varepsilon}^{AGV}_{(1,3)}$	27.75	$\underline{\varepsilon}^{AGV}_{(1,3)}$	26.59

Note: $\overline{\tau}^{AGV}_{(1,i)}$, $\underline{\tau}^{AGV}_{(1,i)}$, $\overline{\tau}^{RC}_{(r,i)}$, $\underline{\tau}^{RC}_{(r,i)}$, $\overline{\tau}^{QC}_{(q,i)}$, $\underline{\tau}^{QC}_{(q,i)}$, $\overline{\tau}^{YC}_{(y,i)}$, and $\underline{\tau}^{YC}_{(y,i)}$ (unit: *min*); $\overline{\varepsilon}^{AGV}_{(1,i)}$ and $\underline{\varepsilon}^{AGV}_{(1,i)}$ (unit: kWh).

Table C.8
Key time instants and remaining energy for the transportation sequence (4-5-2-3).

Container 4	$\overline{\tau}^{QC}_{(1,4)}$	0.00	$\overline{\tau}^{AGV}_{(1,4)}$	2.00	$\underline{\tau}^{QC}_{(1,4)}$	3.00	$\overline{\tau}^{YC}_{(y,4)}$	7.78	$\underline{\tau}^{AGV}_{(1,4)}$	8.78	$\underline{\tau}^{YC}_{(y,4)}$	10.26	$\overline{\varepsilon}^{AGV}_{(1,4)}$	35.60	$\underline{\varepsilon}^{AGV}_{(1,4)}$	33.52
Container 5	$\overline{\tau}^{QC}_{(1,5)}$	10.47	$\overline{\tau}^{AGV}_{(1,5)}$	12.47	$\underline{\tau}^{QC}_{(1,5)}$	13.47	$\overline{\tau}^{YC}_{(y,5)}$	19.15	$\underline{\tau}^{AGV}_{(1,5)}$	20.15	$\underline{\tau}^{YC}_{(y,5)}$	21.45	$\overline{\varepsilon}^{AGV}_{(1,5)}$	32.76	$\underline{\varepsilon}^{AGV}_{(1,5)}$	30.37
Container 2	$\overline{\tau}^{RC}_{(r,2)}$	20.59	$\overline{\tau}^{AGV}_{(1,2)}$	22.59	$\underline{\tau}^{RC}_{(r,2)}$	23.59	$\overline{\tau}^{YC}_{(y,2)}$	28.64	$\underline{\tau}^{AGV}_{(1,2)}$	29.64	$\underline{\tau}^{YC}_{(y,2)}$	31.23	$\overline{\varepsilon}^{AGV}_{(1,2)}$	29.87	$\underline{\varepsilon}^{AGV}_{(1,2)}$	28.65
Container 3	$\overline{\tau}^{QC}_{(1,3)}$	30.65	$\overline{\tau}^{AGV}_{(1,3)}$	32.65	$\underline{\tau}^{QC}_{(1,3)}$	33.65	$\overline{\tau}^{RC}_{(r,3)}$	38.38	$\underline{\tau}^{AGV}_{(1,3)}$	39.38	$\underline{\tau}^{RC}_{(r,3)}$	40.46	$\overline{\varepsilon}^{AGV}_{(1,3)}$	28.03	$\underline{\varepsilon}^{AGV}_{(1,3)}$	26.87

Note: $\overline{\tau}^{AGV}_{(1,i)}$, $\underline{\tau}^{AGV}_{(1,i)}$, $\overline{\tau}^{RC}_{(r,i)}$, $\underline{\tau}^{RC}_{(r,i)}$, $\overline{\tau}^{QC}_{(q,i)}$, $\underline{\tau}^{QC}_{(q,i)}$, $\overline{\tau}^{YC}_{(y,i)}$, and $\underline{\tau}^{YC}_{(y,i)}$ (unit: *min*); $\overline{\varepsilon}^{AGV}_{(1,i)}$ and $\underline{\varepsilon}^{AGV}_{(1,i)}$ (unit: kWh).

Table C.9
Key time instants and remaining energy for the transportation sequence (4-5-3-2).

Container 4	$\overline{\tau}^{QC}_{(1,4)}$	0	$\overline{\tau}^{AGV}_{(1,4)}$	2	$\underline{\tau}^{QC}_{(1,4)}$	3	$\overline{\tau}^{YC}_{(y,4)}$	7.78	$\underline{\tau}^{AGV}_{(1,4)}$	8.78	$\underline{\tau}^{YC}_{(y,4)}$	10.26	$\overline{\varepsilon}^{AGV}_{(1,4)}$	35.6	$\underline{\varepsilon}^{AGV}_{(1,4)}$	33.52
Container 5	$\overline{\tau}^{QC}_{(1,5)}$	10.47	$\overline{\tau}^{AGV}_{(1,5)}$	12.47	$\underline{\tau}^{QC}_{(1,5)}$	13.47	$\overline{\tau}^{YC}_{(y,5)}$	19.15	$\underline{\tau}^{AGV}_{(1,5)}$	20.15	$\underline{\tau}^{YC}_{(y,5)}$	21.45	$\overline{\varepsilon}^{AGV}_{(1,5)}$	32.76	$\underline{\varepsilon}^{AGV}_{(1,5)}$	30.37
Container 3	$\overline{\tau}^{QC}_{(1,3)}$	22.51	$\overline{\tau}^{AGV}_{(1,3)}$	24.51	$\underline{\tau}^{QC}_{(1,3)}$	25.51	$\overline{\tau}^{RC}_{(r,3)}$	30.24	$\underline{\tau}^{AGV}_{(1,3)}$	31.24	$\underline{\tau}^{RC}_{(r,3)}$	32.32	$\overline{\varepsilon}^{AGV}_{(1,3)}$	29.47	$\underline{\varepsilon}^{AGV}_{(1,3)}$	28.31
Container 2	$\overline{\tau}^{RC}_{(r,2)}$	30.6	$\overline{\tau}^{AGV}_{(1,2)}$	31.71	$\underline{\tau}^{RC}_{(r,2)}$	32.71	$\overline{\tau}^{YC}_{(y,2)}$	37.76	$\underline{\tau}^{AGV}_{(1,2)}$	38.76	$\underline{\tau}^{YC}_{(y,2)}$	40.35	$\overline{\varepsilon}^{AGV}_{(1,2)}$	28.21	$\underline{\varepsilon}^{AGV}_{(1,2)}$	26.99

Note: $\overline{\tau}^{AGV}_{(1,i)}$, $\underline{\tau}^{AGV}_{(1,i)}$, $\overline{\tau}^{RC}_{(r,i)}$, $\underline{\tau}^{RC}_{(r,i)}$, $\overline{\tau}^{QC}_{(q,i)}$, $\underline{\tau}^{QC}_{(q,i)}$, $\overline{\tau}^{YC}_{(y,i)}$, and $\underline{\tau}^{YC}_{(y,i)}$ (unit: *min*); $\overline{\varepsilon}^{AGV}_{(1,i)}$ and $\underline{\varepsilon}^{AGV}_{(1,i)}$ (unit: kWh).

For the four feasible AGV transportation sequences, the corresponding makespan values are 41.49, 41.80, 40.46, and 40.35 *min*, respectively. Since no charging operation is triggered in this small-scale instance, the charging duration is zero in all cases. Accordingly, the resulting objective function values are 20.75, 20.90, 20.23, and 20.18 *min*, respectively. It can therefore be observed that the fourth transportation sequence, in which the AGV serves containers in the order 4-5-3-2, yields the minimum objective value and is identified as the optimal solution for this instance.

C.3. Exact validation based on Gurobi

To further verify the correctness and completeness of the proposed mathematical model, this subsection employs Gurobi to obtain the exact solution for the small-scale validation instance described in Appendix C.1, and compares the results with those derived from the manual feasibility analysis.

The Gurobi solution results are summarized in Table C.10. For this instance, the optimal AGV transportation sequence obtained by Gurobi is 4-5-3-2, which is fully consistent with the optimal sequence identified in the manual feasibility analysis. Meanwhile, the RC and YC assignment schemes provided by Gurobi satisfy all model constraints related to continuous equipment operations and safety requirements, and no equipment conflicts are observed.

Table C.10
Exact scheduling solution for the small-scale validation instance obtained by Gurobi.

Container 1	$\overline{\tau}^{RC}_{(2,1)}$	0.00	$\underline{\tau}^{RC}_{(2,1)}$	2.77											
Container 4	$\overline{\tau}^{QC}_{(1,4)}$	0.00	$\overline{\tau}^{AGV}_{(1,4)}$	2.00	$\underline{\tau}^{QC}_{(1,4)}$	3.00	$\overline{\tau}^{YC}_{(1,4)}$	7.78	$\underline{\tau}^{AGV}_{(1,4)}$	8.78	$\underline{\tau}^{YC}_{(1,4)}$	10.26	$\overline{\varepsilon}^{AGV}_{(1,4)}$	35.6	$\underline{\varepsilon}^{AGV}_{(1,4)}$	33.52
Container 5	$\overline{\tau}^{QC}_{(1,5)}$	10.47	$\overline{\tau}^{AGV}_{(1,5)}$	12.47	$\underline{\tau}^{QC}_{(1,5)}$	13.47	$\overline{\tau}^{YC}_{(2,5)}$	19.15	$\underline{\tau}^{AGV}_{(1,5)}$	20.15	$\underline{\tau}^{YC}_{(2,5)}$	21.45	$\overline{\varepsilon}^{AGV}_{(1,5)}$	32.76	$\underline{\varepsilon}^{AGV}_{(1,5)}$	30.37
Container 3	$\overline{\tau}^{QC}_{(1,3)}$	22.51	$\overline{\tau}^{AGV}_{(1,3)}$	24.51	$\underline{\tau}^{QC}_{(1,3)}$	25.51	$\overline{\tau}^{RC}_{(2,3)}$	30.24	$\underline{\tau}^{AGV}_{(1,3)}$	31.24	$\underline{\tau}^{RC}_{(2,3)}$	40.35	$\overline{\varepsilon}^{AGV}_{(1,2)}$	29.47	$\underline{\varepsilon}^{AGV}_{(1,3)}$	28.31
Container 2	$\overline{\tau}^{RC}_{(1,2)}$	22.55	$\overline{\tau}^{AGV}_{(1,2)}$	31.71	$\underline{\tau}^{RC}_{(1,2)}$	32.71	$\overline{\tau}^{YC}_{(1,2)}$	37.76	$\underline{\tau}^{AGV}_{(1,2)}$	38.76	$\underline{\tau}^{YC}_{(1,2)}$	40.35	$\overline{\varepsilon}^{AGV}_{(1,2)}$	27.92	$\underline{\varepsilon}^{AGV}_{(1,2)}$	26.70

Note: $\overline{\tau}^{AGV}_{(1,i)}$, $\underline{\tau}^{AGV}_{(1,i)}$, $\overline{\tau}^{RC}_{(r,i)}$, $\underline{\tau}^{RC}_{(r,i)}$, $\overline{\tau}^{QC}_{(q,i)}$, $\underline{\tau}^{QC}_{(q,i)}$, $\overline{\tau}^{YC}_{(y,i)}$, and $\underline{\tau}^{YC}_{(y,i)}$ (unit: *min*); $\overline{\varepsilon}^{AGV}_{(1,i)}$ and $\underline{\varepsilon}^{AGV}_{(1,i)}$ (unit: kWh).

With respect to key performance indicators, including the maximum completion time and charging duration, the Gurobi solution is consistent with the manual analysis results, yielding values of 40.35 *min* and 0 *min*, respectively. Accordingly, the objective function value is 20.18 *min*.

The above results demonstrate that the proposed mathematical model is able to accurately capture the coupling relationships among multi-equipment collaborative scheduling and AGV energy constraints under the small-scale instance. The exact solution obtained by Gurobi is consistent with the manual feasibility analysis. For RC/YC assignments, as well as certain non-critical start/end times and energy-related variables, the specific values may differ due to the existence of slackness in inequality constraints, and such variations are therefore acceptable.

C.4. Validation based on the DI-iGA algorithm

Based on the above small-scale instance, the proposed DI-iGA algorithm is further applied to the same instance for solution validation. To ensure a fair comparison, all input parameters used in DI-iGA, including processing times, travel times, energy-consumption parameters, and initial battery level settings, are kept identical to those adopted in the Gurobi-based exact solution.

The solution obtained by DI-iGA is reported in Table C.11. The results show that DI-iGA yields the same optimal AGV transportation sequence, namely 4-5-3-2, with a maximum completion time of 40.35 *min*, zero charging duration, and a corresponding objective value of 20.18 *min*. These results are fully consistent with those derived from the manual feasibility analysis and the Gurobi-based exact optimization. Moreover, during the solution process, the proposed DI-iGA algorithm endogenously tightens the inequality constraints, resulting in an equivalent optimal schedule with tighter time and energy variable realizations.

Table C.11
Optimal scheduling solution obtained by DI-iGA for the small-scale validation instance.

Container 1	$\overline{\tau}^{RC}_{(2,1)}$	0.00	$\underline{\tau}^{RC}_{(2,1)}$	2.77											
Container 4	$\overline{\tau}^{QC}_{(1,4)}$	0.00	$\overline{\tau}^{AGV}_{(1,4)}$	2.00	$\underline{\tau}^{QC}_{(1,4)}$	3.00	$\overline{\tau}^{YC}_{(1,4)}$	7.78	$\underline{\tau}^{AGV}_{(1,4)}$	8.78	$\underline{\tau}^{YC}_{(1,4)}$	10.26	$\overline{\varepsilon}^{AGV}_{(1,4)}$	35.6	$\underline{\varepsilon}^{AGV}_{(1,4)}$	33.52
Container 5	$\overline{\tau}^{QC}_{(1,5)}$	10.47	$\overline{\tau}^{AGV}_{(1,5)}$	12.47	$\underline{\tau}^{QC}_{(1,5)}$	13.47	$\overline{\tau}^{YC}_{(2,5)}$	19.15	$\underline{\tau}^{AGV}_{(1,5)}$	20.15	$\underline{\tau}^{YC}_{(2,5)}$	21.45	$\overline{\varepsilon}^{AGV}_{(1,5)}$	32.76	$\underline{\varepsilon}^{AGV}_{(1,5)}$	30.37
Container 3	$\overline{\tau}^{QC}_{(1,3)}$	22.51	$\overline{\tau}^{AGV}_{(1,3)}$	24.51	$\underline{\tau}^{QC}_{(1,3)}$	25.51	$\overline{\tau}^{RC}_{(2,3)}$	30.24	$\underline{\tau}^{AGV}_{(1,3)}$	31.24	$\underline{\tau}^{RC}_{(2,3)}$	32.32	$\overline{\varepsilon}^{AGV}_{(1,2)}$	29.47	$\underline{\varepsilon}^{AGV}_{(1,3)}$	28.31
Container 2	$\overline{\tau}^{RC}_{(1,2)}$	30.6	$\overline{\tau}^{AGV}_{(1,2)}$	31.71	$\underline{\tau}^{RC}_{(1,2)}$	32.71	$\overline{\tau}^{YC}_{(1,2)}$	37.76	$\underline{\tau}^{AGV}_{(1,2)}$	38.76	$\underline{\tau}^{YC}_{(1,2)}$	40.35	$\overline{\varepsilon}^{AGV}_{(1,2)}$	28.21	$\underline{\varepsilon}^{AGV}_{(1,2)}$	26.99

Note: $\overline{\tau}^{AGV}_{(1,i)}$, $\underline{\tau}^{AGV}_{(1,i)}$, $\overline{\tau}^{RC}_{(r,i)}$, $\underline{\tau}^{RC}_{(r,i)}$, $\overline{\tau}^{QC}_{(q,i)}$, $\underline{\tau}^{QC}_{(q,i)}$, $\overline{\tau}^{YC}_{(y,i)}$, and $\underline{\tau}^{YC}_{(y,i)}$ (unit: *min*); $\overline{\varepsilon}^{AGV}_{(1,i)}$ and $\underline{\varepsilon}^{AGV}_{(1,i)}$ (unit: kWh).

In summary, through the comparative validation based on manual feasibility analysis, exact solution obtained by Gurobi, and the proposed DI-iGA algorithm, it can be confirmed that the established mathematical model is capable of consistently capturing the coupling relationships between multi-equipment collaborative scheduling and AGV energy constraints in the small-scale instance. Moreover, the proposed DI-iGA algorithm is able to stably obtain optimal scheduling solutions that are consistent with those derived from the exact solver, without violating any time or energy constraints, thereby demonstrating its effectiveness and reliability.

References

Cai, L., Li, W., Zhou, B., Li, H., Yang, Z., 2024. Robust multi-equipment scheduling for U-shaped container terminals concerning double-cycling mode and uncertain operation time with cascade effects. Transp. Res. Part C Emerging Technol. 158, 104447. https://doi.org/10.1016/j.trc.2023.104447

Chai, X., Zheng, Z., Xiao, J., Yan, L., Qu, B., Wen, P., Wang, H., Zhou, Y., Sun, H., 2022. Multi-strategy fusion differential evolution algorithm for UAV path planning in complex environment. Aerosp. Sci. Technol. 121, 107287. https://doi.org/10.1016/j.ast.2021.107287
Chargui, K., Zouadi, T., Sreedharan, V.R., El Fallahi, A., Reghioui, M., 2023. A novel robust exact decomposition algorithm for berth and quay crane allocation and scheduling problem considering uncertainty and energy efficiency. Omega 118, 102868. https://doi.org/10.1016/j.omega.2023.102868
Ding, J., Dauzère-Pérès, S., Shen, L., Lü, Z., 2023. A novel evolutionary algorithm for energy-efficient scheduling in flexible job shops. IEEE Trans. Evol. Comput. 27 (5), 1470–1484. https://doi.org/10.1109/TEVC.2022.3222791
Gao, Y., Chang, D., Chen, C.-H., Sha, M., 2024. A digital twin-based decision support approach for AGV scheduling. Eng. Appl. Artif. Intell. 130, 107687. https://doi.org/10.1016/j.engappai.2023.107687
Gong, L., Huang, Z., Xiang, X., Liu, X., 2024. Real-time AGV scheduling optimisation method with deep reinforcement learning for energy-efficiency in the container terminal yard. Int. J. Prod. Res. 62 (21), 7722–7742. https://doi.org/10.1080/00207543.2024.2325583
Gupta, S., Deep, K., 2019. A hybrid self-adaptive sine cosine algorithm with opposition based learning. Expert Syst. Appl. 119, 210–230. https://doi.org/10.1016/j.eswa.2018.10.050
He, Y., Song, Z., Liu, Z., 2019. Fast-charging station deployment for battery electric bus systems considering electricity demand charges. Sustainable Cities Soc. 48, 101530. https://doi.org/10.1016/j.scs.2019.101530
Ji, B., Huang, H., Yu, S.S., 2023. An enhanced NSGA-II for solving berth allocation and quay crane assignment problem with stochastic arrival times. IEEE Trans. Intell. Transp. Syst. 24 (1), 459–473. https://doi.org/10.1109/TITS.2022.3213834
Kim, J.-D., Yu, J.-H., Choi, J.-H., Doh, H.-H., 2026. Machine learning-based hybrid preprocessing techniques for UAV spare parts demand forecasting. Eur. J. Ind. Eng. 21 (1), 33–53. https://doi.org/10.1504/EJIE.2026.151158
Kong, L., Ji, M., Yu, A., Gao, Z., 2024. Scheduling of automated guided vehicles for tandem quay cranes in automated container terminals. Comput. Oper. Res. 163, 106505. https://doi.org/10.1016/j.cor.2023.106505
Li, J., Chang, D., Wen, F., 2025a. Digital twin enhanced rescheduling based on hybrid strategy in intermodal container terminal. Comput. Oper. Res. 180, 107053. https://doi.org/10.1016/j.cor.2025.107053
Li, W., Fan, H., Cai, L., Guo, W., Wu, Z., Yang, P., 2024a. Digital twin-driven proactive-reactive scheduling framework for port multi-equipment under a complex uncertain environment. Simul. Modell. Pract. Theory 136, 103011. https://doi.org/10.1016/j.simpat.2024.103011
Li, W., Zhong, L., He, L., Guo, W., 2025b. Integrated scheduling in sea–rail intermodal terminals with flexible transshipment routes. Swarm. Evol. Comput. 93, 101852. https://doi.org/10.1016/j.swevo.2025.101852
Li, Y., Li, L., Liu, R., Pan, E., 2025c. A reinforcement learning hybrid genetic algorithm for charge scheduling optimization in battery swapping stations at automated container terminals. Comput. Ind. Eng. 207, 111285. https://doi.org/10.1016/j.cie.2025.111285
Li, Y., Li, X., Zhang, C., Wu, T., 2024b. Decomposition algorithms for the robust unidirectional quay crane scheduling problems. Comput. Oper. Res. 167, 106670. https://doi.org/10.1016/j.cor.2024.106670
Li, Y., Sun, Z., Hong, S., 2024c. An exact algorithm for multiple-equipment integrated scheduling in an automated container terminal using a double-cycling strategy. Transp. Res. Part E Logist. Transp. Rev. 186, 103565. https://doi.org/10.1016/j.tre.2024.103565
Lou, P., Zhong, Y., Hu, J., Fan, C., Chen, X., 2023. Digital-twin-driven AGV scheduling and routing in automated container terminals. Mathematics 11 (12), 2678. https://doi.org/10.3390/math11122678
Ma, M., Yu, F., Xie, T., Yang, Y., 2024. A hybrid speed optimization strategy based coordinated scheduling between AGVs and yard cranes in U-shaped container terminal. Comput. Ind. Eng. 198, 110712. https://doi.org/10.1016/j.cie.2024.110712
Murakami, K., 2017. A new model and approach to electric and diesel-powered vehicle routing. Transp. Res. Part E Logist. Transp. Rev. 107, 23–37. https://doi.org/10.1016/j.tre.2017.09.004
Park, K., Kim, M., Bae, H., 2024. A predictive discrete event simulation for predicting operation times in container terminal. IEEE Access 12, 58801–58822. https://doi.org/10.1109/ACCESS.2024.3389961
Peng, W., Wang, D., Qiu, H., Chu, F., Yin, Y., 2025. Integrated optimization on double-side cantilever yard crane scheduling and green vehicle path planning at U-shaped yard. IEEE Trans. Intell. Transp. Syst. 26 (3), 3684–3699. https://doi.org/10.1109/TITS.2024.3521218
Qin, T., Du, Y., Chen, J.H., Sha, M., 2020. Combining mixed integer programming and constraint programming to solve the integrated scheduling problem of container handling operations of a single vessel. Eur. J. Oper. Res. 285 (3), 884–901. https://doi.org/10.1016/j.ejor.2020.02.021
Slama, I., Ben-Ammar, O., Dolgui, A., Masmoudi, F., 2021. Genetic algorithm and monte carlo simulation for a stochastic capacitated disassembly lot-sizing problem under random lead times. Comput. Ind. Eng. 159, 107468. https://doi.org/10.1016/j.cie.2021.107468
Song, X., Chen, N., Zhao, M., Wu, Q., Liao, Q., Ye, J., 2024. Novel AGV resilient scheduling for automated container terminals considering charging strategy. Ocean Coastal Manage. 250, 107014. https://doi.org/10.1016/j.ocecoaman.2023.107014
Tang, K., Zhang, Y., Yang, C., He, L., Zhang, C., Zhou, W., 2024a. Optimization for multi-resource integrated scheduling in the automated container terminal with a parallel layout considering energy-saving. Adv. Eng. Inf. 62, 102660. https://doi.org/10.1016/j.aei.2024.102660
Tang, Y., Ye, Z., Chen, Y., Lu, J., Huang, S., Zhang, J., 2024b. Regulating the imbalance for the container relocation problem: a deep reinforcement learning approach. Comput. Ind. Eng. 191, 110111. https://doi.org/10.1016/j.cie.2024.110111
Trade, U. N. C.o., Development, 2024. Review of Maritime Transport: Navigating Maritime Chokepoints. United Nations Publications, NEW YORK.
Wang, C., Liu, K., Zhang, C., Miao, L., 2024. Distributionally robust chance-constrained optimization for the integrated berth allocation and quay crane assignment problem. Transp. Res. Part B Methodol. 182, 102923. https://doi.org/10.1016/j.trb.2024.102923
Wang, J., Guo, Q., Sun, H., Chen, M., 2023a. Collaborative optimization of logistics and electricity for the mobile charging service system. Appl. Energy 336, 120845. https://doi.org/10.1016/j.apenergy.2023.120845
Wang, J., Zhang, Y., Tang, K., Zhou, W., Yang, C., 2025a. Dynamic charging strategies for battery-powered IGV based on multi-agent simulation in automated container terminals. Flex Serv. Manuf. J. . https://doi.org/10.1007/s10696-025-09595-9
Wang, Q., Tong, X., Li, Y., Wang, C., Zhang, C., 2025b. Integrated scheduling optimization for automated container terminal: a reinforcement learning-based approach. IEEE Trans. Intell. Transp. Syst. 26 (7), 10019–10035. https://doi.org/10.1109/TITS.2025.3556882
Wang, R., Li, J., Bai, R., 2023b. Prediction and analysis of container terminal logistics arrival time based on simulation interactive modeling: a case study of ningbo port. Mathematics 11 (15), 3271. https://doi.org/10.3390/math11153271
Wang, X., Jin, Z., 2025. Collaborative optimization of multi-equipment scheduling and intersection point allocation for U-shaped automated sea-rail intermodal container terminals. IEEE Trans. Autom. Sci. Eng. 22, 7373–7393. https://doi.org/10.1109/TASE.2024.3428392
Wang, Z., Zeng, Q., Liu, B., Qu, C., Wang, H., 2025c. A tailored two-stage algorithm for quay crane and automated guided vehicle scheduling problems. IEEE Trans. Intell. Transp. Syst. 26 (4), 5049–5066. https://doi.org/10.1109/TITS.2025.3545433
Xia, H., Zhu, J., 2023. Improved STN models and heuristic rules for cooperative scheduling in automated container terminals. CMES 138 (2), 1637–1661. https://doi.org/10.32604/cmes.2023.029576
Xing, Z., Liu, H., Wang, T., Lin, Y.H., Chew, E.P., Tan, K.C., Li, H., 2025. AGV charging scheduling with capacitated charging stations at automated ports. Transp. Res. Part E Logist. Transp. Rev. 197, 104080. https://doi.org/10.1016/j.tre.2025.104080
Xu, M., Meng, Q., 2019. Fleet sizing for one-way electric carsharing services considering dynamic vehicle relocation and nonlinear charging profile. Transp. Res. Part B Methodol. 128, 23–49. https://doi.org/10.1016/j.trb.2019.07.016
Yang, X., Hu, H., Cheng, C., 2025. Collaborative scheduling of handling equipment in automated container terminals with limited AGV-mates considering energy consumption. Adv. Eng. Inf. 65, 103133. https://doi.org/10.1016/j.aei.2025.103133
Yang, X., Hu, H., Jin, J., 2023a. Battery-powered automated guided vehicles scheduling problem in automated container terminals for minimizing energy consumption. Ocean Coastal Manage. 246, 106873. https://doi.org/10.1016/j.ocecoaman.2023.106873
Yang, Y., Sun, S., He, S., Jiang, Y., Wang, X., Yin, H., Zhu, J., 2023b. Research on the multi-equipment cooperative scheduling method of sea-rail automated container terminals under the loading and unloading mode. J. Mar. Sci. Eng. 11 (10), 1975. https://doi.org/10.3390/jmse11101975

Yu, J., Tang, G., Song, X., Yu, X., Qi, Y., Li, D., Zhang, Y., 2018. Ship arrival prediction and its value on daily container terminal operation. Ocean Eng. 157, 73–86. https://doi.org/10.1016/j.oceaneng.2018.03.038
Yu, M., Liu, X., Xu, Z., He, L., Li, W., Zhou, Y., 2023. Automated rail-water intermodal transport container terminal handling equipment cooperative scheduling based on bidirectional hybrid flow-shop scheduling problem. Comput. Ind. Eng. 186, 109696. https://doi.org/10.1016/j.cie.2023.109696
Zhang, S., Qiu, B., Tian, J., 2025. Design and development of an optimisation model and simheuristic framework for the on-demand delivery problem with driver-experience-based stochastic travel time. Eur. J. Ind. Eng. 20 (1), 127–155. https://doi.org/10.1504/EJIE.2025.147178
Zhang, X., Hong, Z., Xi, H., Li, J., 2024a. Optimizing multiple equipment scheduling for U-shaped automated container terminals considering loading and unloading operations. Comput. Aided Civ. Infrastruct. Eng. 39 (20), 3103–3124. https://doi.org/10.1111/mice.13275
Zhang, X., Li, H., Sheu, J.-B., 2024b. Integrated scheduling optimization of AGV and double yard cranes in automated container terminals. Transp. Res. Part B Methodol. 179, 102871. https://doi.org/10.1016/j.trb.2023.102871
Zhao, R., Liang, C., 2025. Optimizing AGV utilization and battery life in automated container terminals: focus on a novel charging strategy and reinforcement learning algorithm. J. Clean. Prod. 519, 145939. https://doi.org/10.1016/j.jclepro.2025.145939
Zhao, Z., Chen, J., Shen, M., Liang, Y., Wan, Z., Wang, H., 2025. Multi-equipment integrated scheduling for stereo container terminals. Transp. Res. Part E Logist. Transp. Rev. 201, 104259. https://doi.org/10.1016/j.tre.2025.104259
Zhen, L., Zhang, Q., Tan, Z., Wang, S., . Scheduling AGVs in ports with battery charging and swapping. IISE Trans. 0 (0), 1–18. https://doi.org/10.1080/24725854.2025.2468722
Zhen, L., Zhuge, D., Wang, S., Wang, K., 2022. Integrated berth and yard space allocation under uncertainty. Transp. Res. Part B Methodol. 162, 1–27. https://doi.org/10.1016/j.trb.2022.05.011
Zhong, L., Li, W., Gao, K., He, L., Zhou, Y., 2024. An improved NSGAII for integrated container scheduling problems with two transshipment routes. IEEE Trans. Intell. Transp. Syst. 25 (10), 14586–14599. https://doi.org/10.1109/TITS.2024.3388468
Zhou, W., Zhang, Y., Tang, K., He, L., Zhang, C., Tian, Y., 2024. Co-optimization of the operation and energy for AGVs considering battery-swapping in automated container terminals. Comput. Ind. Eng. 195, 110445. https://doi.org/10.1016/j.cie.2024.110445
Zhu, J., Ma, F., 2024. Scheduling of twin automatic stacking cranes and automated guided vehicle considering buffer mode on automated container terminal. Comput. Ind. Eng. 193, 110271. https://doi.org/10.1016/j.cie.2024.110271